

APPENDIX A

CSO SOLIDS DEPOSITION MODELING

---



# KING COUNTY SEDIMENT MANAGEMENT PLAN

## 2018 UPDATE

---

### APPENDIX A: CSO SOLIDS DEPOSITION MODELING

**Part 1. Summary of CSO Solids Deposition Modeling**

**Part 2. Simple Analytical Near-Field Sediment Deposition Model for  
CSO Discharges**

**Part 3. EFDC Sediment Deposition Modeling Report for SMP Update**

**Prepared for**

King County Department of Natural Resources and Parks Sediment Management Program  
Sediment Management Plan Update Project

**Prepared by**

King County Department of Natural Resources and Parks  
Wastewater Treatment Division

**September 2018**

This page intentionally left blank.

# Appendix A, Part 1: Summary of CSO Solids Deposition Modeling

This page intentionally left blank.

**TABLE OF CONTENTS:**

**PART 1 – SUMMARY OF CSO SOLIDS DEPOSITION MODELING**

1 INTRODUCTION.....3

2 MODELING APPROACH .....3

    2.1 Characteristic Discharge Flow Rate.....5

    2.2 Solids Concentrations and Settling Velocity .....7

    2.3 Pipe Diameter, Depth, Ambient Velocity and Salinity .....8

    2.4 Bathymetric Data.....9

3 SIMPLE MODEL CONFIGURATION .....9

4 EFDC MODEL CONFIGURATION.....12

5 CSO DEPOSITION RATES.....12

6 SUMMARY AND CONCLUSIONS.....14

7 REFERENCES.....17

**List of Tables**

Table 1 CSO Outfall Sites Selected for Comparing EFDC and Simple Model Sediment Deposition Rates.....4

Table 2 Characteristic CSO Discharge Flows and Durations. Flows Sorted from Smallest to Largest (Lower 1/3 to Upper 1/3); Durations Sum to 10 Days ....7

Table 3 Suspended Solid Characteristics Used in the Models.....8

Table 4 Outfall Discharge Depths, Pipe Diameter, and Ambient Velocity and Salinity (EFDC Model) .....9

Table 5 Data Requirements for Simple Models, in Addition to Suspended Solids Characteristics in Table 3 .....11

Table 6 Predicted CSO Solids Deposition Rates from Simple Model and EFDC .....13

**List of Figures**

Figure 1 Illustration of a histogram of positive CSO flow values divided into three equal segments, the average flow  $q_i$  for each segment, and the percent probability of each segment occurring (shown at top of chart). .....6

Figure 2 Relative difference in the average sediment deposition rate (within 100 feet) predicted by the Simple and EFDC models .....15

Figure 3 Relative difference in the total sediment deposition predicted by the Simple and EFDC models within 255 m (neutrally buoyant) or 450 m (submerged buoyant) .....15

## 1 INTRODUCTION

This appendix describes how the accumulation rates of CSO solids in receiving sediments were estimated for each CSO discharge. Two models were developed and compared. King County developed a one dimensional spreadsheet calculation, or Simple Model, to estimate the depositional rate of CSO solids and the distance from the CSO discharge those deposits would occur. This model retains the most important physical processes but omits details on site specific geometry and current patterns that would be included in a full three-dimensional model of the discharge. Previous work indicated that a three-dimensional hydrodynamic model such as the Environmental Fluid Dynamics Code (EFDC) could reproduce accumulation patterns from CSO discharges when run with a grid scale equal to the CSO pipe diameter (King County 2011).

Six CSOs from the King County system were identified as candidate locations to compare the two models. These sites were selected to cover the range of conditions for King County's CSO discharges and be separated from other discharges (storm water). The six CSO sites were simulated in EFDC, and the resulting depositional patterns were used to check the one-dimensional screening model results. An additional eight CSOs were then modeled with the Simple Model only, and three CSO were modeled in the EFDC Model only.

This part of this appendix (Appendix A, Part 1) summarizes the CSO modeling approach and results. The predicted deposition rates are used to predict the potential for exceedances of the SMS in surface sediments near each CSO outfall in the main body of this SMP document. The other two parts of this appendix document the detailed modeling methods and assumptions for the Simple Model (Appendix A, Part 2) and the EFDC Model (Appendix A, Part 3).

## 2 MODELING APPROACH

The sediment deposition rates at 14 of King County's CSO discharge locations were simulated using a simplified spreadsheet calculation (Simple Model). Six of these CSO locations were also simulated with the EFDC three-dimensional hydrodynamic model (Table 1), and eight were simulated with the Simple Model only. Three were simulated with the EFDC Model only. Sediment deposition rates were compared at sites with predictions from both models.

**Table 1**  
**CSO Outfall Sites Selected for Comparing EFDC and**  
**Simple Model Sediment Deposition Rates**

CSO Number	CSO Discharge	Average Annual Discharge Volume (MG/year)	Type of Modeling Performed	Rationale for Model Selection
<b>Central Basin of Puget Sound</b>				
048a	North Beach PS Overflow (wet well)	5.4 (prior to control)	EFDC and the Simple Model	Compare EFDC and Simple Models
006	S Magnolia Overflow	19	EFDC and the Simple Model	Compare EFDC and Simple models
052	53rd Ave. SW PS Overflow	0.11	EFDC and the Simple Model	Compare EFDC and Simple models
054	63rd Ave. SW Overflow	1.2	Simple Model	Simple Model considered sufficient for CSO with low discharge volumes/ no historical exceedances
055	SW Alaska St. Overflow	0.01	Simple Model	Simple Model considered sufficient for CSO with no historical exceedances
056	Murray St. PS Overflow	9.1	EFDC and Simple Model	Compare EFDC and Simple models
057	Barton St. PS Overflow	2.7	EFDC and the Simple Model	Compare EFDC and Simple Models
<b>Elliott Bay</b>				
029	Kingdome RS Overflow	16	Simple Model	Simple Model considered more accurate for discharge location
<b>West Waterway</b>				
036	Chelan Ave. RS Overflow	5.7	EFDC	EFDC considered more accurate for Chelan
037	Harbor Ave. RS Overflow	6.6	Simple Model	Simple Model considered sufficient for CSO mixing with creek before discharge
<b>Lake Washington Ship Canal/Lake Union/Portage Bay</b>				
003	Ballard Siphon Overflow	0.94	Simple Model	Simple Model considered sufficient for CSO

CSO Number	CSO Discharge	Average Annual Discharge Volume (MG/year)	Type of Modeling Performed	Rationale for Model Selection
004	11th Ave. NW Overflow	8.9	Simple Model	Simple Model considered sufficient for CSO
008	3rd Ave. W Overflow	9.8	EFDC and Simple Model	Compare EFDC and Simple models
007	Canal St. Overflow	0.19	Simple Model	Simple Model considered sufficient for CSO
009	Dexter Ave. RS Overflow	16	Simple Model	Simple Model considered sufficient for CSO
015	University RS Overflow	88	EFDC and Simple Model	Compare EFDC and Simple models
014	Montlake RS Overflow	22	EFDC and Simple Model	Compare EFDC and Simple models
<b>Lake Washington</b>				
012/049	Belvoir PS Overflow/30th Ave. NE Overflow	0.65	Simple Model	Simple Model considered sufficient for CSO
<b>Lower Duwamish Waterway</b>				
041	Brandon St. RS Overflow	30	EFDC and Simple model	Compare EFDC and Simple models

EFDC – Environmental Fluid Dynamics Code  
 MG – million gallons  
 PS – pump station  
 RS – regulator station

## 2.1 Characteristic Discharge Flow Rate

A set of three characteristic discharge flow rates were simulated for each CSO instead of simulating a CSO discharge time series. For modeling purposes, the time series of CSO discharges was replaced with a set of flows equally spaced over the flow range of the CSO time series. The discharge was simulated for a period proportional to the duration each flow range occurred in the original CSO discharge time series. The characteristic discharge flow rates were determined from observed or simulated CSO discharge time series. See example diagram in Figure 1.

The discharge flow rate changes the initial momentum, primarily affecting how far offshore surface discharges travel. Three characteristic discharge flow rates were used to characterize the CSO discharge time series, as the model is relatively insensitive to the initial momentum.

The model simulations were configured with a 10-day continuous discharge duration to allow multiple tidal cycles to advect the discharge effluent. The same 10-day duration was used for fresh water discharges, for consistency. Ten days of continuous discharge can represent years of CSO overflow events, depending on the particular CSO and the number and magnitude of overflow events for the CSO. Therefore, the simulated sediment accumulation was scaled by the ratio of the average annual discharge volume to the volume discharged over the 10-day period to obtain the average annual deposition rate for each CSO.

Table 2 provides the discharge flow rate and the corresponding simulation duration for each of the three characteristic flow rates. The durations for each set of three flow rates add up to 10 days, the total simulation period.

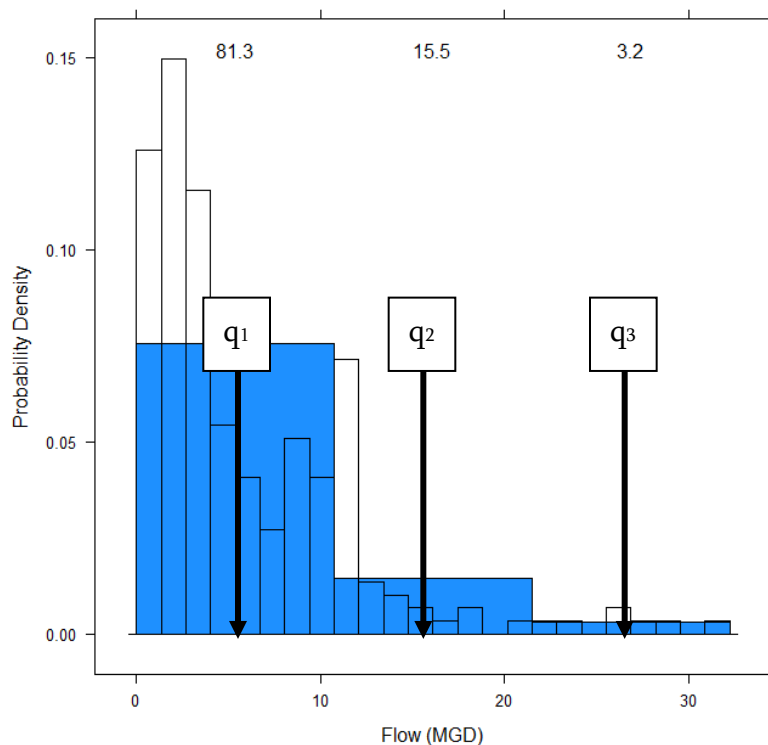


**Figure 1. Illustration of a histogram of positive CSO flow values divided into three equal segments, the average flow  $q_i$  for each segment, and the percent probability of each segment occurring (shown at top of chart).**

**Table 2**  
**Characteristic CSO Discharge Flows and Durations. Flows Sorted from Smallest to Largest (Lower 1/3 to Upper 1/3); Durations Sum to 10 Days**

<b>CSO Discharge</b>	<b>Lower 1/3 (MGD)/(days)</b>	<b>Middle 1/3 (MGD)/(days)</b>	<b>Upper 1/3 (MGD)/(days)</b>
3rd Ave. W Overflow	23.3 / 8.5	69.8 / 1.2	116.3 / 0.3
Montlake RS Overflow	25.1 / 6.1	75.4 / 3.2	125.6 / 0.7
University RS Overflow	38.6 / 5.7	115.9 / 2.6	193.1 / 1.7
53rd Ave. SW PS Overflow	10.1/9.92	30.3/0.05	50.6/0.03
Barton St. PS Overflow	4.0 / 9.2	12.0 / 0.5	20.0 / 0.3
Brandon St. RS Overflow	16.3 / 7.6	48.8 / 2.2	81.3 / 0.2
Chelan Ave. RS Overflow	3.6 / 5.2	10.9 / 2.5	18.1 / 2.3
S Magnolia Overflow	3.0 / 8.1	9.0 / 1.8	15.0 / 0.1
Murray St. PS Overflow	22.4 / 0.5	67.1 / 6.9	111.9 / 2.6
North Beach PS Overflow	1.5 / 8.1	4.5 / 1.7	7.5 / 0.2

MGD – million gallons per day

## 2.2 Solids Concentrations and Settling Velocity

CSO solids concentrations were obtained from sampling CSOs during periods when discharging or when in-pipe flow levels were close to the overflow level. Whole water samples were collected upstream of the regulator gate/weir at flows higher than when most CSOs are recorded and are considered representative of CSO solids. A total solids concentration of 128 mg/L was used, corresponding to the average Total Suspended Solids (TSS) concentration observed in the CSO samples. All CSOs and all discharge flows were assumed to have the same TSS concentration and particle size distribution. Three sediment size classes were used in the modeling, similar to the original model development (King County 2011). The settling velocity for each particle size class was taken from settling tube

measurements on whole water samples collected from CSO discharges collected downstream of the regulator. The settling velocity measurements and relative amount of each particle size class were summarized in the model development report (King County 2011). The settling velocities and mass fraction of the three sediment size classes are summarized in Table 3.

**Table 3**  
**Suspended Solid Characteristics Used in the Models**

Particle Type	Settling Velocity $W_s$ (m/s)	Percent Mass	Conc. (mg/l)
Sand	7.5 E-03	33%	41.6
Silt	6.25 E-04	34%	43.1
Clay	1.50 E-04	34%	43.3

mg/l – milligrams per liter  
m/s – meters per second  
 $W_s$  – settling velocity

### 2.3 Pipe Diameter, Depth, Ambient Velocity and Salinity

Pipe diameters and discharge depth were obtained from facility construction records, summarized below in Table 4. Ambient velocities were obtained from three-dimensional circulation models or current meter records. The ambient velocity was characterized by the depth averaged root mean square velocity. Freshwater discharges had zero ambient salinity, while Puget Sound and Elliott Bay discharges used a constant salinity of 28 practical salinity units (psu). The buoyant CSO discharge is expected to surface in marine waters, so simplifying the ambient stratification to a constant value is not expected to affect the simulation results. In the Lower Duwamish Waterway (LDW) where a thicker fresh/brackish layer overlays the marine water, a winter-time density profile was used for Brandon St. and Chelan Ave. CSOs. The Simple Model doesn't account for vertical density differences, so these CSOs used the marine configuration with a salinity of 28 psu. Temperature was not simulated, as temperature differences have a minor effect on density relative to salinity.

**Table 4**  
**Outfall Discharge Depths, Pipe Diameter, and Ambient Velocity and Salinity (EFDC Model)**

CSO Discharge	Discharge Depth (m)	Pipe Diameter (m)	Ambient Velocity (m/s)	Ambient Salinity (psu)
3rd Ave. W Overflow	12.5	1.52	0.143	0
Montlake RS Overflow	5.7	1.52	0.066	0
University RS Overflow	1	2.13	0.056	0
53rd Ave. SW PS Overflow	5	1.83	0.171	28
Barton St. PS Overflow	6.5	1.52	0.114	28
Brandon St. RS Overflow	0.3	1.83	0.110	28 (simple profile (EFDC))
Chelan Ave. RS Overflow	8.1	0.76	0.350	28 (simple profile (EFDC))
S Magnolia Overflow	6.75	0.91	0.303	28
Murray St. PS Overflow	6.6	1.83	0.327	28
North Beach	5	0.41	0.223	28

EFDC – Environmental Fluid Dynamics Code  
m – meters  
m/s – meters per second  
psu – practical salinity units

## 2.4 Bathymetric Data

Bathymetric data were acquired from King County’s GIS Digital Elevation Model (DGM) to represent the water depth throughout the ambient waterbody.

## 3 SIMPLE MODEL CONFIGURATION

Two Simple Models were developed for two types of waterbodies:

- A neutrally buoyant plume model that characterizes freshwater systems, which are considered quiescent. This model assumes suspended solids settle from within the plume and fall directly into the sediment bed.
- A submerged buoyant plume model that characterizes saltwater systems, which are tidally driven. This model assumes suspended solids settle through the water column where the plume has terminated its rise. At the termination height, solid particles are allowed to settle from the plume. The model accounts for different solids distributions that result from different tidal velocities.

The Simple Models are steady-state, one-dimensional models that simulate the advection of CSO solids mass in the horizontal direction; results are presented as the expected sediment deposition rate with distance from the CSO discharge.

The Simple Models are steady-state models that simulate the advection of particles in one dimension and calculates the distance the particle settles in the vertical direction. When the settling distance exceeds the depth the particle mass is accumulated and converted into a sedimentation depth based on an assumed density of 2500 kg/m<sup>3</sup> and a porosity of 0.4. A variation of the original Simple Model was created to allow tidal velocities to be simulated as the summation of sinusoidally varying velocities, and to simulate the horizontal advection during buoyant plume rise from a submerged discharge. The Simple Models were developed in Excel Workbooks for a freshwater and saltwater discharge; a thorough description of the model and required input data for each waterbody type are given in Appendix A, Part 2.

The input parameters to the Simple Model are slightly different for the fresh water and marine configurations (Table 5). In addition to the characteristics described in Section 2, the Simple Model requires input values for the angle of plume spread, the bathymetry slope, and the plume entrainment coefficient. The bathymetric slope was calculated from a linear fit to the bathymetric profile offshore of the discharge location. The bathymetric slope is not included in the marine model, which assumes the tidal advection will be parallel to the shoreline or bathymetric contours. The angle of plume spread and the plume entrainment coefficient are constant values based on empirical relations (Fisher 1979). See Appendix A, Part 2, for additional detail.

**Table 5**  
**Data Requirements for Simple Models, in Addition to**  
**Suspended Solids Characteristics in Table 3**

<b>Waterbody Type</b>	<b>Discharge Depth (m)</b>	<b>Pipe Diameter (m)</b>	<b>Ambient Velocity (m/s)</b>	<b>Ambient Salinity (o/oo)</b>	<b>Flow (MGD)</b>	<b>Event Duration (days)</b>	<b>Plume Angle <math>\theta</math></b>	<b>Bathymetry Slope m</b>	<b>Entrainment Coefficient</b>
Fresh	NA	Yes	NA	NA	Yes	Yes	Yes	Yes	Yes
Salt	Yes	Yes	Yes	Yes	Yes	Yes	NA	NA	NA

m – meters

m/s – meters per second

MGD – million gallons per day

## 4 EFDC MODEL CONFIGURATION

Previous work by King County (King County 2011) found that if the EFDC Model was configured with a model grid size equal to the discharge pipe diameter, the model could reasonably simulate the initial dilution of the discharge and the resulting sediment deposition. To confirm this conclusion, ten CSO sites were modeled with EFDC in conjunction with sediment sampling. The chemical distribution patterns were compared to the sediment deposition pattern predicted by the EFDC Model. The observed patterns were in qualitative agreement with the model predictions. Model predictions for CSO discharges to marine waters had the largest depositional rate immediately adjacent to the CSO discharge, and sediment sampling around those CSO discharges also tended to have the higher concentrations nearest the discharge. Model predictions for CSO discharges to fresh waters showed a much larger deposition pattern in front of the outfall. Comparison with sediment data had mixed results, with the chemical signature in the sediment data often suggesting other sources are present. However, the predicted depositional area does generally agree with the pattern of highest sediment concentrations. Additional detail on the EFDC Model configuration, simulations, and comparison to sediment data are given in Appendix A, Part 3.

## 5 CSO DEPOSITION RATES

The requirement of a model grid size equal to the discharge pipe diameter for the EFDC Model creates a computationally intensive simulation to predict deposition from a CSO discharge. The Simple Model (see Appendix A, Part 2) was developed to capture the dominant physical processes of the CSO particulate deposition process in a simpler calculation. Simpler to configure and run, deposition from 18 CSO discharges were modeled with the simple model approach. Ten CSO discharges were modeled with an EFDC simulation. The results of the simulations are summarized in Table 6. The EFDC simulations predict the maximum deposition rate occurs in the model cell into which the CSO discharges when the CSO is set to discharge into the bottom vertical layer. This cell ranges from 4 to 20 feet in length, but the deposition rate in cells near the outfall is very dependent on the model grid configuration and if the discharge is in the bottom or next to bottom vertical layer (see Part 3). To account for this modeling sensitivity and better compare the near-field depositional rate, the depositional rate was averaged over a 100-foot radius to compare the Simple Model predictions to the EFDC simulations. As can be seen in Table 6, the Simple Model predicts a greater depositional rate in this area than the

EFDC simulations for freshwater discharges and within a factor of 2 for marine discharges. Note that, for comparison purposes, the EFDC deposition is averaged over a smaller area than predicted by the model (90° vs. up to 360°) to allow a direct comparison to the Simple Model. This change over-predicts the average deposition for EFDC. Thus, the Simple Model was deemed to provide a conservative estimate of the depositional rate of particulate solids discharged from a CSO.

**Table 6**  
**Predicted CSO Solids Deposition Rates from Simple Model and EFDC**

CSO Discharge	Annual Discharge Volume (MG/year)	CSO Deposition Rate Average Within 100 feet (mm/year) <sup>1</sup>	
		Simple Model	EFDC
3rd Ave. W Overflow	9.8	1.0	0.8
Montlake RS Overflow	22	5.2	1.1
University RS Overflow	88	12.5	6.7
53rd Ave. SW PS Overflow	0.11	0.003	0.01
Barton St. PS Overflow	2.7	0.07	0.1
Brandon St. RS Overflow	30	1.8	3.9
Chelan Ave. RS Overflow	5.7	0.03	0.12
S Magnolia Overflow	19	0.13	0.18
Murray St. PS Overflow	9.1	0.07	0.04
North Beach PS Overflow	5.4 (prior to control)	0.01	0.02
63rd Ave. SW Overflow	1.2	0.02	na
SW Alaska St. Overflow	0.01	0.0001	na
Kingdome RS Overflow	16	1.5	na
11th Ave. NW Overflow	8.9	2.1	na
Ballard Siphon Overflow	0.94	0.02	na
Canal St. Overflow	0.19	0.06	na
Dexter Ave. RS Overflow	16	4.9	na
Belvoir PS Overflow/ 30th Ave. NE Overflow	0.65	0.4	na
Harbor Ave. RS Overflow	6.6	0.08	na

Notes:

1. Assumed two 45-degree deposition areas in opposite directions for marine sites (due to tides) and 90-degree deposition area for freshwater sites. Pattern based on EFDC output but normalized to compare model rates.

EFDC – Environmental Fluid Dynamics Code  
na – not applicable (model not run)

MG – million gallons  
PS – pump station

mm – millimeters  
RS – regulator station

## 6 SUMMARY AND CONCLUSIONS

The depositional rate of particulates discharged from CSOs were simulated with both a three-dimensional hydrodynamic model (EFDC) and a one-dimensional spreadsheet calculation, or Simple Model. The depositional patterns predicted from the EFDC Model were in general agreement with sediment samples collected around each CSO, predicting the greatest deposition near the CSO discharge. The predicted depositional rates at ten CSO locations were compared to a simple one-dimensional spreadsheet model that retains the most important physical processes but omits details on site-specific geometry and current patterns that would be included in a full three-dimensional model of the discharge. The Simple Model tended to predict greater sediment depositional rates than the EFDC Model in the near field (100-foot radius) for freshwater discharges and within a factor of 2 for marine discharges.

The neutrally buoyant Simple Model (freshwater discharges) provides higher nearfield deposition rate estimates than the EFDC Model, and therefore provides a more conservative estimate of the potential sediment contamination (Figure 2). The submerged buoyant Simple Model (marine discharges) over- or under-estimated EFDC sediment deposition rates by between 1% and 100% (average ~50%; Figure 2). Because the averaging method used to allow the EFDC Model to directly compare results to the Simple Model inflates the actual predicated near-field EFDC deposition rates, the Simple Model also provides a conservative estimate of the potential sediment contamination. The difference in the Simple Model results and the EFDC Model results show a similar pattern (typically within +60%) when comparing total solids deposition (Figure 3), although the submerged buoyant Simple Model tends to underestimate total deposition, meaning it is less conservative in the far field.

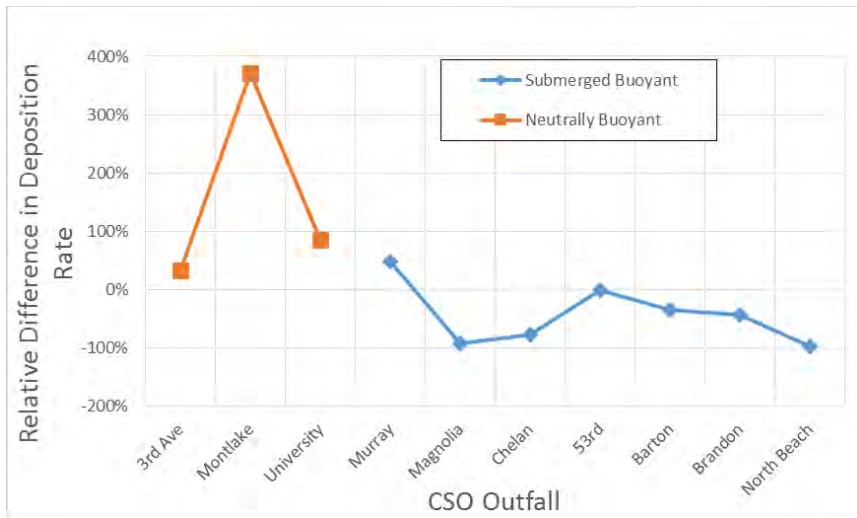


**Figure 2. Relative difference in the average sediment deposition rate (within 100 feet) predicted by the Simple and EFDC models**

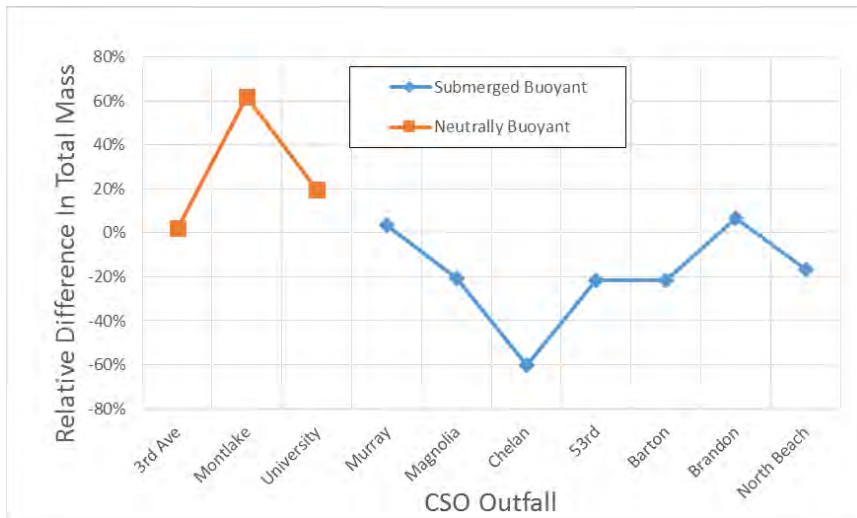


**Figure 3. Relative difference in the total sediment deposition predicted by the Simple and EFDC models within 255 m (neutrally buoyant) or 450 m (submerged buoyant)**

In general, the neutrally buoyant and submerge buoyant (Simple) models over-estimated or produced similar nearfield sediment deposition rates, compared to EFDC Model simulations, respectively. Therefore, the Simple Model provided a conservative estimate of the maximum potential sediment deposition near a CSO outfall. As noted in Part 3 of this Appendix, the EFDC Model tended to predict chemical concentrations near the outfall (areas with highest deposition rates) that were not present in the samples, suggesting the model was conservative

in predictions. With both models providing conservative estimates of nearfield sediment deposition, and the Simple Model being relatively more or similarly conservative, the Simple Model can be considered a screening-type tool that provides a very conservative estimate of the possibility of sediment contamination.

Appendix B describes how the predicted depositional rates calculated in this appendix are combined with characteristic chemical concentrations from solids samples collected from CSOs during periods when discharging or when in-pipe flow levels were close to the overflow level to estimate the potential for exceedances of sediment quality standards. The main body of the SMP uses the information in this appendix and Appendix B to evaluate the potential for CSO discharges to create elevated concentrations of contaminants in sediment.

## 7 REFERENCES

- Fischer, Hugo B., E. John List, Robert C.Y. Koh, Jorg Imberger, and Norman H. Brooks, 1979. Mixing in Inland and Coastal Waters. Academic Press Inc.
- King County, 2011. Discharge modeling for the contaminated sediment cleanup decisions: A summary and supplemental analyses. Department of Natural Resources and Parks, Wastewater Treatment Division.

This page intentionally left blank.

# Appendix A, Part 2: Simple Analytical Near-Field Sediment Deposition Model for CSO Discharges

This page intentionally left blank.

---

# Appendix A, Part II: Simple Analytical Near-Field Sediment Deposition Model for CSO Discharges

---

August 2018



## **King County**

Department of Natural Resources and Parks

### **Wastewater Treatment Division**

King Street Center, KSC-NR-0500  
201 South Jackson Street  
Seattle, WA 98104-3855

For comments or questions, contact:

Jeff Stern

King County Department of Natural Resources and Parks

Wastewater Treatment Division

201 South Jackson Street

MS KSC-NR-0505

Seattle, WA 98104-3855

Jeff.stern@kincounty.gov

Ph. (206) 477-5479

Alternate Formats Available

206-296-6519 TTY Relay: 711

## Contents

1	Introduction.....	1
2	Complex Model Equations.....	1
2.1	Neutrally Buoyant Discharge.....	2
2.2	Submerged Buoyant Discharge.....	4
2.2.1	Model Boundary Limits.....	6
3	Transforming between One and Two Dimensions.....	9
4	Model Data Requirements .....	12
4.1	CSO Outfall Sites.....	13
4.2	Characteristic Discharge Flow Rate.....	13
4.3	Pipe Diameter, Depth, and Ambient Velocity .....	16
4.4	Solids Concentrations and Velocity.....	16
4.5	Simple Model Configuration .....	16
5	Model Comparisons .....	17
5.1	Freshwater Systems .....	17
5.2	Saltwater Systems .....	19
6	Summary.....	25
7	References:.....	28

## Tables

Table 1.	Values for parameters in equation (1.16). Values were obtained from Fischer et. al. (1979). .....	4
Table 2.	Data requirements for the EFDC and simple model.....	13
Table 3.	Ten CSO outfall sites selected for comparing EFDC and simple model sediment deposition rates. .....	13
Table 4.	Characteristic CSO discharge flows and durations, flows are sorted from smallest to largest (lower 1/3 to upper 1/3). Duratiopns sum to ten days.....	15
Table 5.	Outfall discharge depths, pipe diameter, and ambient velocity and salinity.....	16
Table 6.	Combined sewer overflow suspended solid characteristics used in the models, the average total suspended solids concentration was 120 (mg/l).....	16
Table 7.	Data requirements for simple models in addition to suspended solids characteristics in Table 6.17	17

## Figures

Figure 1.	Simplistic interpretation of a plume where $m$ is the rate of change in depth with distance.....	2
Figure 2.	Schematic showing the flow path of a buoyant plume. After the plume rise has terminated, solid particles fall through the water column $H$ and are transport a distance $X_H = HU_{amb}/w_s$ when they reach the sediment bed. ....	5

Figure 3. Sediment deposition per unit load near an outfall for Sand, Silt, and Clay for three different tidal conditions ( $\tau=0.0$  hr,  $\tau=6.0$  hr, and  $\tau=10.8$  hr). Typically the sands deposit well within the 1500 meter boundary, while the silt and clays will travel past the 1500 meter boundary (vertical line at 1500 meters). The solid lines denote solids mass deposition that would be retained in the bounded model, and the dashed lines denote solids mass that would be advected out of the model domain. .... 8

Figure 4. Illustration of annular segments radiating from the outfall, the sediment mass within each annular segment is summed and represents the mass deposited at radius R from the outfall..... 9

Figure 5. Sweep angles  $\phi$  for different velocity cycles and directions. The sweep angles are used for the neutrally buoyant model. .... 10

Figure 6. Converting the one-dimensional radial model  $r$  into two-dimensional annular segments with angle  $\phi$ . The annular segments can be transferred to Cartesian coordinates as well. .... 11

Figure 7. Converting the one-dimensional radial model  $r$  into a two-dimensional rectangle of length  $2r$  and width  $D+2b_w$ , which is 2.4 meters for this graphic. .... 12

Figure 8. Illustration of a histogram of positive CSO flow values divided into three equal segments, the average flow  $q_i$  for each segment, and the percent probability of each segment occurring (shown at top of chart). .... 14

Figure 9. Sediment depth (Sed. Vol./Len.) from the simple and EFDC models at the 3<sup>rd</sup> Avenue CSO site (solid lines) and cumulative sediment mass (dashed lines). .... 17

Figure 10. Sediment depth (Sed. Vol./Area) from the simple and EFDC models at the University Regulator CSO site (solid lines) and cumulative sediment mass (dashed lines).. .... 18

Figure 11. Sediment depth (Sed. Vol./Area) from the simple and EFDC models at the Montlake CSO site (solid lines) and cumulative sediment mass (dashed lines). .... 18

Figure 12. Sediment deposition for  $m = 0.015$  at the 3<sup>rd</sup> Avenue CSO site;  $m$  was 0.032 in Figure 9..... 19

Figure 13. Conceptual display of the forty eight discrete harmonic velocities for each  $\tau$ . The maximum velocity is  $\sqrt{2}V_{RMS}$ , where  $V_{RMS}$  is given in Table 5. The eight colored velocity groups denote the sediment mass distribution series displayed in Figure 14. .... 20

Figure 14. Conceptual sediment depositions for the eight discrete velocity groups noted in Figure 13 and their sum (red curve). .... 20

Figure 15. Simulated sediment deposition (Sed. Vol./Len.) at the Murray CSO site for the simple and EFDC models (solid lines) and cumulative sediment mass (dashed lines). .... 21

Figure 16. Simulated sediment deposition (Sed. Vol./Len.) at the Magnolia CSO site for the simple and EFDC models (solid lines) and cumulative sediment mass (dashed lines). .... 21

Figure 17. Simulated sediment deposition (Sed. Vol./Len.) at the North Beach CSO site for the simple and EFDC models (solid lines) and cumulative sediment mass (dashed lines). .... 22

Figure 18. Simulated sediment deposition (Sed. Vol./Len.) at the 53<sup>rd</sup> CSO site for the simple and EFDC models (solid lines) and cumulative sediment mass (dashed lines). .... 22

Figure 19. Simulated sediment deposition (Sed. Vol./Len.) at the Barton CSO site for the simple and EFDC models (solid lines) and cumulative sediment mass (dashed lines). .... 23

Figure 20. Simulated sediment deposition (Sed. Vol./Len.) at the Brandon CSO site for the simple and EFDC models (solid lines) and cumulative sediment mass (dashed lines). .... 23

Figure 21. Simulated sediment deposition (Sed. Vol./Len.) at the Chelan CSO site for the simple and EFDC models (solid lines) and cumulative sediment mass (dashed lines). .... 24

Figure 22. Simulated sediment deposition at the Chelan CSO site, but using a reduced tidal velocity of  $0.44U_1$  in the simple model. The smaller velocity field allowed more solids deposited within 500 meters of the outfall and provided a better match to the EFDC deposition..... 25

Figure 23. Relative difference in the maximum sediment deposition rate between the simple and EFDC models..... 26

Figure 24. Relative difference in the total sediment mass within 255 m for the freshwater and 450 m for the submerged between the simple and EFDC models..... 27

This page intentionally left blank

## 1 Introduction

If one needs to determine whether a combined sewer overflow (CSO) discharge has the potential to contaminate nearby sediments, then a simple model is likely the most appropriate model for getting a sense of the potential sediment contamination from the CSO discharge. If the simple model results suggest the potential contamination is near an action level, then a more complicated model can be used to refine the assessment. Conversely, if the simple model results suggest the potential contamination is an order of magnitude less than the action level, then one may consider the outfall is not a problem and no further assessment actions are required. Starting with a simple model can save substantial resources and computational time compared to using a significantly more complicated model. This section describes the underlying theory, along with the assumptions and simplifications used to develop a simple model for estimating sediment deposition near CSO discharges.

The appropriateness of simple models was first discussed in a previous effort by King County (2011), where a complicated model was used to assess how geophysical, geochemical, and biological processes affect suspended solid and sorbed chemical deposition near combined sewer overflow (CSO) outfalls. The study found that results could be determined using simple scaling analyses, which identify the salient processes that describe suspended solid deposition; the most salient feature was the horizontal velocity field that carries suspended solids through the waterbody. A simpler model that is based on the salient features will provide similar information as a complex model for significantly less effort. This report investigates sediment deposition simulated by a simple one-dimensional model versus a complex three-dimensional model. Simple models were shown to provide similar spatial sediment deposition patterns compared to the complex models; simple models provide a reasonable methodology for assessing potential suspended solids deposition near CSO outfalls.

## 2 Complex Model Equations

The Environmental Fluid Dynamics Computer Code (EFDC) is considered a complex model that simulates three-dimensional Hydrodynamic and Transport and Fate processes. The hydrodynamics module simulates horizontal and vertical water velocities, which are used in the Transport and Fate module that simulates the transport of suspended solids through the water body. The governing Transport and Fate equations are used to develop a simple model that simulates the transport of suspended solids within a plume.

$$\frac{\partial C}{\partial t} + \frac{\partial(uC)}{\partial x} + \frac{\partial(vC)}{\partial y} + \frac{\partial(wC)}{\partial z} = \frac{\partial}{\partial x} \left( K_x \frac{\partial C}{\partial x} \right) + \frac{\partial}{\partial y} \left( K_y \frac{\partial C}{\partial y} \right) + \frac{\partial}{\partial z} \left( K_z \frac{\partial C}{\partial z} \right) + S_C \quad (1.1)$$

Where  $C$  is concentration of a water quality state variable;  $u$ ,  $v$ , and  $w$  are the velocity components in the  $x$ ,  $y$ , and  $z$  directions;  $K_x$ ,  $K_y$ , and  $K_z$  are the turbulent diffusivities in the  $x$ ,  $y$ , and  $z$  directions; and  $S_C$  is an internal and external source/sink term. In the well-developed plume two conditions allow simplifying the equation: concentration gradients are small along the axis if the plume concentrations are constant in time; also while the lateral concentration gradients are large we are unconcerned about lateral gradients. These conditions allow omitting the turbulent diffusion terms, and the transport of a solid particle within the plume has the form,

$$\frac{\partial(uC)}{\partial x} + \frac{\partial(vC)}{\partial y} + \frac{\partial(wC)}{\partial z} = S_c \quad (1.2).$$

Equation (1.2) is manipulated further for a neutrally buoyant surface plume and a submerged buoyant plume.

## 2.1 Neutrally Buoyant Discharge

This model assumes suspended solids settle from within the plume and fall directly into the sediment bed. The neutrally buoyant plume is assumed to acquire the shape of a triangular prism with depth  $h$  increasing with distance  $r$  from the source, and the width a function of  $r$  and  $\theta$  (Figure 1).

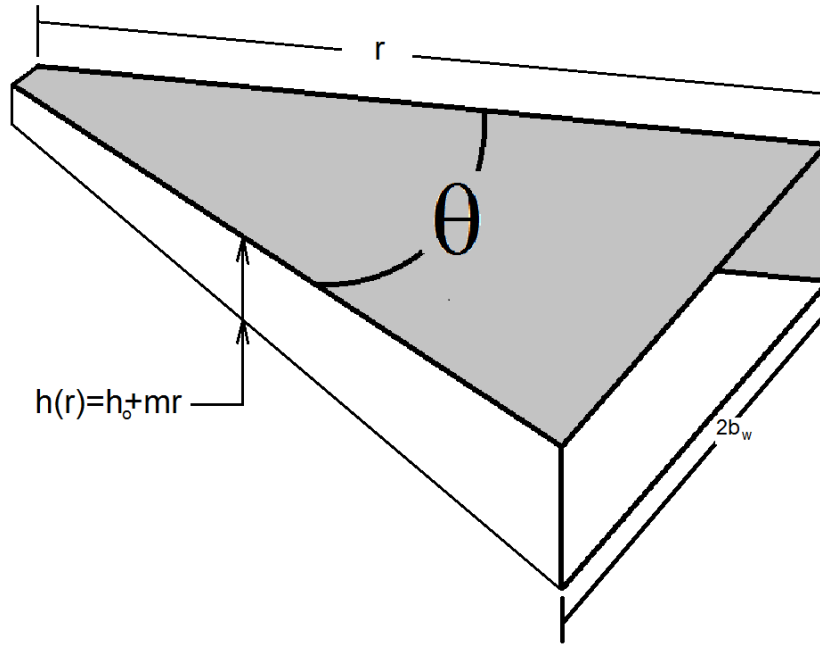


**Figure 1.** Simplistic interpretation of a plume where  $m$  is the rate of change in depth with distance.

Equation (1.2) was transformed into a radial coordinate system for the  $x$  and  $y$  axes and the decay term  $S_c$  was dropped.

$$U(r) \frac{dc}{dr} + w \frac{dc}{dz} = 0 \quad (1.3)$$

Where  $U(r)$  is the average radial velocity in the plume and  $r$  is the radius. Letting  $w$  be the particle settling velocity  $w_s$  and integrating over the plume depth results in the desired differential equation for an expanding plume.

$$U(r) \frac{d(h\bar{c}_s)}{dr} + w_s \bar{c}_s = 0 \quad (1.4)$$

Where  $h$  is the plume depth and  $\bar{c}_s$  is average solids concentration in the plume. The radially dependent flow area characterizes the increase in flow that would occur from entraining ambient water into the plume. The entrained flow was assumed to be proportional to the average plume flow (Fischer et. al., 1979).

$$\frac{dq}{dr} = \frac{2\alpha q}{b_w} \quad (1.5)$$

Where  $q$  is the average plume flow,  $\alpha$  is the entrainment coefficient, and  $b_w$  is half the plume width; equation (1.5) has solution.

$$q(r) = q_0 \left( \frac{r}{l_Q} \right)^{\frac{\alpha}{\sin(\theta/2)}}, \quad r \geq l_Q \quad (1.6)$$

$$l_Q = \sqrt{\frac{\pi}{4} D} \quad (1.7)$$

$$b_w = r \sin\left(\frac{\theta}{2}\right) \quad (1.8)$$

Where  $q_0$  is the pipe discharge flow rate and  $D$  is the discharge pipe diameter, and equations (1.7) and (1.8) are from Fischer et. al. (1979).  $q(r)$  is the average plume velocity and is used to solve for  $U(r)=q(r)/A(r)$ , where  $A(r)$  is the plume cross-sectional area;  $U(r)=q(r)/A(r)$  is substituted into equation (1.4).

$$\frac{q(r)}{A(r)} \frac{d(h\bar{c})}{dr} = -w_s \bar{c} \quad (1.9)$$

$$\frac{d(h\bar{c})}{dr} = -w_s \bar{c} \frac{A(r)}{q(r)} \quad (1.10)$$

$$\bar{c} \frac{dh}{dr} + h \frac{d\bar{c}}{dr} = -w_s \bar{c} \frac{A(r)}{q(r)} \quad (1.11)$$

$$\frac{d\bar{c}}{dr} = -\frac{\bar{c}}{h(r)} \left( \frac{w_s A(r)}{q(r)} + \frac{dh(r)}{dr} \right) \quad (1.12)$$

$$\frac{d\bar{c}}{\bar{c}} = - \left( \frac{2w_s r \sin\left(\frac{\theta}{2}\right)}{q_0 \left(\frac{r}{l_Q}\right)^\beta} + \frac{m}{h_0 + mr} \right) dr \quad (1.13)$$

Where  $\beta = \alpha / \sin(\theta/2)$  and  $A(r) = 2b_w(h_0 + mr)$  and rearranging equation (1.13).

$$\frac{d\bar{c}}{\bar{c}} = - \left( \frac{2l_Q^\beta w_s \sin(\theta/2)}{q_0} r^{1-\beta} + \frac{m}{h_0 + mr} \right) dr \quad (1.14)$$

In equation (1.14), the first term on the right describes solids loss through settling and the second term describes dilution of the solids by entrainment and the expanding plume area.

The solution to equation (1.4) is,

$$\bar{c} = \frac{\bar{c}_0 h_0}{h_0 + mr} \exp \left( \frac{-2l_Q^\beta \sin(\theta/2) w_s r^{2-\beta}}{q_0 (2-\beta)} \right) \quad (1.15)$$

Where  $\bar{c}$  is suspended solids concentration in the plume and  $\bar{c}_0$  is the initial CSO suspended solids concentration. From equation (1.15) one obtains the percent solids deposited into the sediment bed.

$$s' = 1 - \frac{h_0}{h_0 + mr} \exp \left( \frac{-2l_Q^\beta \sin(\theta/2) w_s r^{2-\beta}}{q_0 (2-\beta)} \right) \quad (1.16)$$

Where  $s'$  is the percent of total solids mass that deposited into sediment bed and values for parameters are given in Table 1.

**Table 1.** Values for parameters in equation (1.16). Values were obtained from Fischer et. al. (1979).

Plume Parameters	Value
$b_w/r$	0.107
$\alpha$	5.35%
$\theta$	$2\tan^{-1}(b_w/r)$
$m$	Bed slope $< m < (b_w/r)/2$

## 2.2 Submerged Buoyant Discharge

The response of a submerged buoyant plume can be described in three phases: the first two describe it as it emerges from the outfall pipe and then rises and the third when the rise terminates. In the first two phases, the model assumes all suspended solids stay within the plume while it transitions from a horizontal to vertical profile where it rises to the termination height. When the plume reaches a termination height solid particles are allowed to settle from the plume. At the termination height solid particles fall through the water column  $H$  to reach the sediment bed. During this time the solids are transported horizontally by the ambient velocity  $U_{amb}$  to distance  $X_H$  (Figure 2) where the suspended solids are assumed to be uniformly distributed over the water column. The distance  $X_H$  will be

unchanging only for a constant ambient velocity, but in a tidally influenced waterbody  $X_H$  will change accordingly with the tidal velocity.

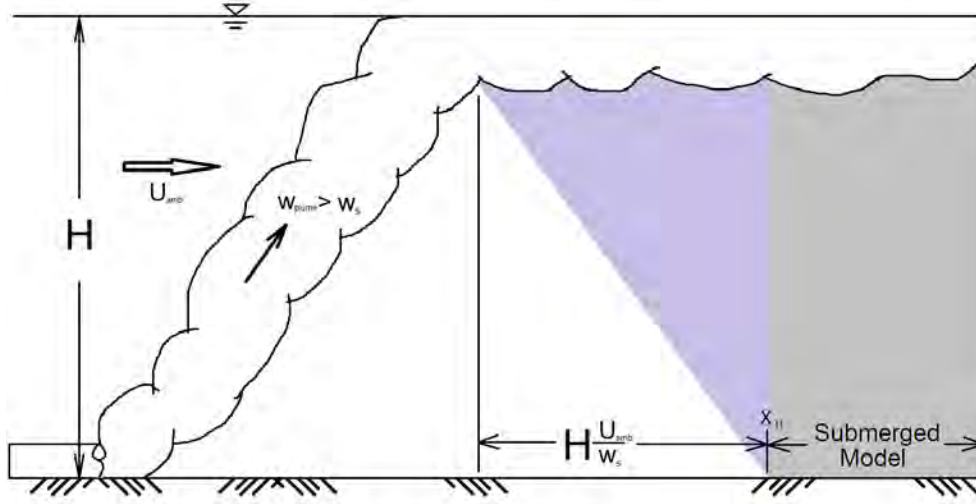


**Figure 2.** Schematic showing the flow path of a buoyant plume. After the plume rise has terminated, solid particles fall through the water column  $H$  and are transport a distance  $X_H = HU_{amb}/w_s$  when they reach the sediment bed.

In a tidally influenced salt water body, the terminated plume will be carried with a tidally varying velocity field, and in the simplest case the plume will be advected back-and-forth, along a straight line, passing over the outfall with each ebb and flood. The ebb-and-flood action smears the sediment deposition over a larger horizontal length than would happen with a constant velocity of similar value, and for many discharge events over sufficient time half the sediment will be deposited on the ebb side and the other half on the flood side of the outfall. The maximum deposition will occur at some distance away from the outfall because for each ebb or flood event the average  $X_H$  is greater than zero. The governing equation for this condition has form,

$$\frac{\partial \bar{c}}{\partial t} + U(t) \frac{\partial \bar{c}}{\partial x} = \frac{w_s \bar{c}}{H} \quad (1.17).$$

Where  $U(t)$  is the tidal velocity. Equation (1.17) can be simplified by substituting,

$$\bar{c}(x,t) = e^{-\beta t} w(x,t) \quad (1.18)$$

and solving for  $w(x,t)$ , where  $\beta = w_s/H$ . The simplified equation has form,

$$\frac{\partial w}{\partial t} + U(t) \frac{\partial w}{\partial x} = 0 \quad (1.19).$$

Equation (1.19) is the advection equation and has the general solution,

$$w(x, t) = F \left( x - \int_t U(t) dt \right) \quad (1.20).$$

Where  $F \left( x - \int_t U(t) dt \right)$  describes the translation of an arbitrarily shaped pulse having speed  $U(t)$  and constant shape, the integral defines the travel distance over the temporal duration  $t$ . Substituting equation (1.20) into equation (1.18) gives the general solution to equation (1.17).

$$\bar{c}(x, t) = \bar{c}_0 e^{-\beta t} F \left( x - \int_t U(t) dt \right) \quad (1.21)$$

Where  $c_0$  is an instantaneous load at time zero. For this study  $F \left( x - \int_t U(t) dt \right)$  shall be the Dirichlet Delta function, which has form,

$$F(x - U(t)t) = \begin{cases} 1, & x = \int_t U(t) dt \\ 0, & x \neq \int_t U(t) dt \end{cases} \quad (1.22).$$

The travel distance  $x$  at time  $t$  is determined from the tidal velocity, which has form  $U(t) = u \sin(\omega t)$ , where  $u$  is the velocity amplitude and  $\omega$  is the tidal frequency. Equation (1.21) describes the fate of an instantaneous unit of mass as it is transported by the velocity field  $U(t)$ ; the equation can be modified for a continuous injection of mass at some rate  $\dot{c}$ . The continuous injection is equivalent to injecting a unit load of  $\dot{c} \delta t$  at each time interval  $\delta t$ , which is an infinitesimally small unit of time. The mass resulting from a continuous injection is the sum of all the unit loads prior to the time of observation.

$$\bar{c}(x, t) = \int_0^t \dot{c}(\tau) e^{-\beta(t-\tau)} F \left( x - u \int_{\tau}^{t+\tau} \sin(\omega(t)) dt \right) d\tau \quad (1.23)$$

Equation (1.23) describes the distribution of a continuous injection of mass within a tidally varying velocity field; however, the Dirichlet Delta function cannot be expressed in terms of elementary functions and is therefore not directly solvable and is usually solved numerically.

### 2.2.1 Model Boundary Limits

In tidally influenced systems, the tidal velocities can potentially transport discharged solids very large distances away from the outfall and transport them back-and-forth over the outfall. These conditions could require a very large modeling domain unless practical reasons can justify smaller modeling domains. In configuring the EFDC model, a practical model domain was derived from initial work assessing suspended solid deposition length scales for the Brandon CSO; analyses suggested typical CSO solids would deposit within 100 meters of the outfall (King County, 2011). Therefore, model boundaries were located 1500 meters from the outfall and should have minimal impact on deposition near the outfall.

The 1500 meter boundary location also assumed that suspended solids transported past the boundary were unlikely to travel back over the outfall, but would be dispersed and advected distant from the outfall. At the boundary EFDC does not track solids advected out of the boundary, and inflowing solid concentrations were zero. The simple model was configured without boundary constraints, suspended solids were allowed to deposit into the sediment bed during the ebb and flood tides. Effects of the ebb and flood condition are most pronounced for the silt and clay sediment classes; however, the returning mass that settles within 0 to 100 meters is negligible (Figure 3).

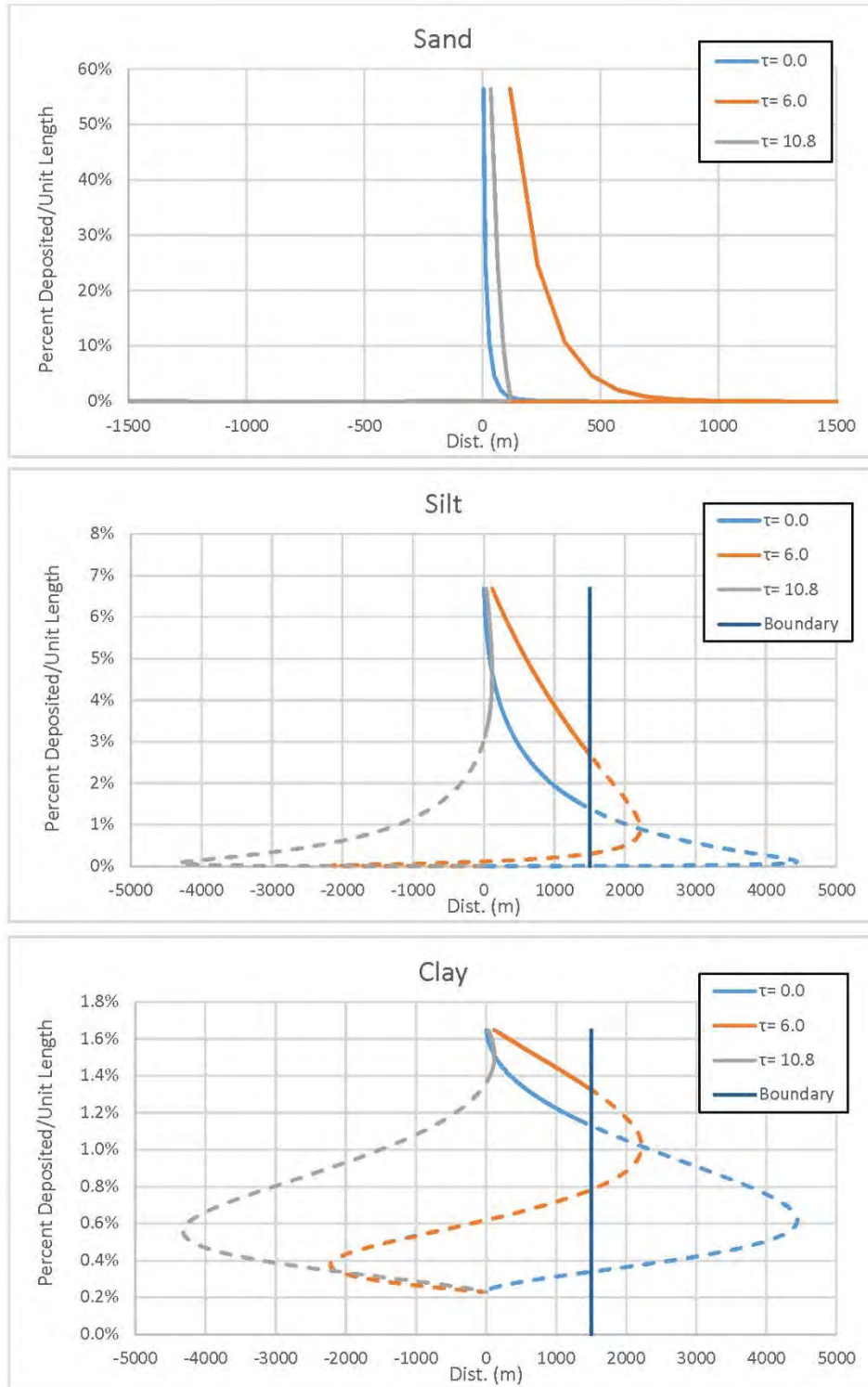


**Figure 3.** Sediment deposition per unit load near an outfall for Sand, Silt, and Clay for three different tidal conditions ( $\tau=0.0$  hr,  $\tau=6.0$  hr, and  $\tau=10.8$  hr). Typically the sands deposit well within the 1500 meter boundary, while the silt and clays will travel past the 1500 meter boundary (vertical line at 1500 meters). The solid lines denote solids mass deposition that would be retained in the bounded model, and the dashed lines denote solids mass that would be advected out of the model domain.

### 3 Transforming between One and Two Dimensions

A three dimensional water quality model produces a two-dimensional (2D) sediment space, but the simple model produces a one-dimension (1D) sediment space; comparing the simulated sediment depositions requires either transforming from 2D to 1D or from 1D to 2D. To compare the simple model against the complex 3D model, the 2D simulated results were transformed into one-dimensional form. The transformation was accomplished by summing the sediment mass within annular segments radiating from the outfall (Figure 4); the transformed 2D results were compared against the 1D simulations provided by the simple model.

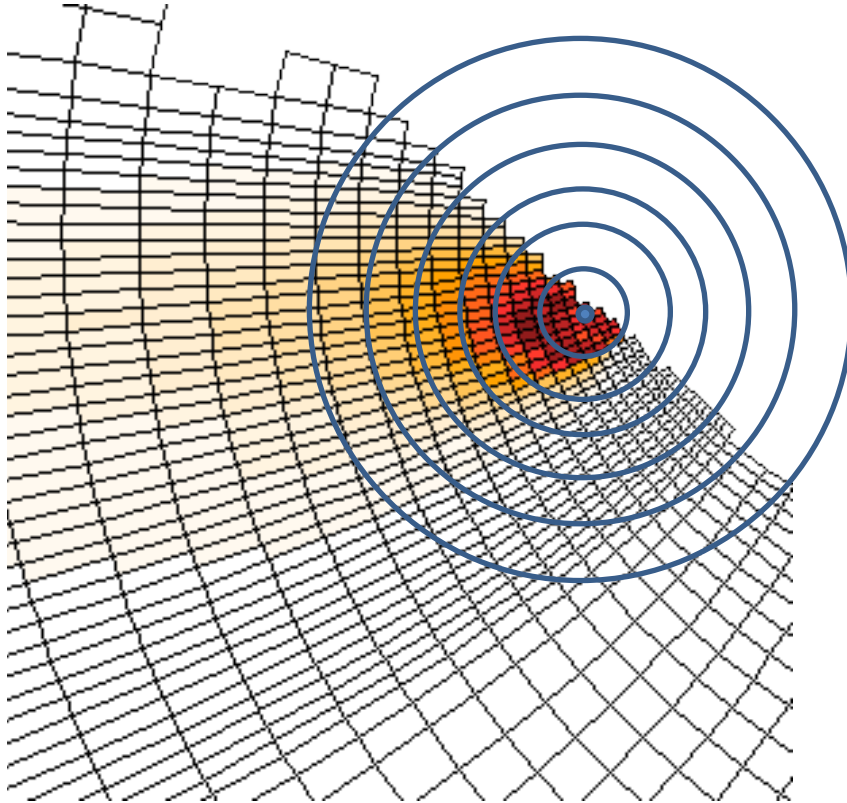


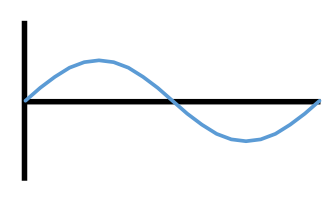
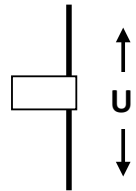
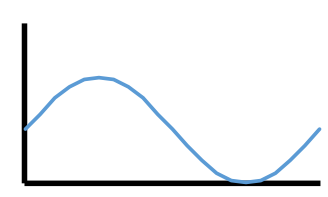
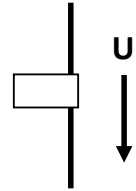
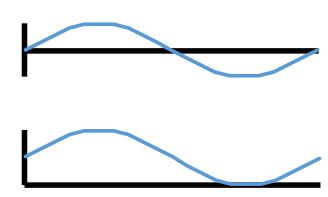
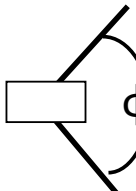
**Figure 4.** Illustration of annular segments radiating from the outfall, the sediment mass within each annular segment is summed and represents the mass deposited at radius R from the outfall.

The simple 1D model can be converted into 2D by transforming the radial distance into a two-dimensional coordinate system that is either radial or Cartesian. The CSO outfall sites presented in this report characterized two different geophysical features: a shoreline discharge into a waterbody with an orthogonal ambient flow, and an offshore submerged discharge into a waterbody with a tidal orthogonal ambient flow.

The shoreline located discharge is converted into two dimensions by transforming the one-dimensional radial distance into a sector with angle  $\phi$  and annular segments; the annular segments match the one-dimensional radial segments. The mass in each segment is divided by the annular segment area giving Mass/Area (Figure 6).

$$A_{as} = \frac{\varphi}{2} (r_{i+1}^2 - r_i^2) \quad (1.24)$$

Where  $A_{as}$  is the annular segment area and  $r_{i+1}$  and  $r_i$  are the one-dimensional radial distances for segments  $i+1$  and  $i$ . The angle  $\varphi$  is based on the ambient flow characteristics at the outfall site and physical boundaries that block flow (Figure 5). The minimum sweep angle is the plume angle  $\varphi \geq \theta$  (Table 1). The annular segments can be converted into Cartesian coordinates using spatial interpolation methods (Figure 6).

Velocity Cycle	Velocity Direction	$\varphi$
		180
		90
		$\theta \leq \varphi$ $\varphi \leq \phi$

**Figure 5.** Sweep angles  $\varphi$  for different velocity cycles and directions. The sweep angles are used for the neutrally buoyant model.

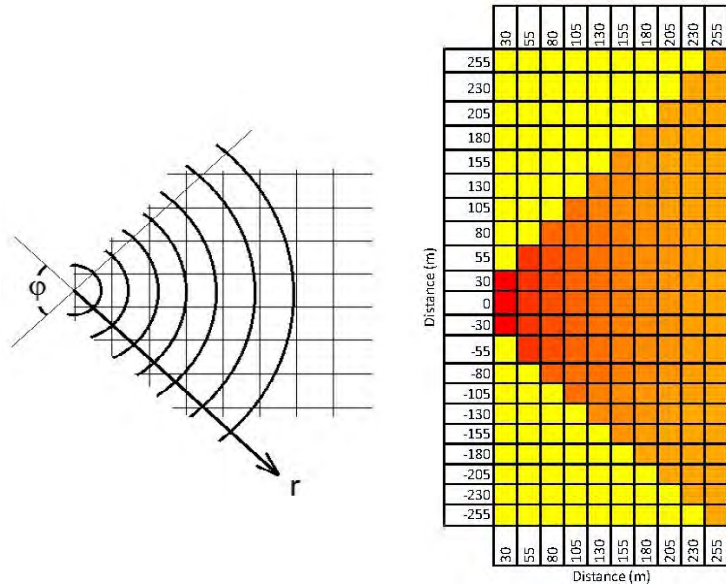


**Figure 6.** Converting the one-dimensional radial model  $r$  into two-dimensional annular segments with angle  $\phi$ . The annular segments can be transferred to Cartesian coordinates as well.

For an offshore submerged discharge in a tidally influenced flow environment, the simple model simulated sediment deposition along an ebb and flood transect (§ 2.2) of one dimension. Radial depositional areas were estimated with two methods: a rectangular area having width equal to the plume termination width  $D+2b_w$  where  $D$  is the pipe diameter and  $b_w$  is the plume half-width at elevation  $z$ ; a sector area comprising annular segments with angle  $\phi$ . The deposition length is twice the simulated length mirrored about  $r=0$  and the mass is divided by two to account for the ebb and flood tides (§ 2.2 and Figure 7).

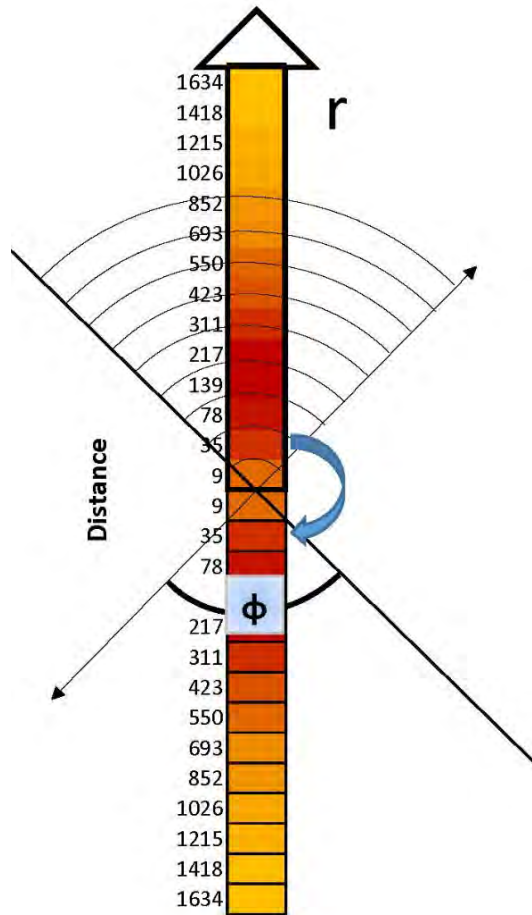


**Figure 7.** Converting the one-dimensional radial model  $r$  into a one-dimensional rectangle of length  $2r$  and width  $D+2b_w$ , or converting it into two-dimensional annular segments with angle  $\phi$ .

#### 4 Model Data Requirements

The EFDC and simple model require the same types of information to configure and run (Table 2), but the simple model data requires less spatial and temporal dimensions. Both models will have the same pipe diameter, characteristic discharge rates and durations, and characteristic solids (settling velocity and concentrations), but EFDC requires detailed spatial bathymetry, shoreline, and hydrodynamic boundary conditions. In this case, the simple model depth and ambient velocity will be obtained from the EFDC model, but bottom slope will be obtained from drawings or bathymetric depth data.

**Table 2.** Data requirements for the EFDC and simple model.

Model	EFDC	Simple
Data Requirements	Pipe Diameter	Pipe Diameter
	Discharge Flow	Discharge Flow
	Bathymetry	Bottom Slope
	Shoreline Geography	Sweep Angle based on Geography
	Discharge Depth	Discharge Depth
	Tidal and Density BC	Peak Velocity
	Solids Settling Velocity	Solids Settling Velocity
	Salinity	Salinity
	Solids Concentration	Solids Concentration

#### 4.1 CSO Outfall Sites

Ten CSO outfall locations were selected for comparing sediment deposition rates between EFDC and the simple model; the ten locations were simulated in the EFDC modeling effort. The EFDC model sites were selected because it was thought there were limited proximal non-CSO discharges were present that could confound the CSO chemical signature.

**Table 3.** Ten CSO outfall sites selected for comparing EFDC and simple model sediment deposition rates.

CSO Site	Waterbody Type
3 <sup>rd</sup> Avenue	Fresh
Montlake	Fresh
University	Fresh
53rd	Salt
Barton	Salt
Brandon	Salt
Chelan	Salt
Magnolia	Salt
Murray	Salt
NorthBeach	Salt

#### 4.2 Characteristic Discharge Flow Rate

Modeling CSO time series can become computationally time intensive when series longer than a couple weeks are simulated, but a couple weeks of discharges is insufficient to characterize the potential range in CSO discharge flow rates and durations. CSOs are sporadic events of short duration (hours) with long periods of zero flow between events (days to months) when sediment deposition is governed by ambient geo-physical and chemical conditions. Instead of simulating the entire CSO discharge time series, a characteristic discharge flow rate was simulated.

Characteristic discharge flow rates were determined from a measured or simulated (Crawford, 2014) CSO discharge time series. The discharge series contains positive and zero flow values with any positive values

sampled at equal intervals. Positive values characterize the discharge flow rate and are collated into a histogram and the binned flow rates are divided into three equal segments. Within each segment, the average flow rate and the probability of that segment occurring is calculated (Figure 8). The segment probability is used to calculate the temporal duration of the average segment flow.

$$\Delta t_i = p_i \Delta t_d, \quad i = 1, 2, 3 \quad (1.25)$$

Where  $\Delta t_i$  is the duration of the  $i^{\text{th}}$  segment,  $p_i$  is the probability of the  $i^{\text{th}}$  segment, and  $\Delta t_d$  is the cumulative temporal duration of all the flow events

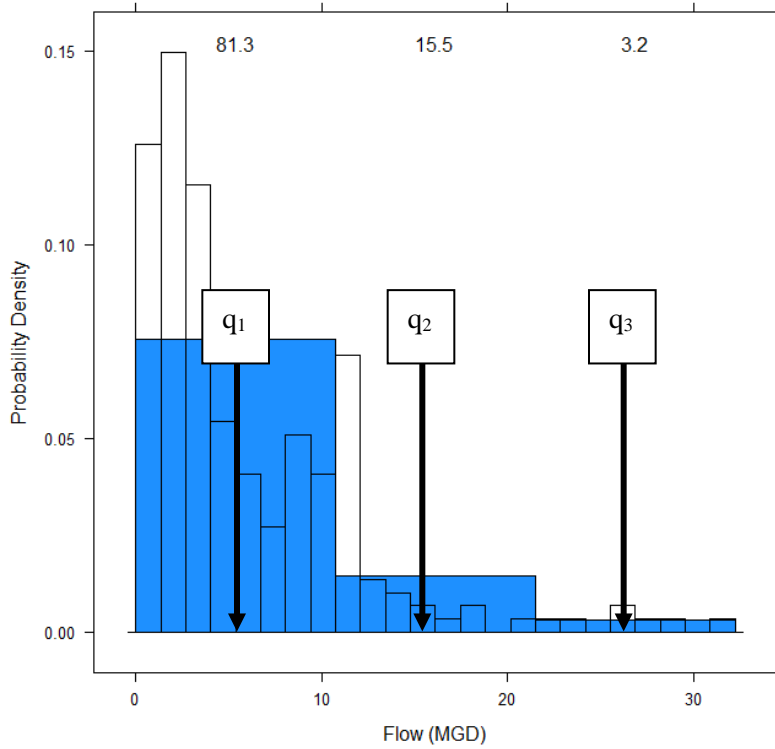


**Figure 8.** Illustration of a histogram of positive CSO flow values divided into three equal segments, the average flow  $q_i$  for each segment, and the percent probability of each segment occurring (shown at top of chart).

The applied characteristic flow rates describe a typical flow condition that occurred over some interval of time that will discharge a known solids mass.

$$m_{Ti} = c_s q_i \Delta t_i \quad (1.26)$$

$$m_{Ti} = c_s q_i p_i \Delta t_d \quad (1.27)$$

Where  $m_{Ti}$  is total solids mass discharged by the  $i^{\text{th}}$  characteristic flow rate. Equation (1.27) is the solids mass deposited during the CSO event; however, the characteristic mass deposition rate should account for those time intervals when the CSO is not discharging.

For this study  $\Delta t_d$  equaled ten days for all CSO sites to assure enough tidal cycles occurred during the simulations. Because the actual temporal duration of all the flow events is different from ten days, the model results must be corrected to the actual temporal duration and for the time when the CSO is not discharging, which required the duration of the monitoring period, and the duration of the positive flow events..

$$\frac{\Delta t_{hyd}}{\Delta t_{obs}} = \frac{\Delta t_d}{S_f} \quad (1.28)$$

$$S_f = \Delta t_{obs} \frac{\Delta t_d}{\Delta t_{hyd}} \quad (1.29)$$

Where  $\Delta t_{obs}$  is the duration of the monitoring period,  $\Delta t_{hyd}$  is the duration of all positive flow events, and  $S_f$  is the scaling factor and has units of time, it is the equivalent monitoring period duration required to scale  $\Delta t_d$  to  $\Delta t_{hyd}$ . The characteristic mass deposition rate is equation (1.27) divided equation (1.29).

$$d_{Ti} = c_0 q_i P_i \Delta t_d / S_f \quad (1.30)$$

Where  $d_{Ti}$  is characteristic mass deposition rate for flow  $q_i$ . Equation (1.30) is the deposition rate for the observed or simulated CSO discharge hydrographs, it can be adjusted to different discharge periods using time averaged discharge volumes. Adjusting equation (1.30) requires all computations are done using the same temporal duration (such as years, months, or days), it is adjusted by multiplying by the ratio of the time averaged discharge volumes.

$$d_{Tj} = d_{Ti} \frac{V_j}{V_i} \quad (1.31)$$

Where  $d_{Tj}$  is the mass deposition rate for discharge conditions having volume  $V_j$ , and  $V_i$  is the discharge volume for flow  $q_i$ . Characteristic flow rates and durations are given in Table 4, values were obtained from the EFDC modeling (Appendix A, Part 3).

**Table 4.** Characteristic CSO discharge flows and durations, flows are sorted from smallest to largest (lower 1/3 to upper 1/3). Durations sum to ten days.

CSO site	Lower 1/3 (MGD)/(days)	Middle 1/3 (MGD)/(days)	Upper 1/3 (MGD)/(days)
3 <sup>rd</sup> Avenue	23.3 / 8.5	69.8 / 1.2	116.3 / 0.3
Montlake	25.1 / 6.1	75.4 / 3.2	125.6 / 0.7
University	38.6 / 5.7	115.9 / 2.6	193.1 / 1.7
53rd	10.1/9.92	30.3/0.05	50.6/0.03
Barton	4.0 / 9.2	12.0 / 0.5	20.0 / 0.3
Brandon	16.3 / 7.6	48.8 / 2.2	81.3 / 0.2
Chelan	3.6 / 5.2	10.9 / 2.5	18.1 / 2.3
Magnolia	3.0 / 8.1	9.0 / 1.8	15.0 / 0.1

Murray	22.4 / 0.5	67.1 / 6.9	111.9 / 2.6
Northbeach	1.5 / 8.1	4.5 / 1.7	7.5 / 0.2

### 4.3 Pipe Diameter, Depth, and Ambient Velocity

Pipe diameters, discharge depth, and ambient velocities were obtained from the EFDC modeling (Appendix A, Part 3); ambient velocities are the depth averaged root mean square simulated by EFDC.

**Table 5.** Outfall discharge depths, pipe diameter, and ambient velocity and salinity.

CSO Site	Discharge Depth (m)	Pipe Diameter (m)	RMS* Ambient Velocity (m/s)	Ambient Salinity (o/oo)
3 <sup>rd</sup> Avenue	12.5	1.52	0.143	0
Montlake	5.7	1.52	0.066	0
University	1	2.13	0.056	0
53rd	5	1.83	0.171	28
Barton	6.5	1.52	0.114	28
Brandon	0.3	1.83	0.110	28
Chelan	8.1	0.76	0.350	28
Magnolia	6.75	0.91	0.303	28
Murray	6.6	1.83	0.327	28
NorthBeach	5	0.41	0.223	28
* Root-Mean-Square				

### 4.4 Solids Concentrations and Velocity

CSO solids concentrations were obtained from Appendix A, Part 3 and settling velocities were from King County (2011). Three suspended solids types were used in the EFDC model, the three solids characterize distributions measured in the County's sewer conveyance system during wet weather events (Table 6).

**Table 6.** Combined sewer overflow suspended solid characteristics used in the models, the average total suspended solids concentration was 120 (mg/l).

Particle Type	Settling Velocity $W_s$ (m/s)	Percent of Total Suspended Solids Mass	Suspended Solid Conc. (mg/l)
Sand	7.5E-03	33%	41.6
Silt	6.25E-04	34%	43.1
Clay	1.50E-04	34%	43.3

### 4.5 Simple Model Configuration

The simple models were developed in Excel Workbooks for a freshwater and saltwater discharge; input data for each waterbody type are given in Table 7. Once the last data value is entered, the sediment deposition is instantly calculated along the radius.

**Table 7.** Data requirements for simple models in addition to suspended solids characteristics in Table 6.

Waterbody Type	Discharge Depth (m)	Pipe Diameter (m)	Ambient Velocity (m/s)	Ambient Salinity (o/oo)	Flow (MGD)	Event Duration (days)	Plume Angle $\theta$	Bathymetry Slope $m$	Entrainment Coefficient
Fresh	NA	Yes	NA	NA	Yes	Yes	Yes	Yes	Yes
Salt	Yes	Yes	Yes	Yes	Yes	Yes	NA	NA	NA

## 5 Model Comparisons

The simple and EFDC sediment deposition modeling results were compared to see if the simple model could reasonably replicate EFDC sediment deposition. EFDC sediment deposition was transformed into one-dimension (see Section 3) and then compared to the simple model. The models are compared on the predicted effective sedimentation rate, which is the sum of the three solid settling velocities and three characteristic discharge flow rates

### 5.1 Freshwater Systems

The neutrally buoyant model was used for freshwater environments and it over-estimated sediment deposition immediate to the outfall but compared more favorably at locations distant from the outfall. The simple model allowed more solids to deposit immediate to the outfall compared to the EFDC model (Figure 9-Figure 11). The immediate deposition is driven by the plume depth term  $m$  in  $h_0/(h_0 + mr)$  from equation (1.16); where  $m$  was constrained by empirical constants or the sediment bed slope (Table 1). A more comparable sediment deposition could be obtained if  $m$  was calibrated to the EFDC profile (Figure 12), but one cannot provide a compelling physically based argument for the derived value. The simple model reasonably replicated the radial extent of the simulated EFDC sediment deposition.

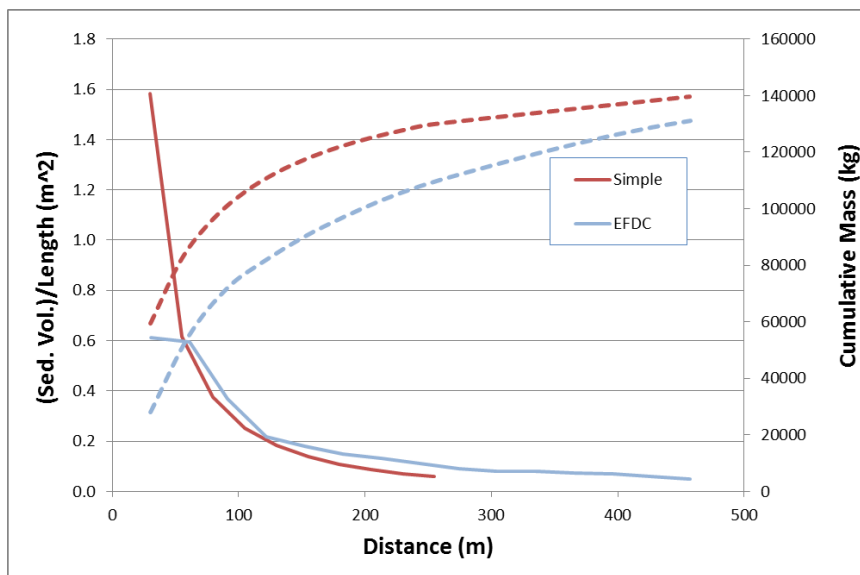


**Figure 9.** Sediment depth (Sed. Vol./Len.) from the simple and EFDC models at the 3<sup>rd</sup> Avenue CSO site (solid lines) and cumulative sediment mass (dashed lines).

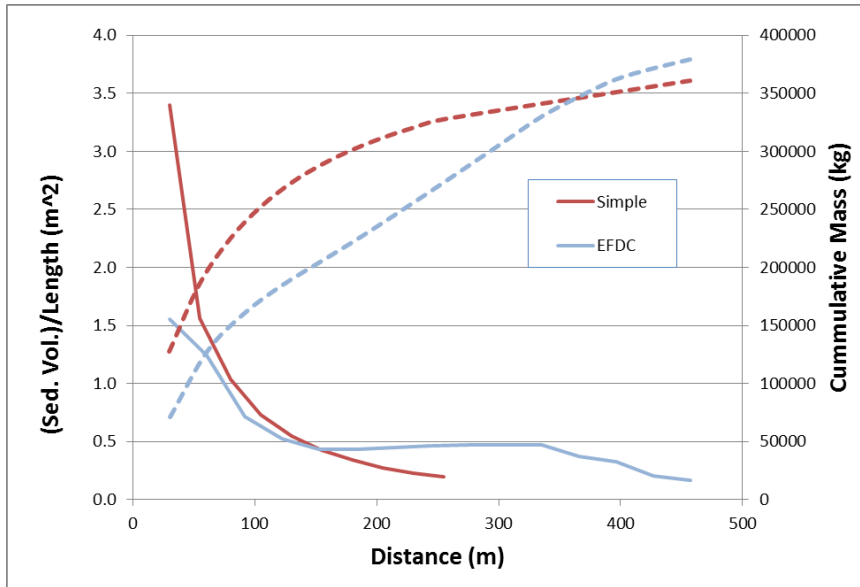


**Figure 10.** Sediment depth (Sed. Vol./Area) from the simple and EFDC models at the University Regulator CSO site (solid lines) and cumulative sediment mass (dashed lines)..

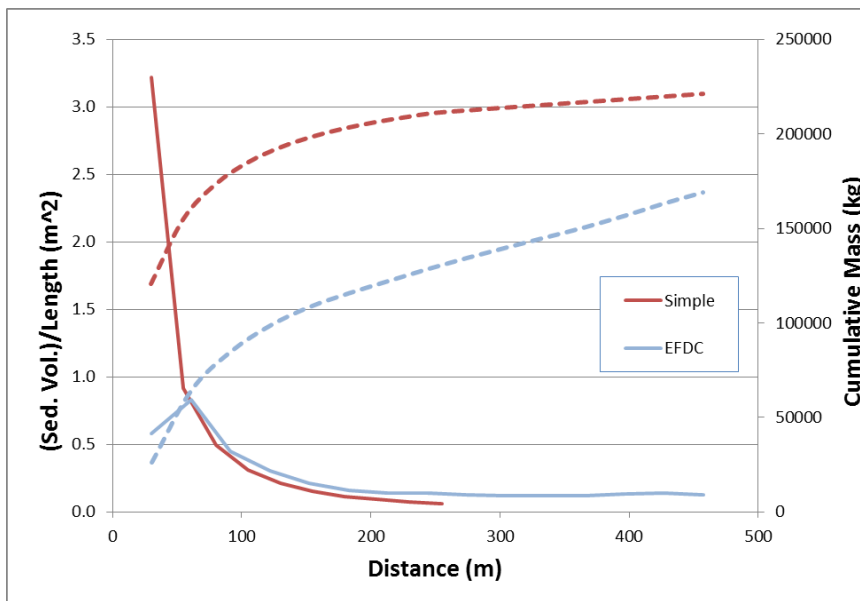


**Figure 11.** Sediment depth (Sed. Vol./Area) from the simple and EFDC models at the Montlake CSO site (solid lines) and cumulative sediment mass (dashed lines).

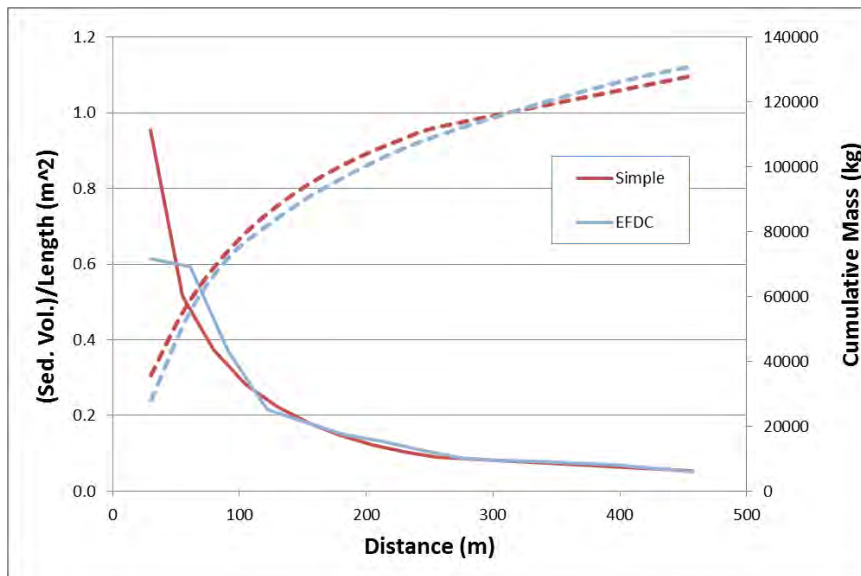


**Figure 12.** Sediment deposition for  $m = 0.015$  at the 3<sup>rd</sup> Avenue CSO site;  $m$  was 0.032 in Figure 9.

## 5.2 Saltwater Systems

The submerged buoyant plume model was used for saltwater environments. The saltwater CSO outfall sites discharged into tidally influenced waterbodies, which transport the suspended solids under a continuously oscillating velocity that smears the deposition pattern. In the simple model, the oscillating velocity was replicated as 48 discrete harmonic velocity series (Figure 13); the 48 discrete depositional patterns were summed to form a composite sediment deposition pattern (Figure 14). The maximum harmonic velocity was scaled as  $\sqrt{2}V_{RMS}$  where  $V_{RMS}$  is the root-mean-square velocity calculated from the simulated EFDC velocity (Table 5).

The Brandon CSO configuration was slightly different from the other saltwater outfalls. Brandon is located on the shoreline and essentially discharges at the water surface, it is not a submerged outfall but the discharged plume is still subject to tidally varying flows. For these reasons, the buoyant plume model assumed sediment deposition started at the outfall for all tidal conditions ( $X_H=0$ ).

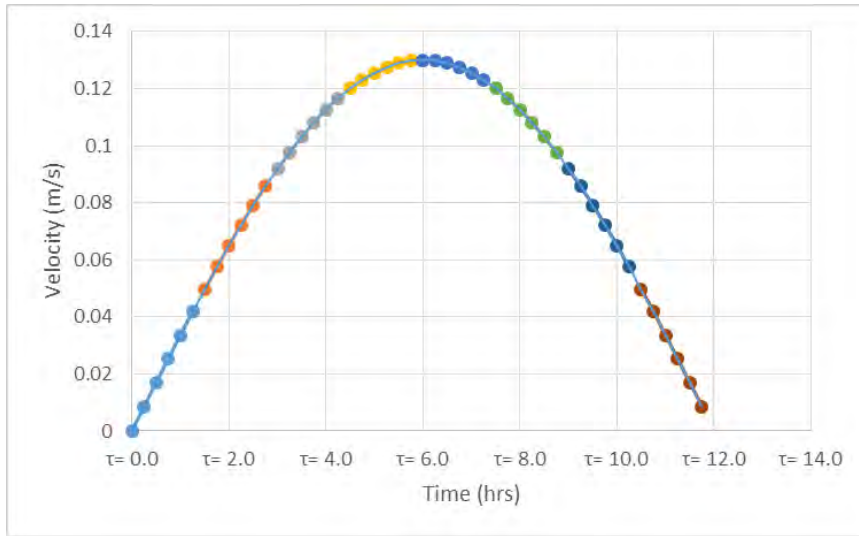


**Figure 13.** Conceptual display of the forty eight discrete harmonic velocities for each  $\tau$ . The maximum velocity is  $\sqrt{2}V_{RMS}$ , where  $V_{RMS}$  is given in Table 5. The eight colored velocity groups denote the sediment mass distribution series displayed in Figure 14.

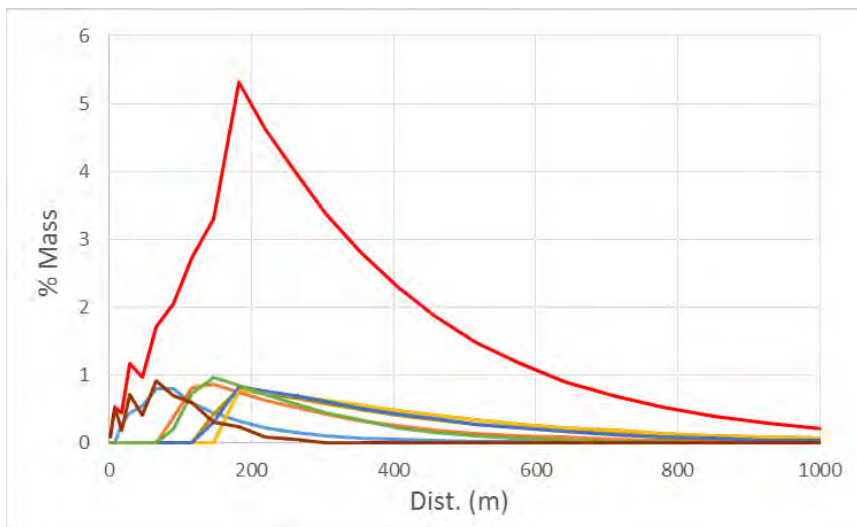


**Figure 14.** Conceptual sediment depositions for the eight discrete velocity groups noted in Figure 13 and their sum (red curve).

Compared to EFDC sediment depositions, the simple model peak deposition rate is displaced farther from the outfall and is typically less than that computed by EFDC (Figure 15-Figure 21), and the simple model transports more sediment mass farther away from the outfall than EFDC as indicated by the lower mass accumulation rate with distance. The simple model appears more capable at characterizing EFDC results for outfalls that discharge into open waters at sites like Murray, North Beach, 53<sup>rd</sup>, Barton, and to some extent Magnolia (Figure 15-Figure 19). At geographically bounded outfall sites, the simple model reasonably replicated EFDC results for the Brandon CSO (Figure 20), but was unable to replicate EFDC results for the Chelan CSO (Figure 21). For all model results, sediment deposition mass was governed by the sands because the silts and clays traveled two to three orders of magnitude farther than the sands.

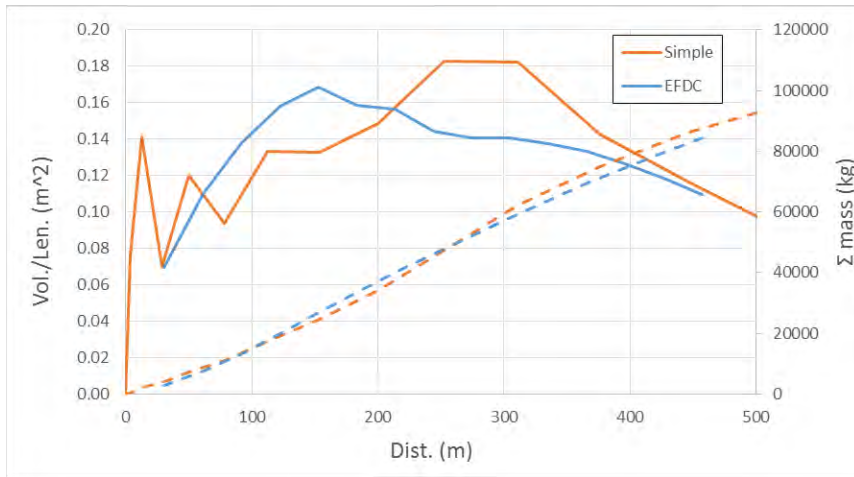


**Figure 15.** Simulated sediment deposition (Sed. Vol./Len.) at the Murray CSO site for the simple and EFDC models (solid lines) and cumulative sediment mass (dashed lines).

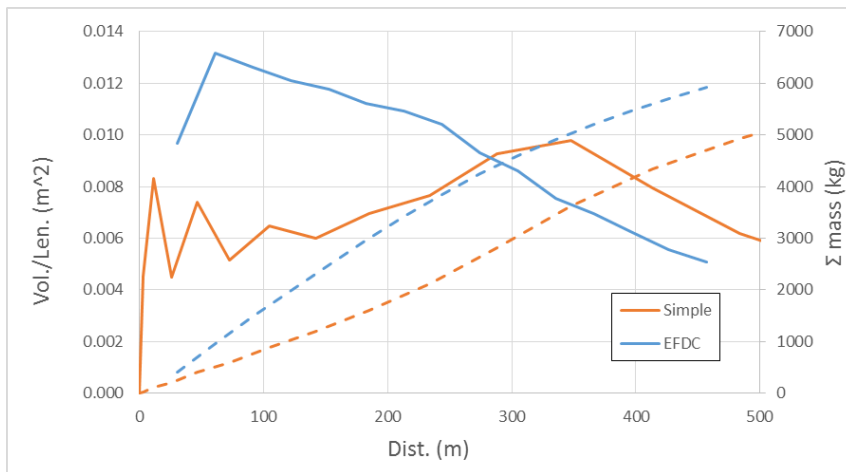


**Figure 16.** Simulated sediment deposition (Sed. Vol./Len.) at the Magnolia CSO site for the simple and EFDC models (solid lines) and cumulative sediment mass (dashed lines).

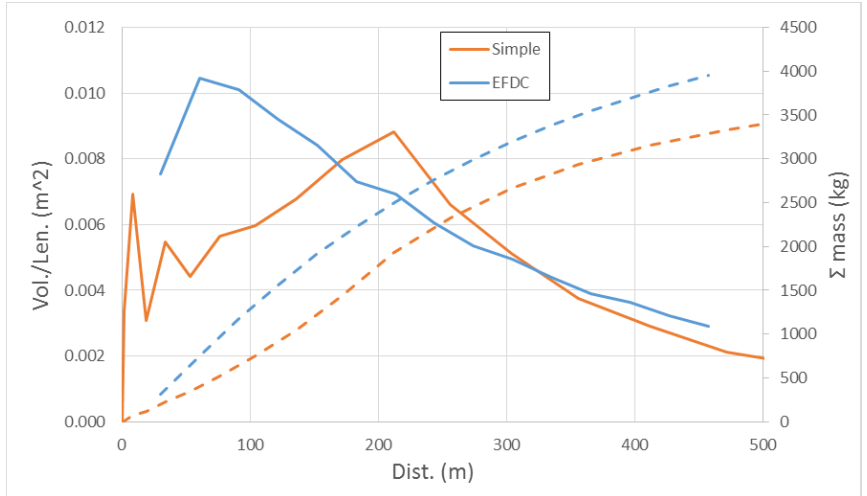


**Figure 17.** Simulated sediment deposition (Sed. Vol./Len.) at the North Beach CSO site for the simple and EFDC models (solid lines) and cumulative sediment mass (dashed lines).

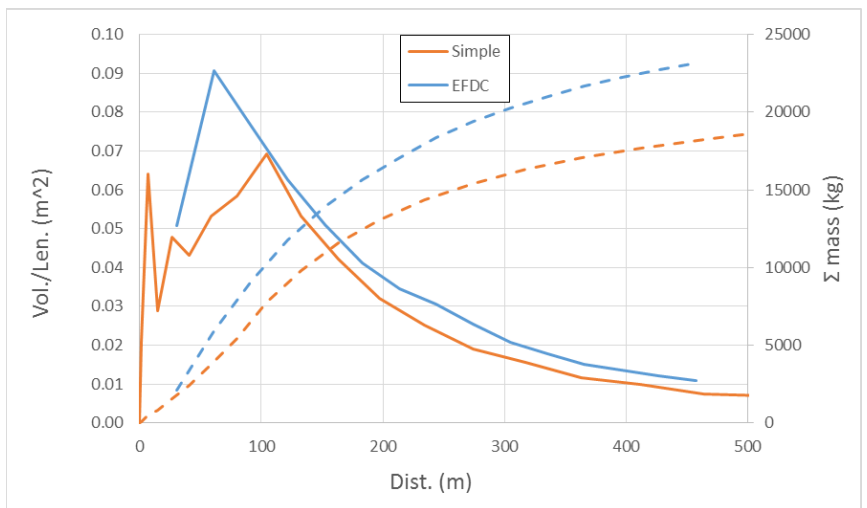


**Figure 18.** Simulated sediment deposition (Sed. Vol./Len.) at the 53<sup>rd</sup> CSO site for the simple and EFDC models (solid lines) and cumulative sediment mass (dashed lines).

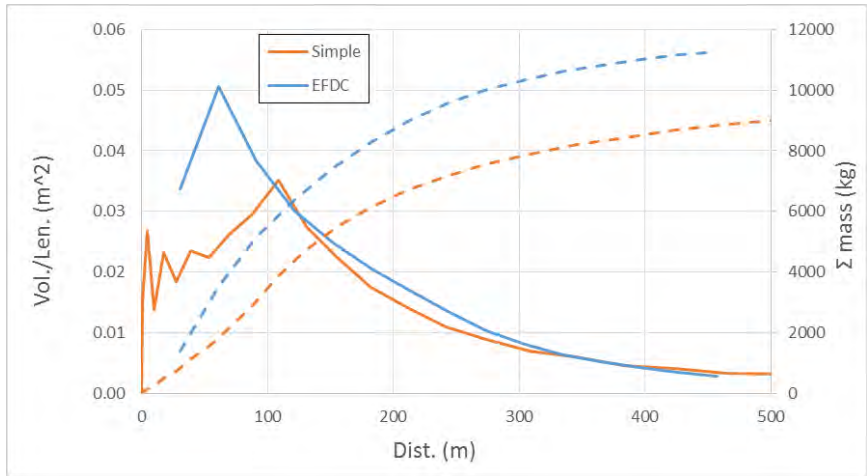


**Figure 19.** Simulated sediment deposition (Sed. Vol./Len.) at the Barton CSO site for the simple and EFDC models (solid lines) and cumulative sediment mass (dashed lines).

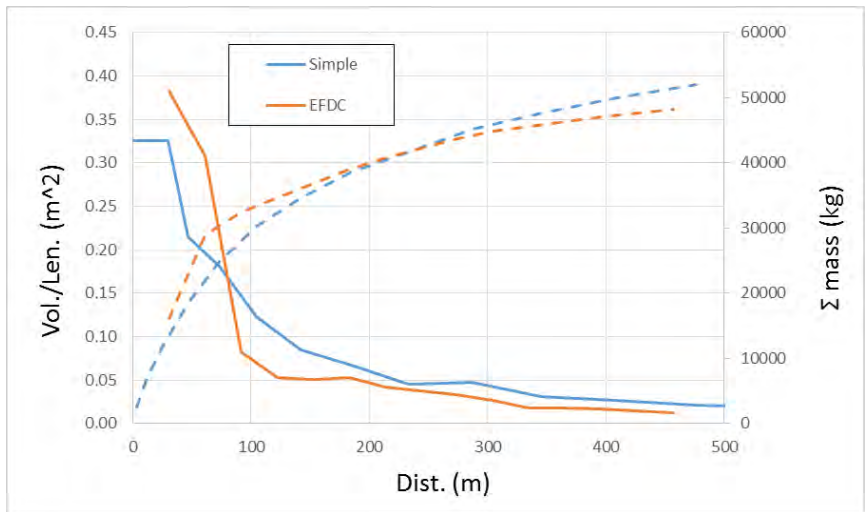


**Figure 20.** Simulated sediment deposition (Sed. Vol./Len.) at the Brandon CSO site for the simple and EFDC models (solid lines) and cumulative sediment mass (dashed lines).

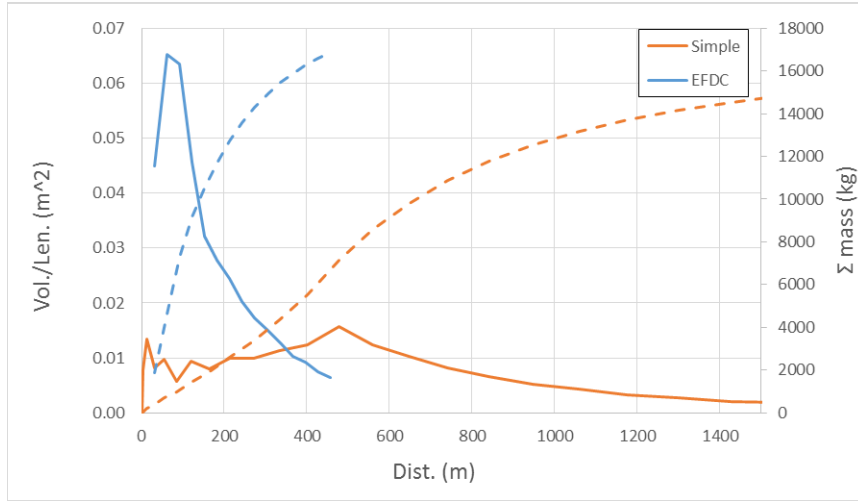


**Figure 21.** Simulated sediment deposition (Sed. Vol./Len.) at the Chelan CSO site for the simple and EFDC models (solid lines) and cumulative sediment mass (dashed lines).

The under-estimation at Chelan likely resulted from the complex geometry of the Chelan site, where the West Waterway narrows at the south end of Harbor Island from about 900 ft to 400 ft wide, and the depth decreases from about 65 ft to 25 ft. The applied velocity and depth represent conditions at the outfall site, which characterize the narrow channel. These conditions will transport the discharged solids beyond the 470 meter observation length. A more representative velocity can be estimated by considering the length scales in the wider-deeper and narrow-shallow channels defined by equation (1.32).

$$L_i = H_i \frac{U_i}{w_s} \quad (1.32)$$

Where subscript  $i$  describes the narrow-shallow channel ( $i=1$ ) or the wider-deeper channel ( $i=2$ ). Deposition in the wider-deeper channel relative to the narrow-shallow channel is,

$$L_2 = H_2 \frac{U_2}{w_s} = H_1 \frac{U_1}{w_s} \left( \frac{W_1}{W_2} \right) \quad (1.33)$$

where  $U_1 A_1 = U_2 A_2$  and  $A = WH$

$$L_2 = H_1 \frac{U_1}{w_s} \left( \frac{400}{900} \right) = H_1 \frac{0.44 U_1}{w_s} \quad (1.34)$$

The reduced velocity in the simple model better replicated the EFDC sediment distributions; more sediment mass deposited closer to the outfall (Figure 22).

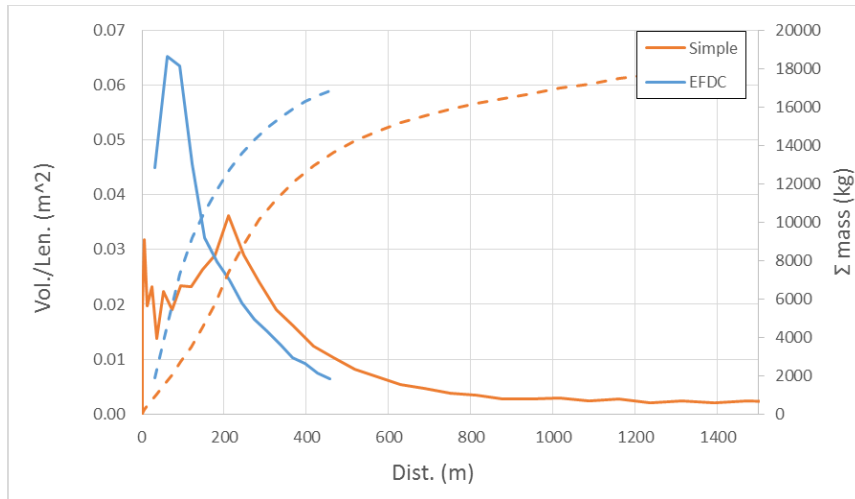


**Figure 22.** Simulated sediment deposition at the Chelan CSO site, but using a reduced tidal velocity of  $0.44U_1$  in the simple model. The smaller velocity field allowed more solids deposited within 500 meters of the outfall and provided a better match to the EFDC deposition.

## 6 Summary

The Neutrally Buoyant model reasonably replicated EFDC sediment deposition patterns for CSOs discharging into freshwater environments, but the Submerged Buoyant model dispersed sediment deposition farther from the outfall compared to EFDC.

The Neutrally Buoyant model tended to over-estimate both the maximum sediment deposition rate by 85% to 371% (Figure 24) and total sediment mass deposition by 19% to 62% (Figure 25). The simple model provides a conservative estimate of the maximum potential sediment deposition near a CSO outfall.

Excluding the Chelan CSO site, the Submerged Buoyant model tended to under-estimate the maximum sediment deposition rate by -1% to -99% (except Murry, which was 47%) and it over-estimated total sediment mass deposition for Brandon and Murray (7% and 4%), and it under-estimated the others by -17% to -22% (Figure 24 and Figure 25). Sediment deposition rates for both models were calculated using the sector area comprising annular segments for an angle of 45 degrees (Figure 7). These comparisons fitted EFDC results within a 45 degree sector, which is typically a smaller depositional area than that simulated by EFDC. This difference is apparent for the simulated EFDC Murray outfall results where EFDC distributed solids outside of the 45 degree sector (Figure 23); thus, the simulated EFDC depositional rates would be smaller than those presented in this report and relative difference between EFDC and simple model results would be smaller than that presented in Figure 24.

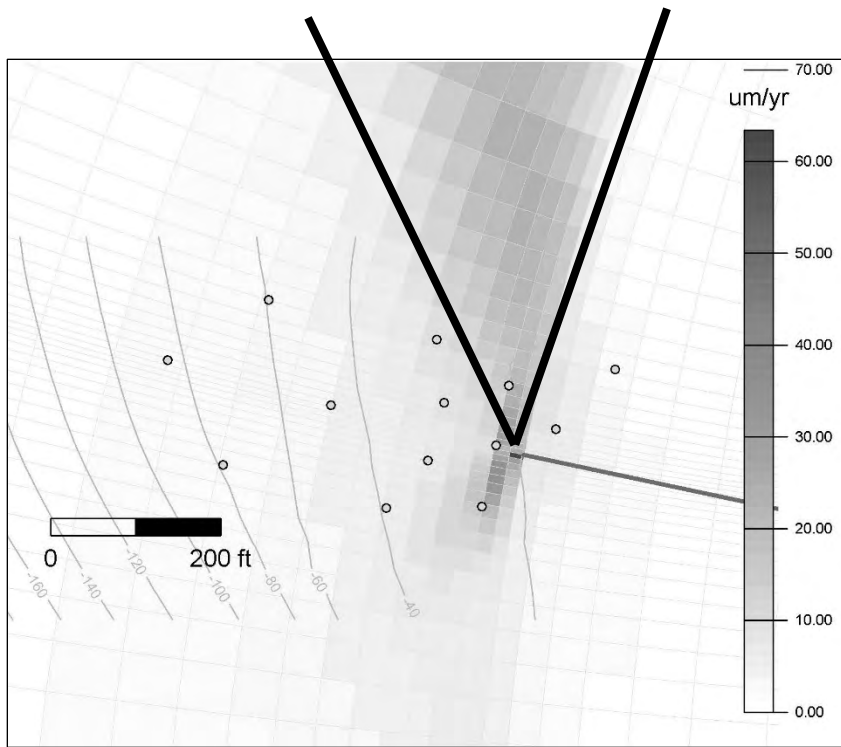


**Figure 23.** Simulated sediment deposition rates by EFDC for the Murray outfall and a superimposed 45 degree sector atop EFDC results.

This approach tended to under-estimated the sediment deposition rate compared to EFDC; however, all results were within a factor of two, which is reasonable range considering screening level applications are looking for orders of magnitude differences. Thus, the simple submerged buoyant plume model provides a reasonable screening level estimate of the potential maximum deposition rate. The simple model is sensitive to geographical boundaries that can create significant changes in field velocities.

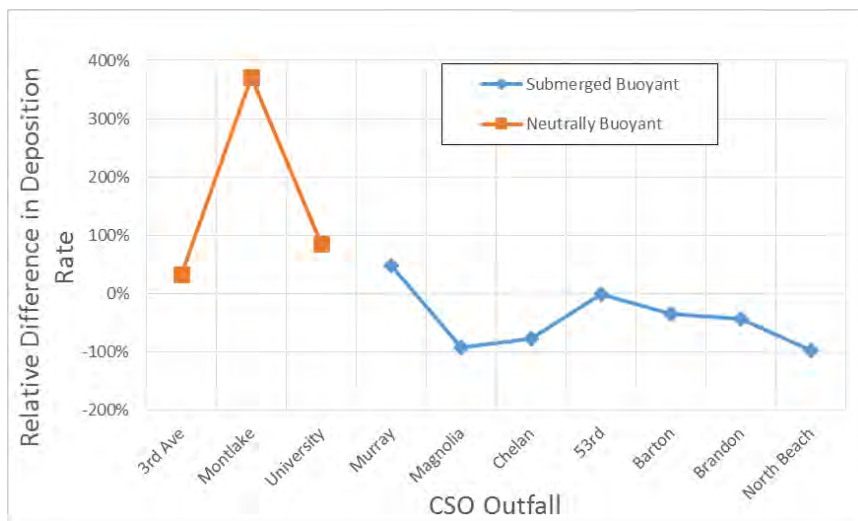


**Figure 24.** Relative difference in the maximum sediment deposition rate between the simple and EFDC models.

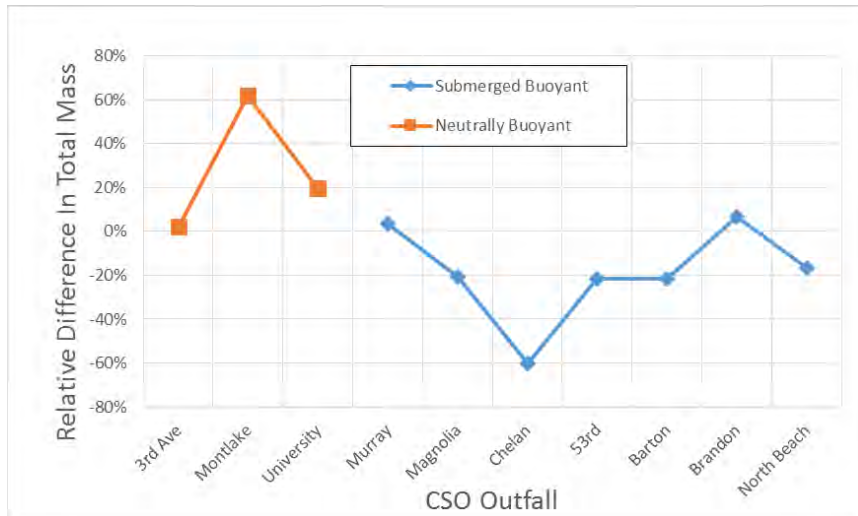


**Figure 25.** Relative difference in the total sediment mass within 255 m for the freshwater and 450 m for the submerged between the simple and EFDC models

This report compared sediment deposition patterns between two models, but because all models are estimates and therefore incorrect in some manner, this report cannot determine which model provides the better prediction. Both models were used against each other to help improve the conceptual understanding on what processes and configurations affect the settling of suspended solids from a plume. EFDC results suggested the Submerged Buoyant model required a more explicit tidal velocity influence, and the Submerged Buoyant results suggested EFDC submerged outfalls must be elevated above the sediment bed layer. With these observations and modifications, both models converged to a qualitatively similar sediment deposition pattern indicating the maximum sediment deposition is located near, but some distance from, the outfall. Neither model has been verified against observed sediment deposition rates, but the EFDC model was compared against observed sediment chemical concentrations (King County, 2018). For freshwater discharges with high deposition rates, modeled sediment deposition rates had a similar and consistent pattern to the sediment chemical pattern at the University CSO. At marine CSOs where very low deposition rates are predicted, the sediment chemistry data had no discernible pattern, thus no conclusion could be made about pattern similarity and consistency between predicted sediment deposition and sediment chemistry. An indiscernible pattern was expected because a simple uncertainty analysis indicated that it would be difficult to observe a pattern at very low deposition rates (King County, 2018). The study concluded that EFDC is predictive of general deposition patterns, and it is useful as a screening level model. Due to several assumptions in the comparison that conservatively estimate deposition rates nearer the outfall, one can also consider the simple model is useful a screening level model for CSO outfalls, particularly in fresh and open waters.

## **7 References:**

Crawford, Bruce, 2014. Memorandum: 2014 No Impact Release Rates. King County.

Fischer, Hugo B., E. John List, Robert C. Y. Koh, Jorg Imberger, and Norman H. Brooks, 1979. Mixing in Inland and Coastal Waters. Academic Press Inc..

King County, 2011. Discharge modeling for the contaminated sediment cleanup decisions: A summary and supplemental analyses. Department of Natural Resources and Parks, Wastewater Treatment Division.

King County, 2018. Appendix A Part III: EFDC Sediment Deposition Modeling Report for Sediment Management Plan Update.

# Appendix A, Part 3: EFDC Sediment Deposition Modeling Report for SMP Update

This page intentionally left blank.

---

**Appendix A Part III  
EFDC Sediment Deposition  
Modeling Report  
for Sediment Management Plan  
Update**

---

July 2018



## **King County**

Department of  
Natural Resources and Parks  
**Wastewater Treatment Division**

***For comments or questions, contact:***

Jeff Stern  
King County Wastewater Treatment Division  
201 South Jackson Street  
KSC-NR-0512  
Seattle, WA 98104-3856  
206-263-6447  
[jeff.stern@kingcounty.gov](mailto:jeff.stern@kingcounty.gov)

This information is available in  
alternative formats on request at  
206-684-1280 (voice) or 711 (TTY).

# Contents

---

<b>Contents .....</b>	<b>i</b>
<b>1 Introduction .....</b>	<b>1</b>
1.1 Problem Definition and Background .....	1
1.2 Description of Study Area .....	1
1.2.1 Lake Washington .....	1
1.2.2 Lake Union and the Ship Canal .....	2
1.2.3 Duwamish .....	2
1.2.4 Puget Sound .....	2
<b>2 Modeling Goals and Objectives.....</b>	<b>4</b>
2.1 Modeling Objectives.....	4
<b>3 Modeling Approach and Selection .....</b>	<b>5</b>
3.1 Modeling Approach .....	5
3.2 Model Description .....	5
<b>4 EFDC Model Setup .....</b>	<b>6</b>
4.1 Model Domain .....	6
4.2 Model Configuration.....	7
4.2.1 Solids Concentrations and Settling Velocity .....	7
4.3 Boundary Conditions .....	8
4.3.1 CSO Discharge Rates and Volumes .....	8
4.3.2 Ambient Currents.....	10
4.3.3 Ambient Density Stratification .....	11
4.4 Calibration Strategy .....	12
<b>5 Model Results .....</b>	<b>13</b>
5.1 Methods Overview.....	13
5.2 Results.....	13
5.2.1 North Beach Pump Station .....	13
5.2.2 South Magnolia CSO.....	15
5.2.3 53rd Avenue Pump Station.....	16
5.2.4 Murray Avenue Pump Station .....	17
5.2.5 Barton Street Pump Station.....	18
5.2.6 Brandon Street CSO .....	19
5.2.7 Chelan Avenue CSO.....	20
5.2.8 3rd Avenue West CSO.....	22
5.2.9 University Regulator.....	23
5.2.10 Montlake CSO .....	24
<b>6 Sensitivity and Uncertainty.....</b>	<b>26</b>
<b>7 Model Evaluation .....</b>	<b>30</b>
7.1 Evaluation Procedure .....	30
7.2 Verification Evaluation.....	32
7.2.1 North Beach Pump Station .....	34
7.2.2 South Magnolia CSO.....	38
7.2.3 53rd Avenue Pump Station.....	43
7.2.4 Murray Avenue Pump Station .....	47
7.2.5 Barton Street Pump Station.....	54
7.2.6 Brandon Street CSO .....	58
7.2.7 Chelan Avenue CSO.....	65

7.2.8	3rd Avenue West CSO .....	69
7.2.9	University Regulator.....	73
7.2.10	Montlake CSO .....	80
7.3	Verification Summary.....	84
<b>8</b>	<b>Model Output Quality (Usability) Assessment .....</b>	<b>87</b>
<b>9</b>	<b>References.....</b>	<b>88</b>
<b>Appendix A.</b>	<b>Data Tables .....</b>	<b>89</b>

## Tables

Table 1.	CSO discharge locations.....	7
Table 2.	Suspended solids characteristics used in the models.....	8
Table 3.	Characteristic CSO discharge flows and durations. Flows are sorted from smallest to largest (lower 1/3 to upper 1/3); durations sum to 10 days.....	9
Table 4.	Current speeds predicted by EFDC simulations.....	10
Table 5.	Duration simulated in EFDC.....	13

## Figures

Figure 1.	Images of a square grid of size $[-\pi/2, \pi/2] \times [-\pi/2, \pi/2]$ under the (conformal) map $z \mapsto \sin(z)$ . The two "focal points" are the points $\pm 1$ .....	6
Figure 2.	Illustration of a histogram of positive CSO flow values divided into three equal segments, the average flow $q_i$ for each segment, and the percent probability of each segment occurring (shown at top of chart).....	9
Figure 3.	Boundary salinity profile used for Brandon, Chelan models.....	12
Figure 4.	North Beach predicted depositional rates.....	14
Figure 5.	Magnolia predicted depositional rates.....	15
Figure 6.	53rd Ave. CSO predicted depositional rates.....	16
Figure 7.	Murray Ave. CSO predicted depositional rates.....	18
Figure 8.	Barton St. CSO predicted depositional rates.....	19
Figure 9.	Brandon St. CSO predicted depositional rates.....	20
Figure 10.	Chelan Ave. CSO predicted depositional rates.....	22
Figure 11.	3rd Ave. West CSO predicted depositional rates.....	23
Figure 12.	University Regulator CSO predicted depositional rates.....	24
Figure 13.	Montlake CSO predicted depositional rates.....	25
Figure 14.	53rd Ave. CSO predicted depositional rates with CSO input to bottom layer.....	28
Figure 15.	Percent difference in predicted depositional rate with no CSO input to bottom layer compared to base simulation.....	29
Figure 16.	Range of concentrations observed in CSO solids and ambient sediments.....	32
Figure 17.	North Beach sediment concentrations for selected compounds.....	36
Figure 18.	Parameter-parameter plot of sediment concentrations at North Beach CSO.....	37
Figure 19.	Sediment concentrations versus predicted sediment depositional rates at North Beach CSO.....	38
Figure 20.	Magnolia sediment concentrations for selected compounds.....	40
Figure 21.	Parameter-parameter plot of sediment concentrations at Magnolia CSO.....	41
Figure 22.	Sediment concentrations versus predicted sediment depositional rates at Magnolia CSO.....	42
Figure 23.	South Magnolia Outfall in relation to Elliott Bay Marina.....	43
Figure 24.	53rd Ave. sediment concentrations for selected compounds.....	45
Figure 25.	Parameter-parameter plot of sediment concentrations at 53rd Ave. CSO.....	46
Figure 26.	Sediment concentrations versus predicted sediment depositional rates at 53rd Ave. CSO.....	47

Figure 27. Murray Ave. CSO sediment concentrations for selected compounds. ....	49
Figure 28. Parameter–parameter plot of sediment concentrations at Murray CSO. ....	50
Figure 29. Sediment concentrations versus predicted sediment depositional rates at Murray Ave. CSO. ....	51
Figure 30. Murray Ave. CSO sediment concentrations without PAH values at CSO-MY-9. ....	52
Figure 31. Parameter–parameter plot at Murray CSO without PAH values at CSO-MY-9. ....	53
Figure 32. Sediment concentrations versus predicted sediment depositional rates at Murray Ave. CSO without PAH values at CSO-MY-9. ....	54
Figure 33. Barton St. CSO sediment concentrations for selected compounds.....	56
Figure 34. Parameter–parameter plot of sediment concentrations at Barton St. CSO. ....	57
Figure 35. Sediment concentrations versus predicted sediment depositional rates at Barton St. CSO.....	58
Figure 36. Brandon St. CSO sediment concentrations for selected compounds.....	60
Figure 37. Parameter–parameter plot of sediment concentrations at Brandon St. CSO. ....	61
Figure 38. Sediment concentrations versus predicted sediment depositional rates at Brandon St. CSO....	62
Figure 39. Brandon St. CSO sediment concentrations without PAH values at CSO-BR-3.....	63
Figure 40. Parameter–parameter plot at Brandon St. CSO without PAH values at CSO-BR-3. ....	64
Figure 41. Sediment concentrations versus predicted sediment depositional rates at Brandon St. CSO without PAH values at CSO-BR-3.....	65
Figure 42. Chelan Ave. CSO sediment concentrations for selected compounds. ....	67
Figure 43. Parameter–parameter plot of sediment concentrations at Chelan Ave. CSO. ....	68
Figure 44. Sediment concentrations versus predicted sediment depositional rates at Chelan Ave. CSO... ..	69
Figure 45. 3rd Ave. W CSO sediment concentrations for selected compounds. ....	71
Figure 46. Parameter–Parameter plot of sediment concentrations at 3rd Ave. W CSO. ....	72
Figure 47. Sediment concentrations versus predicted sediment depositional rates at 3rd Ave. West CSO. .....	73
Figure 48. University Regulator CSO sediment concentrations for selected compounds. ....	75
Figure 49. Parameter–parameter plot of sediment concentrations at University CSO. ....	76
Figure 50. Sediment concentrations versus predicted sediment depositional rates at University Regulator CSO.....	77
Figure 51. University Regulator CSO sediment concentrations without values at CSO-UR-11. ....	78
Figure 52. Parameter–parameter plot at University Regulator CSO without values at CSO-UR-11. ....	79
Figure 53. Sediment concentrations versus predicted sediment depositional rates at University Regulator CSO without values at CSO-UR-11.....	80
Figure 54. Montlake CSO sediment concentrations for selected compounds.....	82
Figure 55. Parameter–parameter plot of sediment concentrations at Montlake CSO. ....	83
Figure 56. Sediment concentrations versus predicted sediment depositional rates at Montlake CSO. ....	84

# 1 Introduction

---

## 1.1 Problem Definition and Background

Combined sewer overflows (CSOs) are untreated discharges of wastewater and stormwater into waterbodies during heavy rainfall events when combined sewers are full. To avoid sewer backups into homes, businesses, and streets during heavy rainfall events, combined sewers in the City of Seattle sometimes overflow into Puget Sound, the Duwamish Waterway, Elliott Bay, Lake Union, the Lake Washington Ship Canal, and Lake Washington. Although the wastewater in CSOs is greatly diluted by stormwater, CSOs carry particulate matter and chemicals into local waterbodies. After CSO discharge, the particulate matter is transported, dispersed, and eventually settles to the sediment surface. The depositing particulates are one contributor to sediment quality in the vicinity of CSO outfalls.

Often, sediment quality adjacent to a CSO discharge reflects multiple point and non-point sources that are both ongoing and historical. To understand the contribution of CSO discharges to sediment quality, King County developed a predictive tool (model) to simulate contamination of sediments from near-shore discharges such as CSOs and storm drains (King County 2011). The three-dimensional hydrodynamic model, EFDC, was found to be able to implement all the components identified for the predictive tool.

This report documents the implementation of EFDC at 10 CSO discharge locations selected for minimal nearby discharges. These 10 locations were selected to be representative of the discharge receiving water conditions of all KC CSOs and areas that lacked sediment characterization. At each of these 10 locations, a dense grid of sediment samples was collected to confirm the model predictions. Comparison of the sediment quality data to the model deposition patterns indicate qualitative agreement.

## 1.2 Description of Study Area

King County's wastewater conveyance system includes 39 CSOs that discharge into Lake Washington, Lake Union, the ship canal, and Puget Sound.

### 1.2.1 Lake Washington

Lake Washington is the largest of the three major lakes in King County, and the second largest natural lake in the state of Washington. Lake Washington's two major influent streams are the Cedar River at the southern end, which contributes about 57 percent of the annual hydraulic load, and the Sammamish River, which contributes 27 percent of the annual hydraulic load. The majority of the immediate watershed is highly developed and urban in nature, with 63 percent fully developed.

The basin of Lake Washington is a deep, narrow, glacial trough with steeply sloping sides, sculpted by the Vashon ice sheet—the last continental glacier to move through the Seattle area. The lake is 20.6 ft above mean lower low tide in Puget Sound and it is connected to Puget Sound by Lake Union and the ship canal, which was constructed in 1916. The ship canal represents the only discharge from Lake Sammamish and Lake Washington via the locks and dam at the

western end of the lake. Prior to construction of the ship canal, the only significant inflow to Lake Washington was from the Sammamish River in the north. Mercer Island lies in the southern half of the lake, separated from the east shore by a relatively shallow and narrow channel, and from the west shore by a much wider and deeper channel.

No CSO discharges into Lake Washington were simulated with the EFDC model.

### **1.2.2 Lake Union and the Ship Canal**

Construction of the ship canal and Hiram M. Chittenden Locks was completed in 1917 by the U.S. Army Corps of Engineers. The ship canal and Lake Union connect Lake Washington with Puget Sound. To the east, the Montlake Cut connects Union Bay in Lake Washington with Portage Bay. Portage Bay connects to Lake Union, which covers approximately 581 acres and has an average depth of 32 ft. Heading west, the narrow Fremont Cut connects with Salmon Bay and the Hiram Chittenden (Ballard) Locks. The locks allow boats to pass between the fresh water of the ship canal and the salt water of Puget Sound and regulate the water level in the Lake Union/ship canal/Lake Washington system.

Within the Lake Union and ship canal system, deposition patterns from the Montlake CSO, University Regulator, and 3rd Ave. CSO were simulated with the EFDC model.

### **1.2.3 Duwamish**

The Duwamish River originates at the confluence of the Green and Black rivers near Tukwila, Washington, and flows northwest for approximately 12 miles. During the early 20th century, the last 6 miles of the Duwamish River were straightened and channelized into a commercial corridor for ship traffic, officially designated as the Lower Duwamish Waterway (LDW). The river splits at the southern end of Harbor Island to form the East and West Waterways prior to discharging into Elliott Bay.

A federally authorized navigation channel runs down the center of the LDW. This channel is maintained at depths between -30 ft, referenced to mean lower low water (MLLW), in the downstream reach and 15-ft MLLW in the upstream reach (upstream of the SR99/509 Bridge).

Fresh water moving downstream overlies the tidally influenced salt water entering the system. The LDW has a relatively sharp interface between the freshwater outflow at the surface and saltwater inflow (wedge) at depth.

Within the LDW, deposition patterns from Brandon and Chelan CSOs were simulated with the EFDC model.

### **1.2.4 Puget Sound**

Puget Sound is a deep, glacially carved fjord that connects to the Strait of Juan de Fuca through Admiralty Inlet and Deception Pass (Figure 1). The Strait of Juan de Fuca opens into the north Pacific Ocean between Washington state and Vancouver Island. Within the Sound, shallower sills (underwater shallow bars) separate a series of deeper basins.

The Main Basin extends from Tacoma, Washington, to the south end of Whidbey Island in a north-south orientation. Depths in the basin exceed 280 m (700 ft), and are generally uniform across the center portion of the basin, with steep side slopes that level off near the shoreline. Vashon and Maury Islands divide the southern portion of the Main Basin into the East Passage and Colvos Passage.

To the south, South Sound is connected to the Main Basin by Tacoma Narrows. South Sound is generally shallower than the Main Basin, with regions of tidal flats and numerous finger inlets and embayments.

At the north end of the Main Basin, Possession Sound forms one branch of the Triple Junction, leading northward to Port Susan, Saratoga Passage, and Skagit Bay. While much of Port Susan and Saratoga Passage is similar to the Main Basin, with depths near 200 m (600 ft) and steep side slopes, extensive tidal flats also exist. The three largest rivers (by volume) in Puget Sound—the Skagit, Stillaguamish, and Snohomish—empty into Skagit Bay, Port Susan, and Possession Sound, respectively (Figure 3). Skagit Bay is also connected to the Strait of Juan de Fuca by Deception Pass, a narrow, shallow passageway less than 500-m wide.

Hood Canal extends southward from the middle of Admiralty Inlet, almost reaching South Sound. This long, narrow basin has depths greater than 200 m, becoming shallower further south. A sill about 50-m deep separates Hood Canal from Admiralty Inlet.

Within Puget Sound, deposition patterns from CSOs at Barton, Murray, 53rd Ave., Magnolia, and North Beach were simulated with the EFDC model.

## 2 Modeling Goals and Objectives

---

### 2.1 Modeling Objectives

The objective of modeling was to predict the deposition pattern of CSO particulates in the sediments adjacent to each CSO corresponding to current CSO discharge rates.

## 3 Modeling Approach and Selection

---

### 3.1 Modeling Approach

The modeling approach taken was to simulate the discharge of water and solids from a CSO outfall and the subsequent deposition to the sediment bed with a three-dimensional hydrodynamic model. The model grid was locally refined to match the discharge pipe diameter and extended about 1500 m from the discharge point. The CSO discharge was configured as a continuous discharge with a flowrate that matched the observed/predicted distribution of flowrates. The discharge events were assumed to be uncorrelated with tides or ambient conditions, and the model was run for a 10-day period to average over tidal conditions.

This modeling simulated the depositional rate of CSO particulate matter; Appendix B describes how the depositional rate was related to chemical concentrations. In summary, sediment accumulation was assumed to be the sum of the ambient sedimentation and the predicted CSO depositional rate. Ambient sedimentation was estimated from previous studies, typically using geochronological analysis. High and low estimates of chemical concentrations associated with ambient sedimentation were combined with estimates of CSO solids concentrations from low- and high-concentration CSO basins to estimate the sediment concentration. Appendix B compares these concentrations to screening levels (sediment management standards), and establishes threshold deposition rates that could result in screening-level exceedances. This information is used to evaluate the model results of the CSOs in the main body of this document.

Two alternative approaches were considered: continuous simulation and individual event simulation. In a continuous simulation, the model is run for a period of time and CSO discharges occur in the model according to the same timing as observed. To include multiple CSO discharges in the simulation, the simulation would typically need to span multiple years. This approach is computationally inefficient, and is not practical with the model run times. The second approach would simulate each individual CSO discharge event and combines the resulting deposited solids to estimate the total CSO depositional rate. However, with limited data to configure the initial conditions prior to each CSO event, there appeared to be minimal benefits of this approach compared to the approach used.

### 3.2 Model Description

The EFDC model is a state-of-the-art hydrodynamic model that solves three-dimensional, vertically hydrostatic, free surface, turbulent averaged equations of motion for a variable-density fluid. Dynamically coupled transport equations for turbulent kinetic energy, turbulent length scale, salinity, and temperature are also solved. EFDC uses stretched or sigma vertical coordinates and Cartesian or curvilinear, orthogonal horizontal coordinates to represent the physical characteristics of a waterbody. The EFDC model allows for drying and wetting in shallow areas by a mass conservation scheme.

## 4 EFDC Model Setup

---

### 4.1 Model Domain

An orthogonal model grid was configured for each discharge location. Where the waterbody geometry was suitable, a Cartesian grid was used. In most locations, a conformal mapping was used to create a radial domain. This was intended to allow the cell dimensions to increase away from the discharge location and minimize computational time while maintaining an orthogonal grid. The grid is locally refined so that the cell into which the CSO discharges has a cell width equal to the discharge pipe diameter and a cell length 3 times the width.

Grid dimensions grow exponentially from the discharge cell, up to a maximum cell size. This grid is then transformed by a conformal mapping to produce an orthogonal grid with a far-field radial pattern.

The conformal mapping used is:

$$z = \sin(y + j*x)$$

which maps a rectangular region to the inside of a circle.

**Images of a square grid**

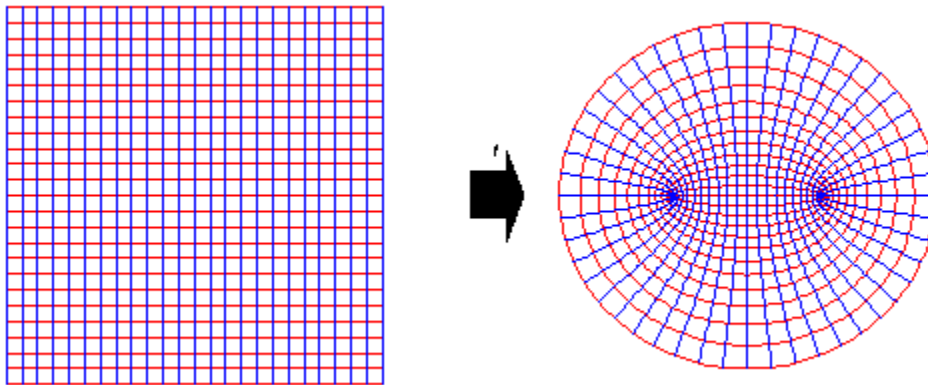


**Figure 1. Images of a square grid of size  $[-\pi/2, \pi/2] \times [-\pi/2, \pi/2]$  under the (conformal) map  $z \mapsto \sin(z)$ . The two "focal points" are the points  $\pm 1$ .**

To keep the focal points outside of the computational domain, the discharge location was set to ensure the focal points would be on land and thus out of the computational domain.

(Figure)

The grid was reduced in size to match the pipe diameter and grid aspect ratio. The cell dimensions were set to increase at a constant rate away from the discharge cell.

**Table 1. CSO discharge locations.**

	<b>Northing</b>	<b>Easting</b>	<b>Discharge Depth (m)</b>	<b>Pipe Diameter (in)</b>
North Beach	1256900	259982	5	16
Magnolia	1254425	234555	6.75	36
53 <sup>rd</sup> Ave.	1253524	216866	5	72
Murray	1254282	200845	6.6	72
Barton	1254813	194850	6.5	60
Brandon	1268200	205972	0.3	72
Chelan	1264135	212943	8.1	30
3rd Ave.	1264117	241548	1	60
University	1276167	240227	1	84
Montlake	1277715	239513	1	60

Subsequent to model development and simulation, the estimated location of the Chelan discharge was revised, moving the discharge location approximately 60 ft northwest of the original and modeled location (Table 1). The revised outfall location is shown on figures of the Chelan model results (Figure 10 and Figure 42), but the sediment sampling locations and model discharge location are based on the previous discharge location coordinates.

The sediment grid was configured as four 2-cm-thick layers, initially empty of sediment. Sediment resuspension was enabled in the model, although transport by bedload movement was disabled. The threshold for resuspension was set at  $0.003 \text{ m}^2/\text{s}^2$ , or  $3 \text{ N}/\text{m}^2$ . The intent was to create a realistic simulation in which sediment accumulation was reduced in high shear stress areas. In most cases, bottom stress is below this threshold and the models are depositional. In the models of Chelan, Murray, and University, multiple model cells exceeded the threshold. In Brandon, Barton, and North Beach, only the CSO discharge created an exceedance within the discharge cell.

## 4.2 Model Configuration

### 4.2.1 Solids Concentrations and Settling Velocity

CSO solids concentrations were obtained from sampling CSOs during periods when the CSO was discharging or when in-pipe water levels were close to the level that causes an overflow. Whole water samples were collected upstream of the regulator gate/weir under conditions similar to CSO discharge events and are considered representative of CSO solids. A total solids concentration of  $128 \text{ mg}/\text{L}$  was used, corresponding to the average total suspended solids (TSS) concentration observed in the CSO samples. Three sediment size classes were used in the modeling, similar to the original model development (King County, 2011). The settling velocity for each particle size class was taken from settling tube measurements on whole water samples collected from CSO discharge events. The settling velocity measurements and relative amount of each particle size class were summarized in the model development report (King County, 2011). The settling velocities and mass fraction of the three sediment size classes are summarized in Table 3.

**Table 2.** Suspended solids characteristics used in the models.

<b>Particle Type</b>	<b>EFDC Sediment Type</b>	<b>Sediment Density (kg/m<sup>3</sup>)</b>	<b>Settling Velocity W<sub>s</sub> (m/s)</b>	<b>Percent mass</b>	<b>Conc. (mg/l)</b>
Sand	Non-cohesive	2500	7.5E-03	33%	41.6
Silt	Cohesive	2500	6.25E-04	34%	43.1
Clay	Cohesive	2500	1.50E-04	34%	43.3

## 4.3 Boundary Conditions

### 4.3.1 CSO Discharge Rates and Volumes

Sediment accumulation patterns adjacent to CSO discharges are the cumulative result of the CSO discharge events. For future and many historic discharge events, a discharge hydrograph is not available. The sediment accumulation should be proportional to the volume discharged. The primary influence of the CSO discharge rate is to determine the initial momentum of the discharge and, consequently, the offshore velocity and trajectory of the discharged effluent. On the assumption that the depositional pattern at a given time was independent of the previous discharge flowrate, the simulation used a series of constant discharge rates. Each discharge rate was set to occur for a duration proportional to its occurrence in historical discharge rates.

The discharge flowrates were collated into a histogram and the simulated duration of each discharge rate was proportional to the portion of flowrates in each histogram segment. Because the model results did not appear particularly sensitive to the discharge flowrate, three segments were used (Figure 2). A histogram with 24 segments was also computed to assist in evaluating how well the three discharge flowrates represented the time series.

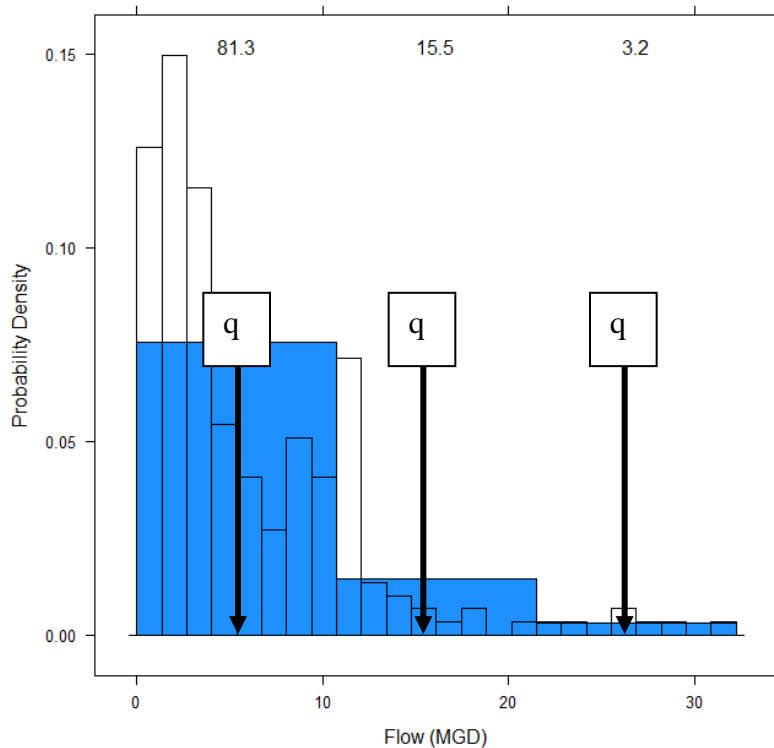


**Figure 2.** Illustration of a histogram of positive CSO flow values divided into three equal segments, the average flow  $q_i$  for each segment, and the percent probability of each segment occurring (shown at top of chart).

Characteristic flowrates and durations are given in Table 3.

**Table 3.** Characteristic CSO discharge flows and durations. Flows are sorted from smallest to largest (lower 1/3 to upper 1/3); durations sum to 10 days.

CSO Site	Data Period	Lower 1/3 (MGD)/(days)	Middle 1/3 (MGD)/(days)	Upper 1/3 (MGD)/(days)	Average EFDC Flow (mgd)
3rd Ave.	6/1/2009 – 1/1/2012	23.3 / 8.5	69.8 / 1.2	116.3 / 0.3	31.6
Montlake	6/1/2009 – 1/1/2012	25.1 / 6.1	75.4 / 3.2	125.6 / 0.7	48.3
University	6/1/2009 – 1/1/2012	38.6 / 5.7	115.9 / 2.6	193.1 / 1.7	84.7
53rd Ave.	10/1/2007 – 1/1/2012	10.1/9.92	30.3/0.05	50.6/0.03	10.3

Barton	1/1/2008 – 1/1/2012	4.0 / 9.2	12.0 / 0.5	20.0 / 0.3	4.8
Brandon	6/1/2009 – 1/1/2012	16.3 / 7.6	48.8 / 2.2	81.3 / 0.2	24.8
Chelan	6/1/2009 – 1/1/2012	3.6 / 5.2	10.9 / 2.5	18.1 / 2.3	8.8
Magnolia	1/1/2010 – 1/1/2012	3.0 / 8.1	9.0 / 1.8	15.0 / 0.1	4.2
Murray	1/1/2009 – 1/1/2012	22.4 / 0.5	67.1 / 6.9	111.9 / 2.6	76.4
North beach	1/1/2009 – 1/1/2011	1.5 / 8.1	4.5 / 1.7	7.5 / 0.2	2.1

### 4.3.2 Ambient Currents

Ambient currents at the time of CSO discharges are unknown. The modeling approach was to prescribe model boundary conditions that would result in a typical current pattern within the model domain. For CSOs discharging into Elliott Bay and Puget Sound, this was achieved by prescribing the tidal elevation along the boundary. The two dominate tidal components, M2 and K1, were used with a delay equal to the tidal phase speed. For CSOs discharging into the ship canal, a characteristic velocity of 3 cm/s was used, based on the wintertime flow from the Hiram M. Chittenden Locks. This was implemented as a constant elevation difference between the upstream and downstream boundary conditions. For CSOs discharging into the LDW, a combination of tidal elevations and constant elevation difference was used to simulate the estuarine nature of the waterway. In this way, no direct specification of the Green River flowrate was required. The resulting mean and root mean square (RMS) currents predicted in the model simulations are summarized in Table 4.

**Table 4. Current speeds predicted by EFDC simulations.**

CSO	Mean (m/s)	RMS (m/s)
3rd Ave.	0.055	0.143
53rd Ave.	0.065	0.171
Brandon	0.091	0.110
Barton	0.035	0.114
Chelan	0.016	0.350
Magnolia	0.055	0.303

Montlake	0.054	0.066
Murray	0.071	0.327
North Beach	0.025	0.223
University	0.037	0.056

### 4.3.3 Ambient Density Stratification

No ambient density stratification was prescribed for CSO discharges to the ship canal, Elliott Bay, or Puget Sound. For CSO discharges to the ship canal, the initial and boundary conditions prescribed zero salinity. For discharges to Elliott Bay and Puget Sound, initial and boundary conditions of 30 psu were selected.

An ambient density stratification for discharges to the LDW (Brandon, Chelan) was set based on a representative wintertime salinity profile, as shown in Figure 3. The 11/17/2009 profile from King County monitoring station LTKE03 near the Spokane Street Bridge was used, augmented by the density profile from King County’s monitoring station LTED04 in Central Elliott Bay for values at depths greater than 11 m. This density profile was prescribed for the upstream and downstream boundary locations in the Chelan model and downstream boundary in the Brandon model.

This density profile was made fresher (less saline) for the upstream boundary in the Brandon model. Salinity at the surface was reduced by 1 psu (minimum of 0 psu), while salinity below 5 m depth was not modified. Between the surface and 5 m, the reduction in salinity varied linearly from 1 psu to zero. The resulting profile is not distinguishable from the downstream profile at the scale shown in Figure 3. This reduction in salinity was based on a comparison of salinity profiles at the Brandon upstream and downstream boundary locations from King County’s Elliott Bay/LDW model. The resulting horizontal salinity gradient provided the freshwater flow, and no volume flux was specified for the Duwamish river. This allowed both upstream and downstream flow at the model boundary to be more realistically simulated.

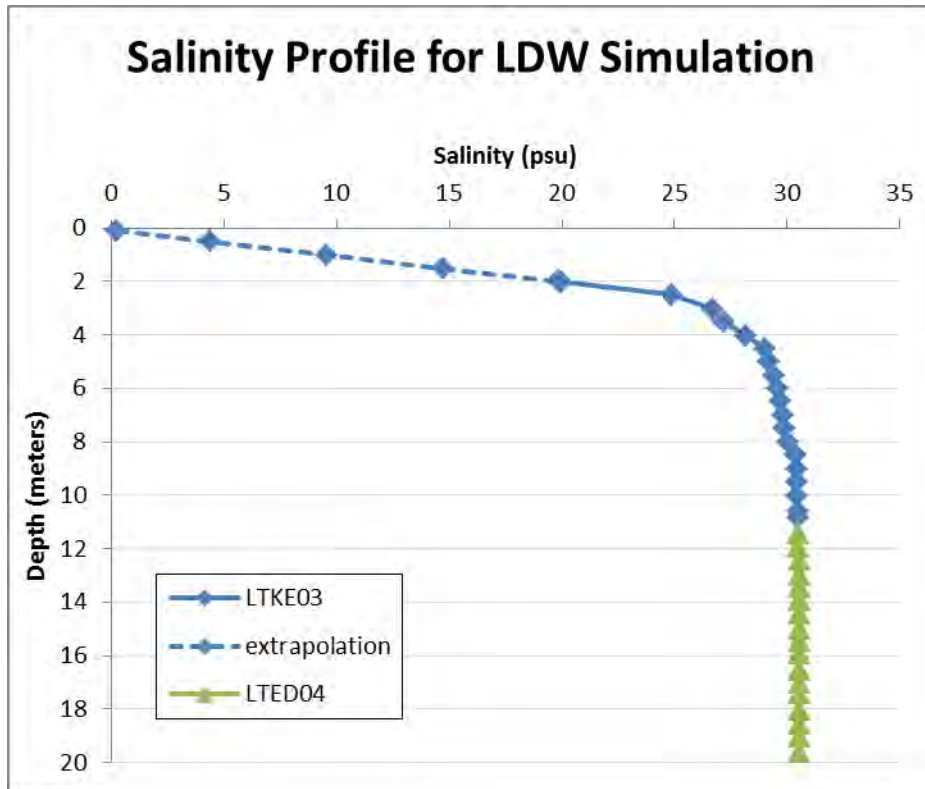


Figure 3. Boundary salinity profile used for Brandon, Chelan models.

#### 4.4 Calibration Strategy

The modeling approach was to configure the model to simulate representative conditions during which CSOs discharge. Because no direct measurements exist of conditions during historic or future CSO discharge events, direct model calibration was not possible.

Where possible, the predicted current pattern was compared to nearby current meter data or simulations to verify the mean and tidal current speeds were similar. The phase shift of the tidal components or the magnitude of the constant elevation offset at boundary cells were adjusted, if necessary.

## 5 Model Results

---

### 5.1 Methods Overview

A separate model was configured for each CSO location. The model grid extended approximately 1500 m from the discharge to limit any boundary effects on the sedimentation pattern. The model was run for 2 days with no discharge and for the following 10 days with the CSO discharging for the flowrates and durations indicated in Table 5. The simulation continued for an additional day to allow all discharged sediment to deposit or leave the model domain. The resulting depth of sediment deposition was normalized by the estimated period for the CSO to discharge the same volume as the simulation. The resulting spatial deposition pattern is discussed below for each simulated CSO.

**Table 5. Duration simulated in EFDC.**

<b>CSO Site</b>	<b>Average EFDC Flow (mgd)</b>	<b>Historic Annual CSO Volume (MG)</b>	<b>Effective Duration of EFDC Simulation (yrs)</b>
3rd Ave.	31.6	9.8	32
Montlake	48.3	23	21
University	84.7	88	9.6
53 <sup>rd</sup> Ave.	10.3	0.14	740
Barton	4.8	3.5	14
Brandon	24.8	30	2.9
Chelan	8.8	5.7	15
Magnolia	4.2	19	2.2
Murray	76.4	12	65
North beach	2.1	5.4	3.9

Sediment samples were collected to confirm the model simulations were reasonable. The sampling plan was developed and the initial round of sampling was conducted before model results were available. Sampling locations were placed based on a momentum length scale around the CSO discharge location (King County 2012). Additional sampling was conducted in two subsequent sampling events to address specific questions.

### 5.2 Results

#### 5.2.1 North Beach Pump Station

The predicted deposition pattern from the North Beach CSO was focused at the immediate end of the outfall. As with all of the submerged marine CSOs, the EFDC model predicted the initial momentum was quickly lost and horizontal spreading of the buoyant CSO discharge appeared to

dominate the advection. Five additional sampling sites were added in a second round of sampling, northeast of the original pattern, and inshore of the discharge location. This ensured that samples surrounded the discharge location after the discharge location was corrected to approximately 50 feet to the northeast after the original sampling but prior to the modeling. The comparison of predicted deposition rate and sediment chemistry is discussed in Section 7. The model predicted a peak deposition rate of 0.2 mm/yr at the outfall, reducing to less than 0.1 mm/yr within 3 ft.

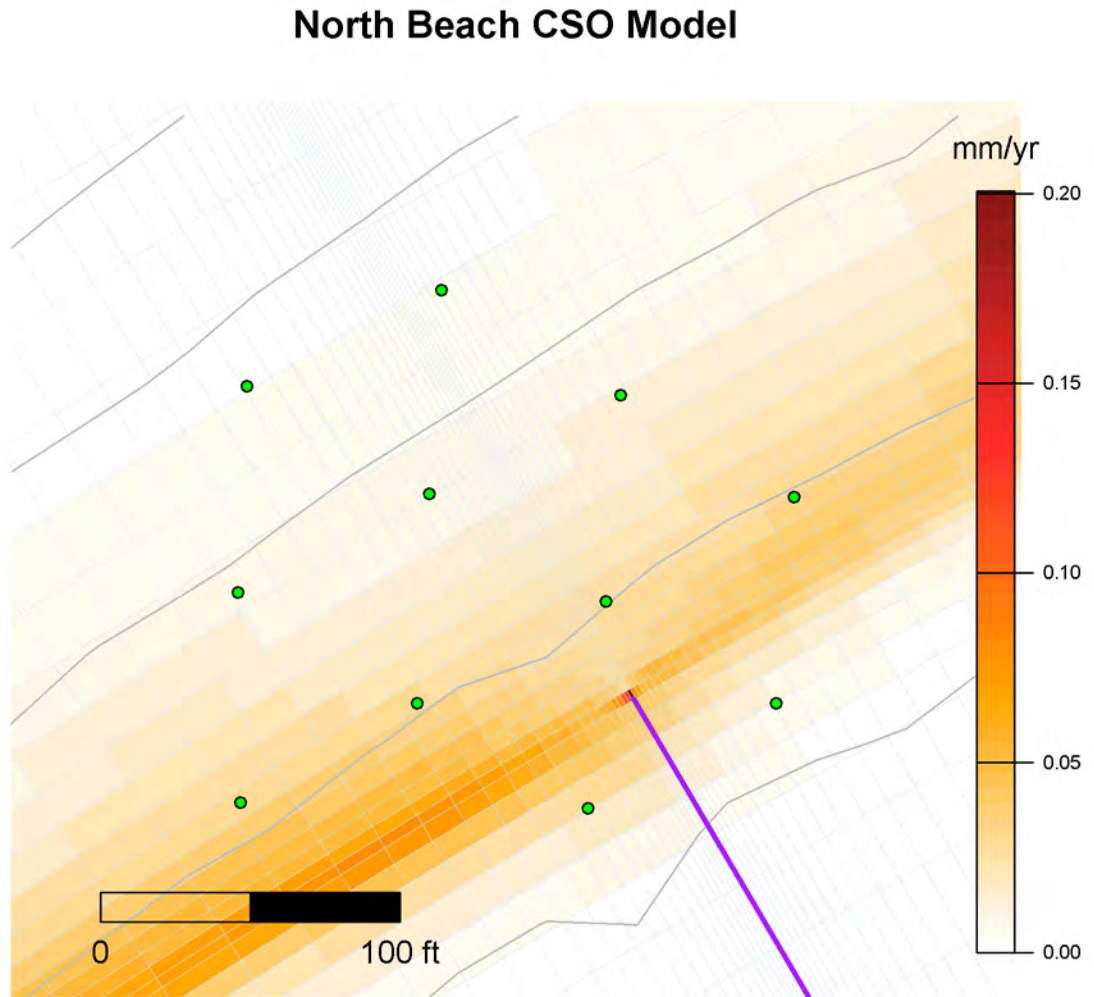


**Figure 4. North Beach predicted depositional rates.**

### 5.2.2 South Magnolia CSO

The predicted deposition pattern from the South Magnolia CSO was generally parallel to the shoreline, along a line roughly over the discharge location. As with all of the submerged marine CSOs, the EFDC model predicted the initial momentum was quickly lost, and horizontal spreading of the buoyant CSO discharge appeared to dominate the advection. An additional sampling site was added in a second round of sampling, to the northeast of the discharge location, to collect sediments in the predicted depositional pattern. The comparison of predicted deposition rate and sediment chemistry is discussed in Section 7. The model predicted a peak deposition rate of 0.4 mm/yr at the outfall, reducing to less than 0.1 mm/yr within 200 ft.

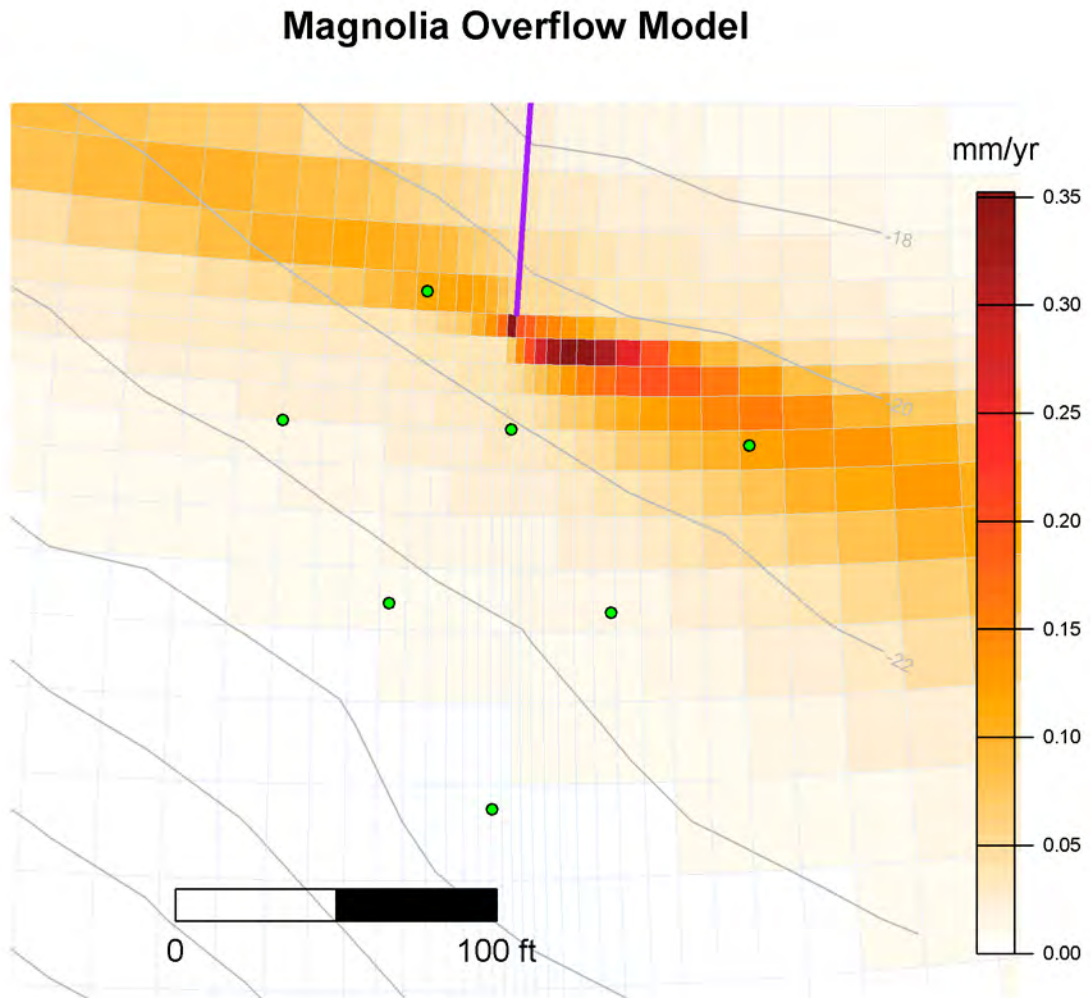


Figure 5. Magnolia predicted depositional rates.

### 5.2.3 53rd Avenue Pump Station

The predicted deposition pattern from the 53rd Ave. Pump Station CSO was generally parallel to the shoreline, and inshore of the CSO discharge location. As with all of the submerged marine CSOs, the EFDC model predicted the initial momentum was quickly lost, and horizontal spreading of the buoyant CSO discharge appeared to dominate the advection. The deposition pattern inshore of the CSO discharge location appears reasonable based on flood tides moving predominately southward around Alki. The EFDC model domain is too small to capture large-scale tidal patterns, so while plausible, this onshore tidal movement is rather uncertain. The model predicted a peak deposition rate of 0.003 mm/yr at the outfall, which is the lowest deposition rate of the CSOs modeled.

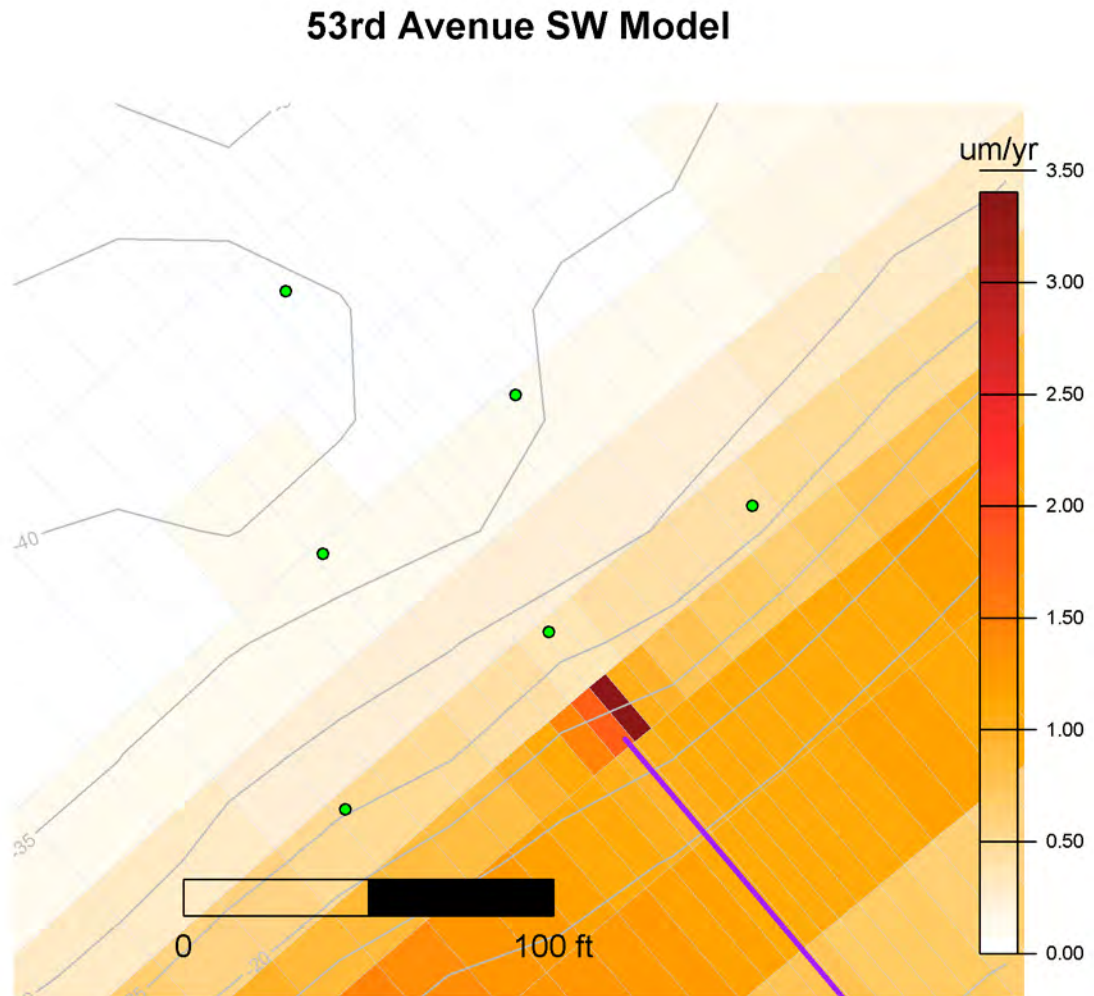


Figure 6. 53rd Ave. CSO predicted depositional rates.

#### **5.2.4 Murray Avenue Pump Station**

The predicted deposition pattern from the Murray Ave. Pump Station CSO was generally parallel to the shoreline, with a greater accumulation north of the discharge location. As with all of the submerged marine CSOs, the EFDC model predicted the initial momentum was quickly lost, and horizontal spreading of the buoyant CSO discharge appeared to dominate the advection. Six additional sampling sites were added in a second round of sampling, surrounding the discharge and to the north-east of the discharge location, to collect sediments in the predicted depositional pattern and samples off- and inshore of the outfall and a nearby outfall. The comparison of predicted deposition rates and sediment chemistry is discussed in Section 7. The model predicted a peak deposition rate of 0.06 mm/yr at the outfall.

## Murray Avenue Model

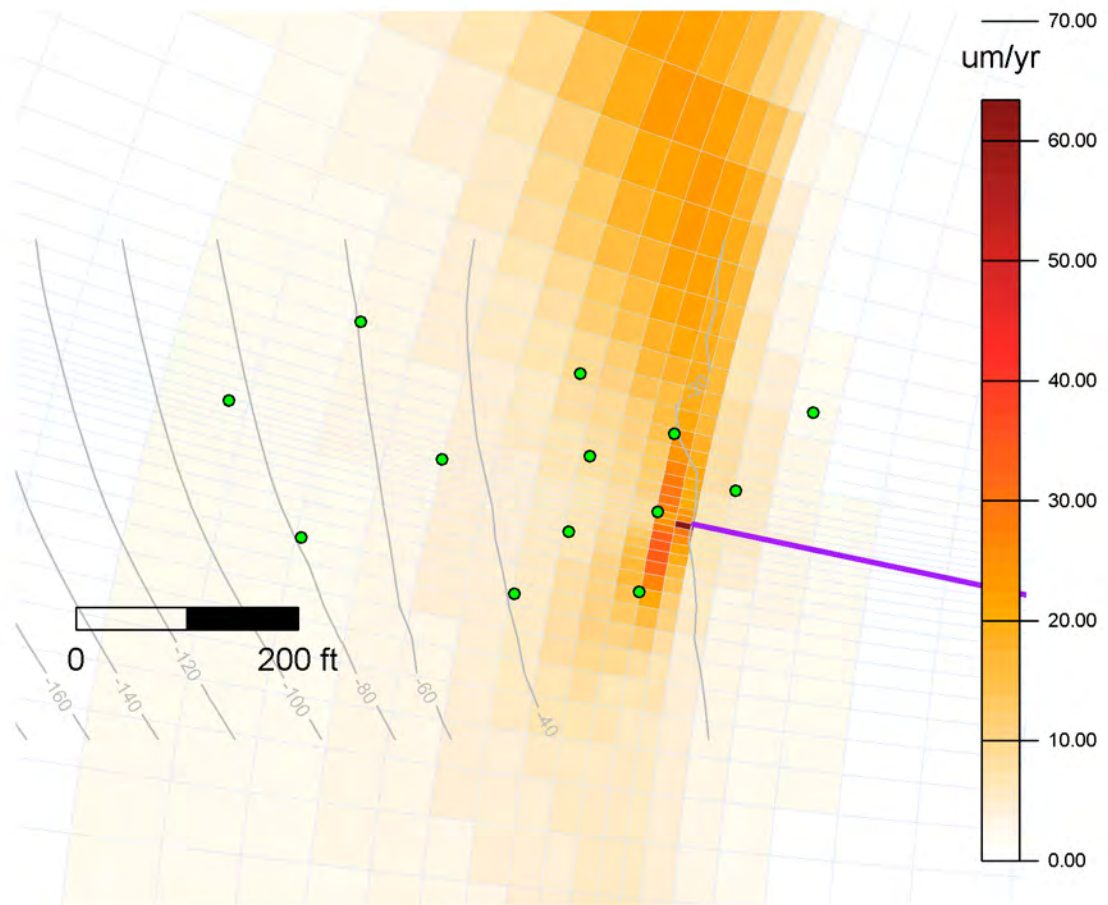
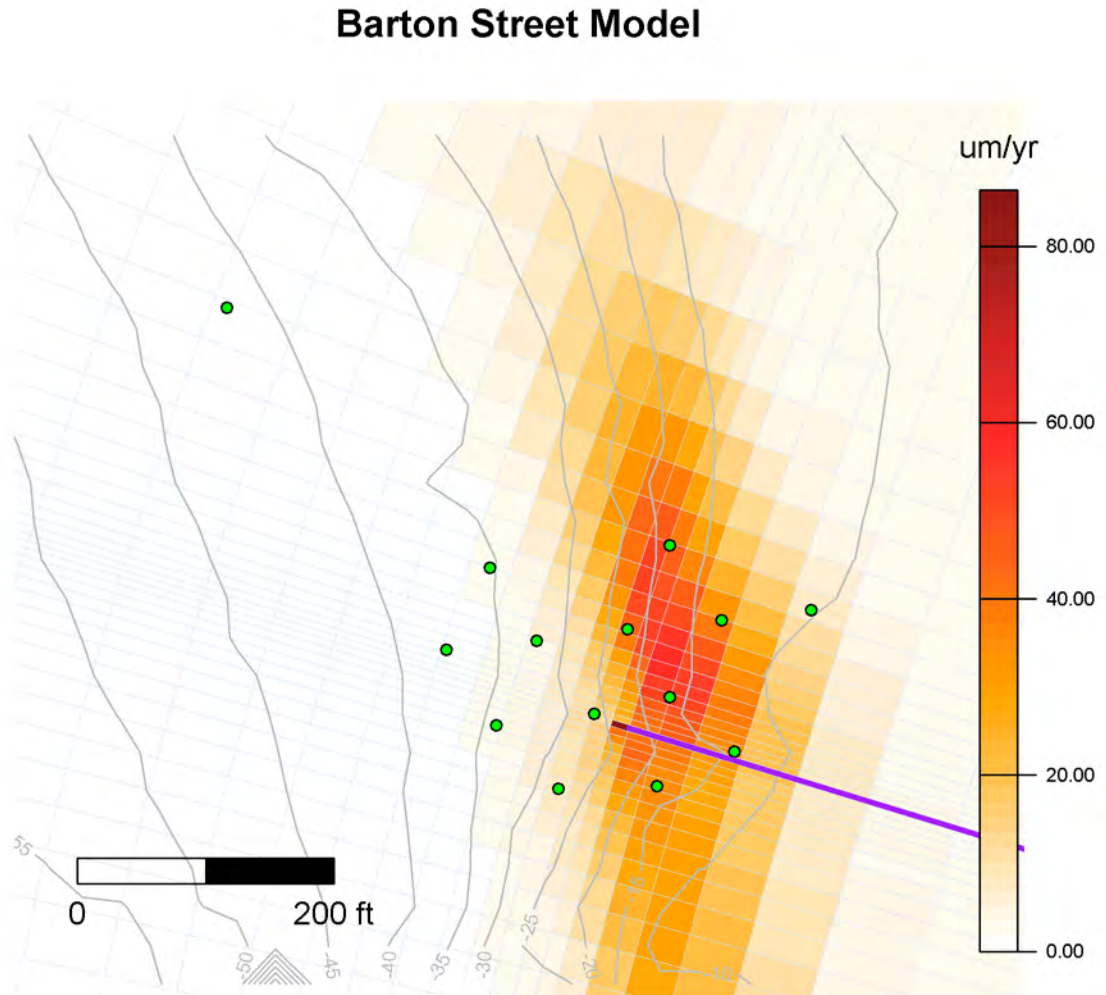


Figure 7. Murray Ave. CSO predicted depositional rates.

### 5.2.5 Barton Street Pump Station

The predicted deposition pattern from the Barton St. Pump Station CSO was generally parallel to the shoreline, and inshore of the CSO discharge location. As with all of the submerged marine CSOs, the EFDC model predicted the initial momentum was quickly lost, and horizontal spreading of the buoyant CSO discharge appeared to dominate the advection. The deposition pattern inshore of the CSO discharge location was unanticipated. The EFDC model domain is too small to capture large-scale tidal patterns, so while plausible, this onshore tidal movement is rather uncertain. Some additional sampling sites were added to the northeast and inshore of the discharge in a second round of sampling to collect sediment in the predicted sediment pattern

and around a nearby outfall. The model predicted a peak deposition rate of 0.09 mm/yr at the outfall.



**Figure 8. Barton St. CSO predicted depositional rates.**

### 5.2.6 Brandon Street CSO

The deposition pattern from the Brandon St. CSO was originally modeled as part of the development of this modeling approach (King County 2011). The predicted pattern is generally similar to the previous modeling results, although the previous results simulated a larger domain. The Brandon discharge is at the surface and the predicted solids deposition pattern appears to follow a momentum jet. The model predicted a peak deposition rate of 46 mm/yr at the outfall,

which is the highest deposition rate of the CSOs modeled. The deposition rate reduced to less than 1 mm/yr within 190 ft and to less than 0.1 mm/yr within 450 ft. Part of this deposition pattern is intertidal, so tidal movements and waves could re-suspend sediments deposited here and spread them more broadly than the initial deposition pattern shown.

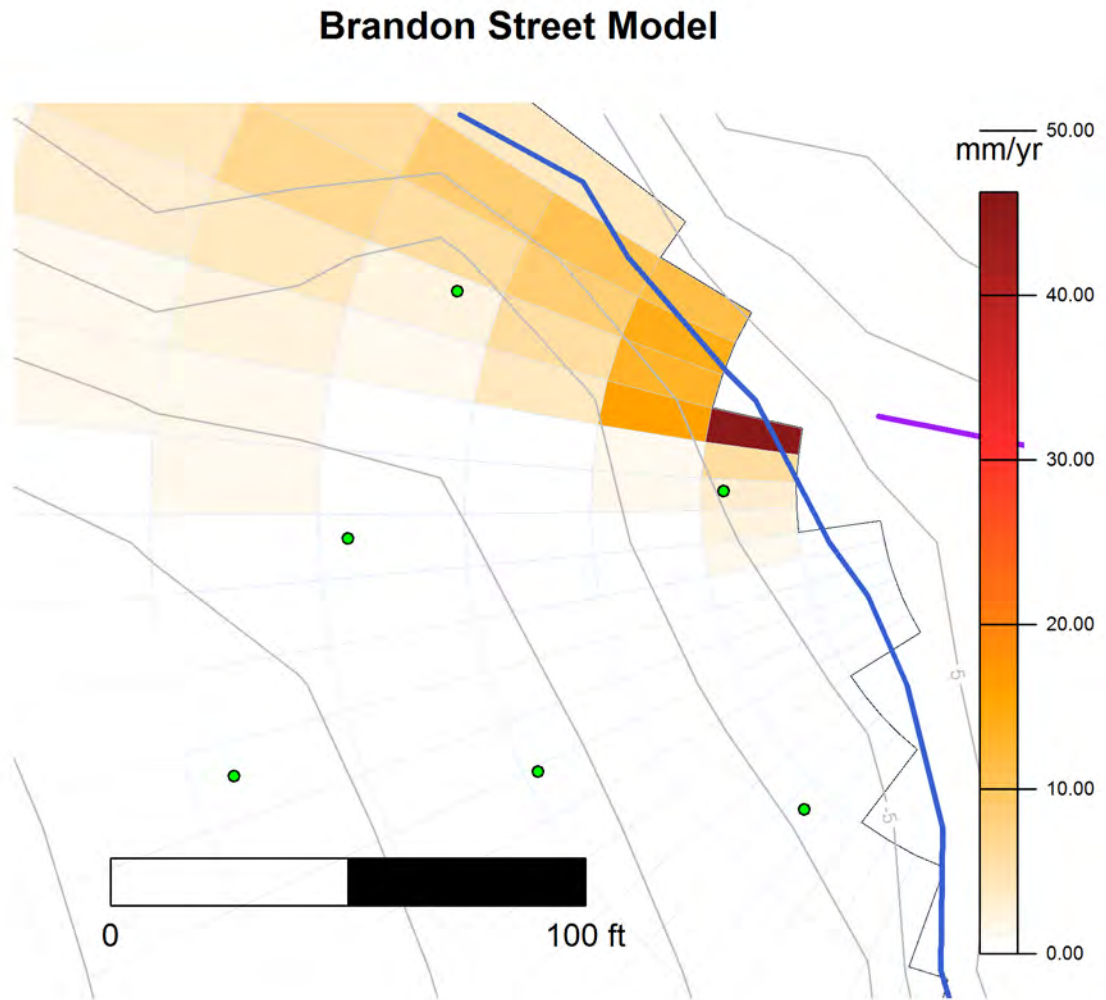


**Figure 9. Brandon St. CSO predicted depositional rates.**

### 5.2.7 Chelan Avenue CSO

The discharge location for the Chelan outfall was revised approximately 60 ft to the northwest subsequent to the completion of sediment sampling and modeling. The figures show the revised

location as well as a secondary overflow location further inshore. All discharges were modeled as exiting the offshore discharge location.

The predicted deposition pattern from the Chelan Ave. CSO was generally parallel to the shoreline, and inshore of the CSO discharge location. As with all of the submerged marine CSOs, the EFDC model predicted the initial momentum was quickly lost, and horizontal spreading of the buoyant CSO discharge appeared to dominate the advection. The deposition pattern inshore of the CSO discharge location appears reasonable from the expected tidal flow pattern around the south end of Harbor Island. The EFDC model domain is large enough to capture the tidal flow patterns around this bend. The model predicted a peak deposition rate of 3 mm/yr at the outfall, reducing to less than 1 mm/yr within 3 ft and to less than 0.1 mm/yr within 230 ft.

Four additional sampling sites were added in a second round of sampling, all located to the east of the original sampling locations. Concentrations for several compounds were higher at station CSO-CH-3 than the other sampling stations, suggesting a source further to the east. The purpose of these additional sites was to determine if there was a long-shore gradient in concentrations and attempt to bound higher concentrations. The influence of the CSO on sediment concentrations was anticipated to show decreasing concentration with distance from the CSO. Over water structures obstructed access and prevented us from locating the stations closer to shore where the model predicts higher sediment deposition.

## Chelan Avenue Model

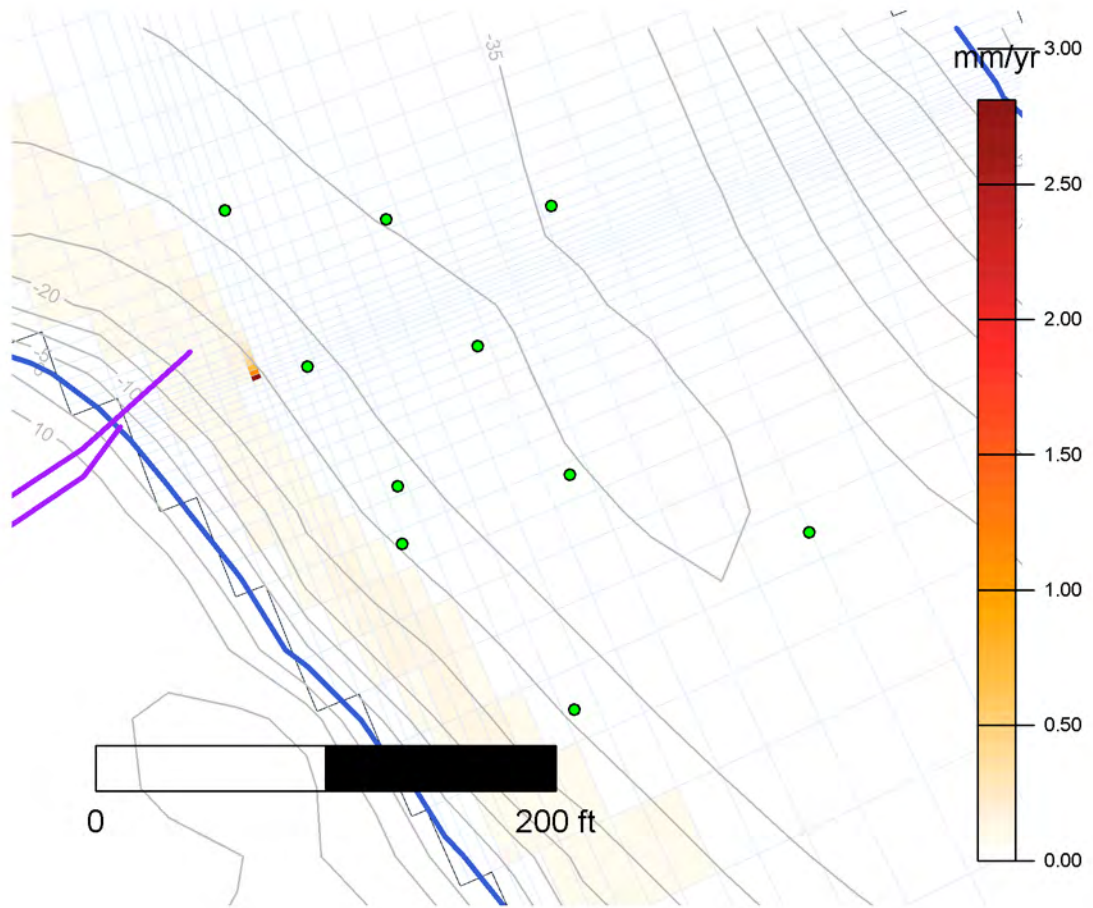
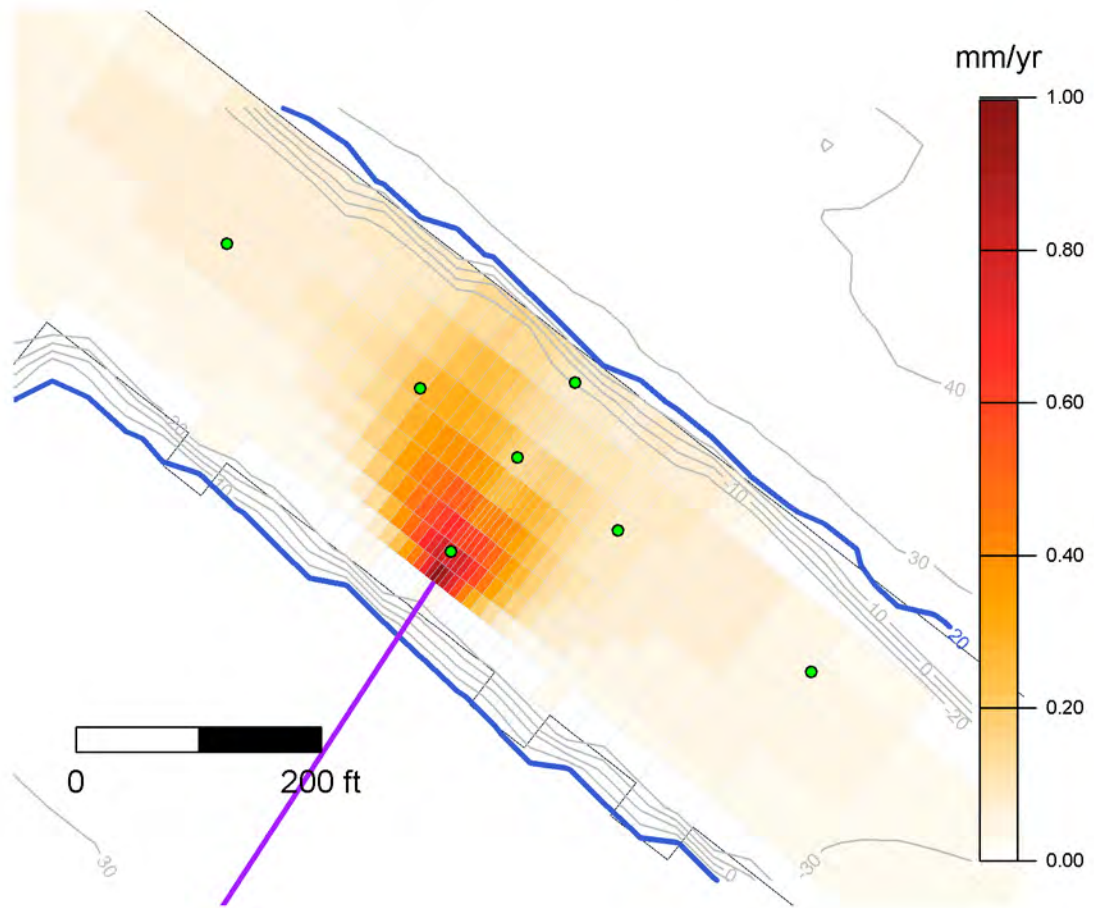


Figure 10. Chelan Ave. CSO predicted depositional rates.

### 5.2.8 3rd Avenue West CSO

Third Ave. West CSO discharges into the ship canal and the EFDC model predicted a sediment deposition pattern predominately offshore of the CSO. As with all of the freshwater CSOs, the EFDC model predicted initial momentum, and spreading of the discharge determined the deposition pattern. The model predicted a peak deposition rate of 1 mm/yr at the outfall, reducing to less than 0.1 mm/yr within 240 ft.

## 3rd Ave West



**Figure 11. 3rd Ave. West CSO predicted depositional rates.**

### 5.2.9 University Regulator

University CSO discharges into fresh water in Portage Bay and the EFDC model predicted a sediment deposition pattern predominately offshore of the CSO. As with all of the freshwater CSOs, the EFDC model predicted initial momentum, and spreading of the discharge determined the deposition pattern. The model predicted a peak deposition rate of 9 mm/yr at the outfall, reducing to less than 1 mm/yr within 210 ft, and to less than 0.1 mm/yr within 1200 ft.

## University Regulator Model

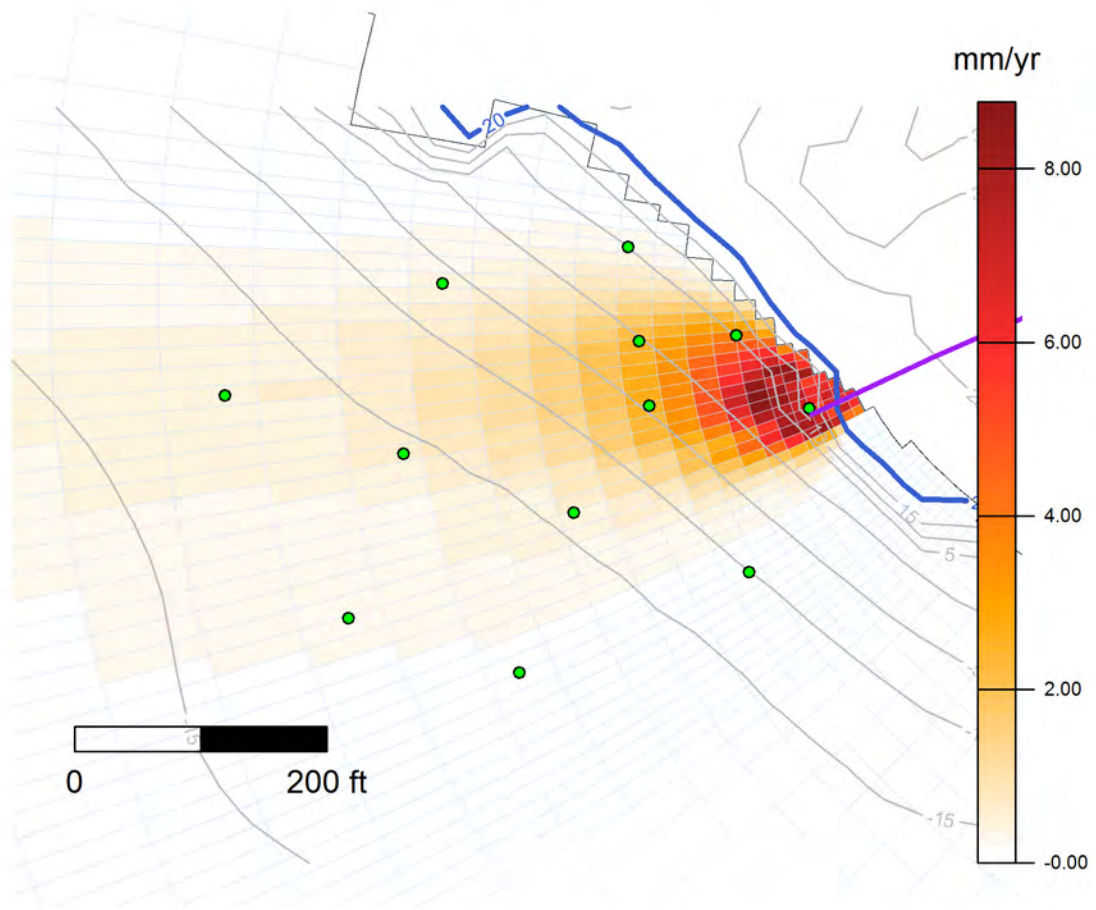


Figure 12. University Regulator CSO predicted depositional rates.

### 5.2.10 Montlake CSO

Montlake CSO discharges into fresh water in the ship canal, and the EFDC model predicted a sediment deposition pattern predominately offshore of the CSO. As with all of the freshwater CSOs, the EFDC model predicted initial momentum, and spreading of the discharge determined the deposition pattern. The model predicted a peak deposition rate of 1.3 mm/yr at the outfall, reducing to less than 1 mm/yr within 45 ft, and to less than 0.1 mm/yr within 1100 ft.

## Montlake CSO Model

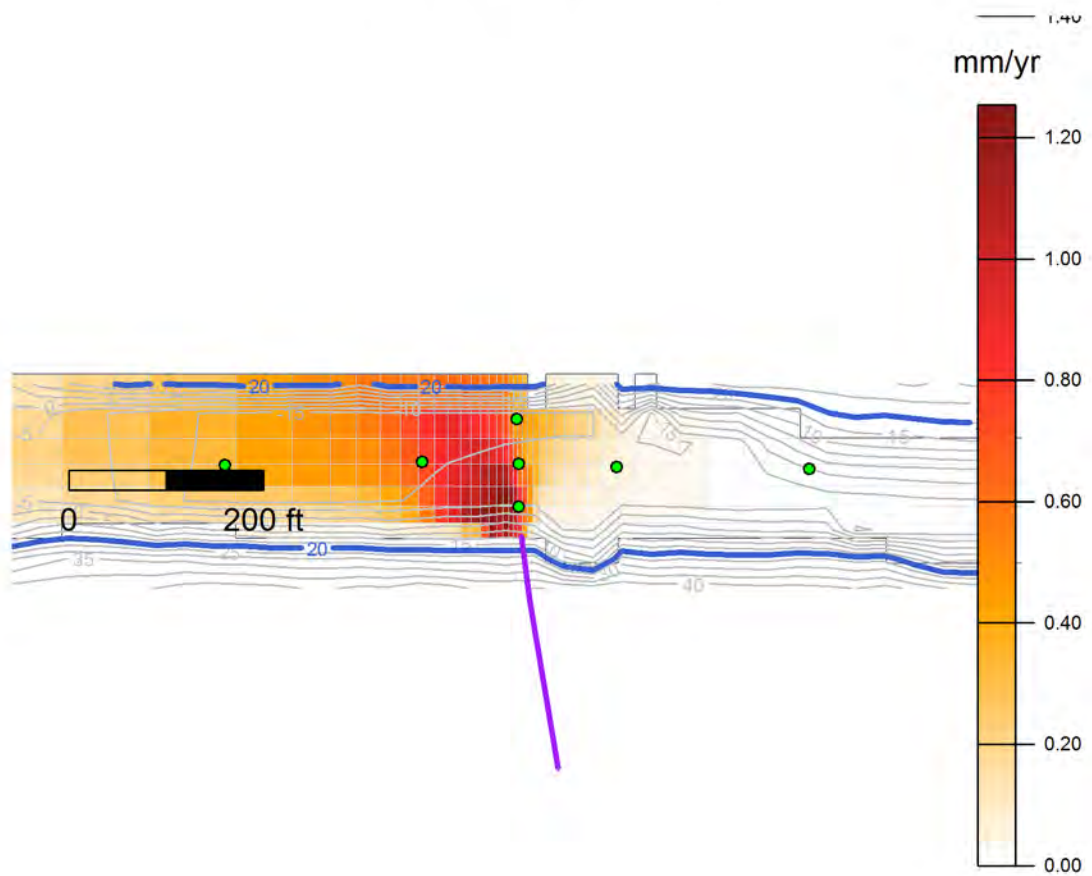


Figure 13. Montlake CSO predicted depositional rates.

## 6 Sensitivity and Uncertainty

---

Model predictions are a function of the input parameters and the model configuration. With limited data available to characterize many of these parameters, the model predictions have a high amount of uncertainty associated with them. Recognizing this uncertainty, a mostly qualitative discussion of factors affecting model predictions follows.

The modeled deposition rate is directly proportional to the discharged solids mass. Thus, a change in the annual discharge volume or average TSS concentration will change the deposition rate by a similar amount. The annual discharge volume was calculated by averaging historic discharges. Because all of the CSO discharges modeled had sensors monitoring the overflows, typically level sensors, the discharge rate is expected to be relatively close to the actual discharge rate within the limitations of the measurement equipment. However, most of the CSOs modeled do not have TSS measurements during CSO events. A characteristic value based on the mean TSS concentration at locations with measurements was used. Although TSS concentrations are generally similar at the CSOs with measurements, the appropriate concentration at any other CSO may be higher or lower than assumed. However, since CSOs comprise between 85 and 95 percent stormwater by volume when discharging, the differences are not expected to be large.

The modeling approach used here attempts to estimate sediment deposition rates as the statistical mean of multiple events. In this approach, individual events are not simulated, but a discharge is simulated with properties equivalent to the mean of multiple events. With CSO locations that do not discharge frequently, the sediment accumulation may reflect only a few discharge events. The mean values used in the modeling may not be a representative average of a small number of discharge events. This could change both the amount of predicted sediment accumulation and the spatial pattern of deposition.

The modeling does not reflect any correlations between the input parameters. In calculating the solids mass discharged from a CSO, no consideration is made to the possibility that TSS concentrations may tend to decrease at higher flowrates. Likewise, no consideration is given to the possibility that CSO events occur during periods of heavy rainfall, which may tend to be associated with higher winds or higher stream/freshwater inflows.

Model simulations were configured with the CSO discharges entering the model at a similar location to current conditions. In the vicinity of the discharge, the model grid was refined to have a cell width equal to the discharge pipe diameter. This results in the model having only a very approximate representation of the discharge jet/plume dynamics. It was recognized that this could bias the model results for CSOs with marine discharges at the bottom of the water column. In this case, the discharge is buoyant and most solid material is likely carried upward with the buoyant plume. However, when the discharge is introduced into the model in the bottom cell, this is not the case. A buoyant discharge will create an upward vertical velocity in the model, but the vertical velocity is prescribed to be zero at the sediment bed. As a result, the settling rate is calculated as the product of the settling velocity and concentration in the bottom cell. To examine the impact of this approximation, a sensitivity run was conducted with the 53rd St. CSO. Originally, half of the discharge entered the discharge cell at the lowest vertical layer and half was placed in the second layer above the bottom. With a discharge depth of 7 m or 23 ft

relative to mean sea level and each layer comprising 10% of the depth, this creates a discharge location of 4.6 ft by 6 ft, or 27.6 sq ft, close to the cross-sectional pipe area of 28.3 sq ft. This was modified to have the entire discharge enter into the second layer above the bottom.

While this also doubles the discharge velocity and momentum, the discharge momentum for 53rd is quite small and the increase was not anticipated to make a significant change to the simulation. The deposition pattern with the discharge to the bottom layer (Figure 14) is largely similar to the pattern without discharging to the bottom layer (Figure 6), except the magnitude of deposition in the cells adjacent to the discharge is greatly reduced. The percent difference between the sensitivity simulation and the original is shown in Figure 15. The depositional rate adjacent and inshore from the discharge is reduced with no discharge to the bottom layer, while depositional rates offshore and further from the discharge tend to be increased. The most significant differences occurred within 100-200 ft of the discharge.

As a result of this sensitivity investigation, the submerged discharges into marine waters were reconfigured to exclude the discharge into the bottom layer to avoid significant over prediction of depositional rates in the vicinity of the discharge.

### 53rd Avenue SW Model

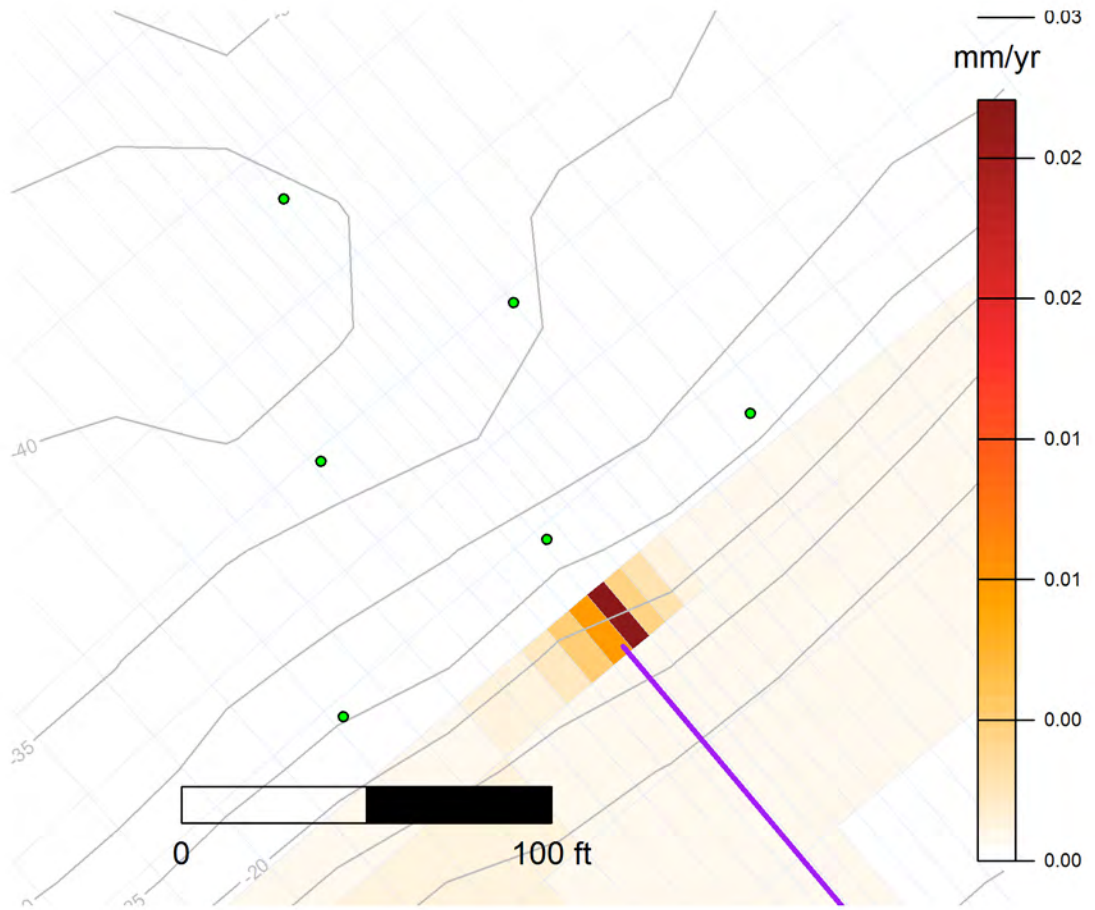
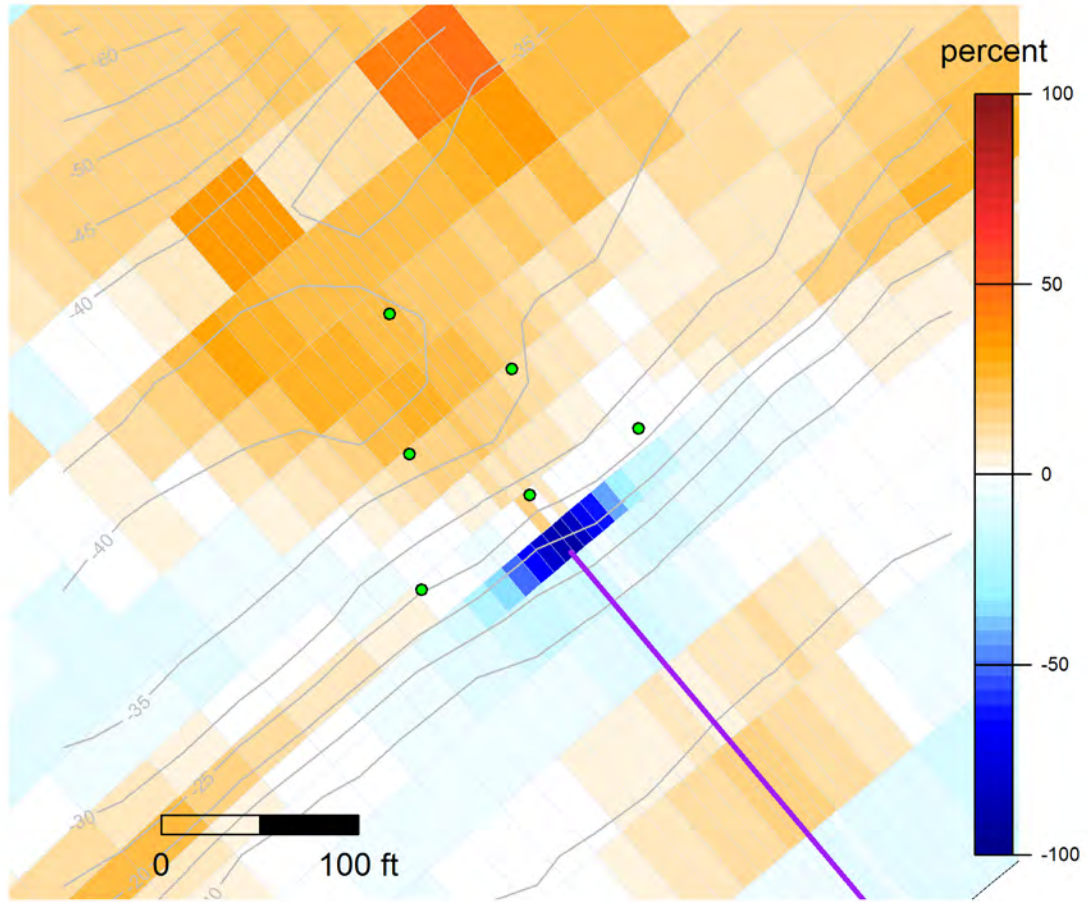


Figure 14. 53rd Ave. CSO predicted depositional rates with CSO input to bottom layer.

### 53rd Avenue SW



**Figure 15. Percent difference in predicted depositional rate with no CSO input to bottom layer compared to base simulation.**

## 7 Model Evaluation

---

### 7.1 Evaluation Procedure

The EFDC model predictions were qualitatively compared to sediment data collected around each CSO discharge. Presumably, higher sediment deposition rates should correspond to higher sediment concentrations for those chemicals with higher concentrations in CSO discharges than in the ambient sedimentation. Because of the large amount of uncertainty in the volume of previous CSO discharges, the chemical concentrations associated with those discharges, and the historic ambient conditions, a quantitative comparison was not undertaken. The qualitative comparison focused on comparing the spatial depositional pattern predicted by the model with the spatial variation in chemical concentrations.

Compounds that are expected to be good indicators for deposited CSO solids were identified by comparing the concentrations measured in solids collected from the CSO system to the concentrations measured in the collected ambient sediment samples. Chemicals were screened to identify likely candidates as those compounds that

- had a high concentration in CSO solids relative to ambient sediment concentrations, operationally defined as the 10th percentile concentration from the ambient sediment samples collected around the CSO outfalls.
- had a large range of concentration observed in the ambient sediments, defined as the ratio of the 90th percentile value to the 10th percentile value.
- had concentrations above the minimum detection limit (MDL) in at least 25% of samples.

Based on this screen, the following nine chemicals were used to compare sediment chemistry to model-predicted sediment deposition rates:

- Copper—copper piping plus brake pad wear
- Lead—historic tracer from gasoline
- Mercury—historically high concentrations from dentistry, industrial uses
- Silver—historically high concentrations from photo finishing
- Phenanthrene—a low molecular weight PAH (LPAH)
- Fluoranthrene—high molecular weight PAH (HPAH)
- Pyrene—an HPAH
- Bis(2-ethylhexyl)phthalate—common plasticizer
- Total polychlorinated biphenyls (PCBs)—historic industrial uses, urban stormwater runoff

In addition, cadmium and dibenzofuran were identified for fresh water.

Not used was 4-Methylphenol, which was identified as being present at a very high concentration in CSO solids relative to ambient sediments, but never detected in ambient sediments above the MDL. 4-methylphenol is produced by bacterial fermentation of protein in

the human large intestine, and known to be excreted in feces and urine. Likewise, hexachlorobenzene had high concentrations in CSO solids relative to ambient sediment concentrations, but was not detected in the ambient sediments.

Total LPAHs also met the screening criteria, but were not used because phenanthrene was expected to be a more sensitive compound. Total LPAHs are the sum of the following: naphthalene, acenaphthylene, acenaphthene, fluorene, phenanthrene, and anthracene.

Figure 16 presents the range of concentrations observed in solids collected from CSOs, freshwater sediments, and marine sediments for each of the nine chemicals. The concentrations for the freshwater and marine sediments are those collected for this CSO deposition model calibration, and are typically within 200 ft of a CSO discharge. Despite the potential contribution the CSO discharges may have to these sediment concentrations, the concentration associated with the CSO discharge tends to be higher than the ambient sediment concentrations.

The sensitivity of sediment concentrations to reflect the depositional pattern from a local source depends on the source concentration and depositional rate as well as the spatial variability of sediment concentrations resulting from other natural and anthropogenic sources. The minimum depositional rate that could be observed in sediment concentrations can be estimated using the following example.

Consider a hypothetical location where deposition from a nearby CSO discharge had a concentration factor of 10 larger than the ambient sediment concentration. Further, assume the analytical method is accurate to +/- 20% so that a 40% difference between two samples would be statistically significant at a 95% confidence level. Assuming constant, steady-state conditions, the sediment concentration at a location could be expressed as:

$$C = \frac{C_{CSO}D_{CSO} + C_A D_A}{D_{CSO} + D_A}$$

where C is the concentration and D represents the depositional rate of solids from the CSO and ambient sources. If the discharge concentration is 10 times the ambient concentration, and the concentration at the hypothetical location is required to be 140% of the ambient concentration ( $C_A$ ), the above equation can be rearranged to show that the corresponding depositional rate from the discharge needs to exceed 5% of the ambient sedimentation rate. With a typical ambient sedimentation rate of 1 cm/yr, this indicates that changes in sediment concentrations from discharge depositional rates below 0.4 mm/yr are unlikely to be distinguishable. If the concentration in the CSO discharge was a factor of 100 larger than the ambient sediment concentration, a similar analysis suggests depositional rates below 0.04 mm/yr are unlikely to be distinguishable.

Of the nine chemicals shown in Figure 16, bis(2-ethylhexyl)phthalate has the greatest range between median CSO solids concentration and median sediment concentrations.

## Solids/Sediment Concentration

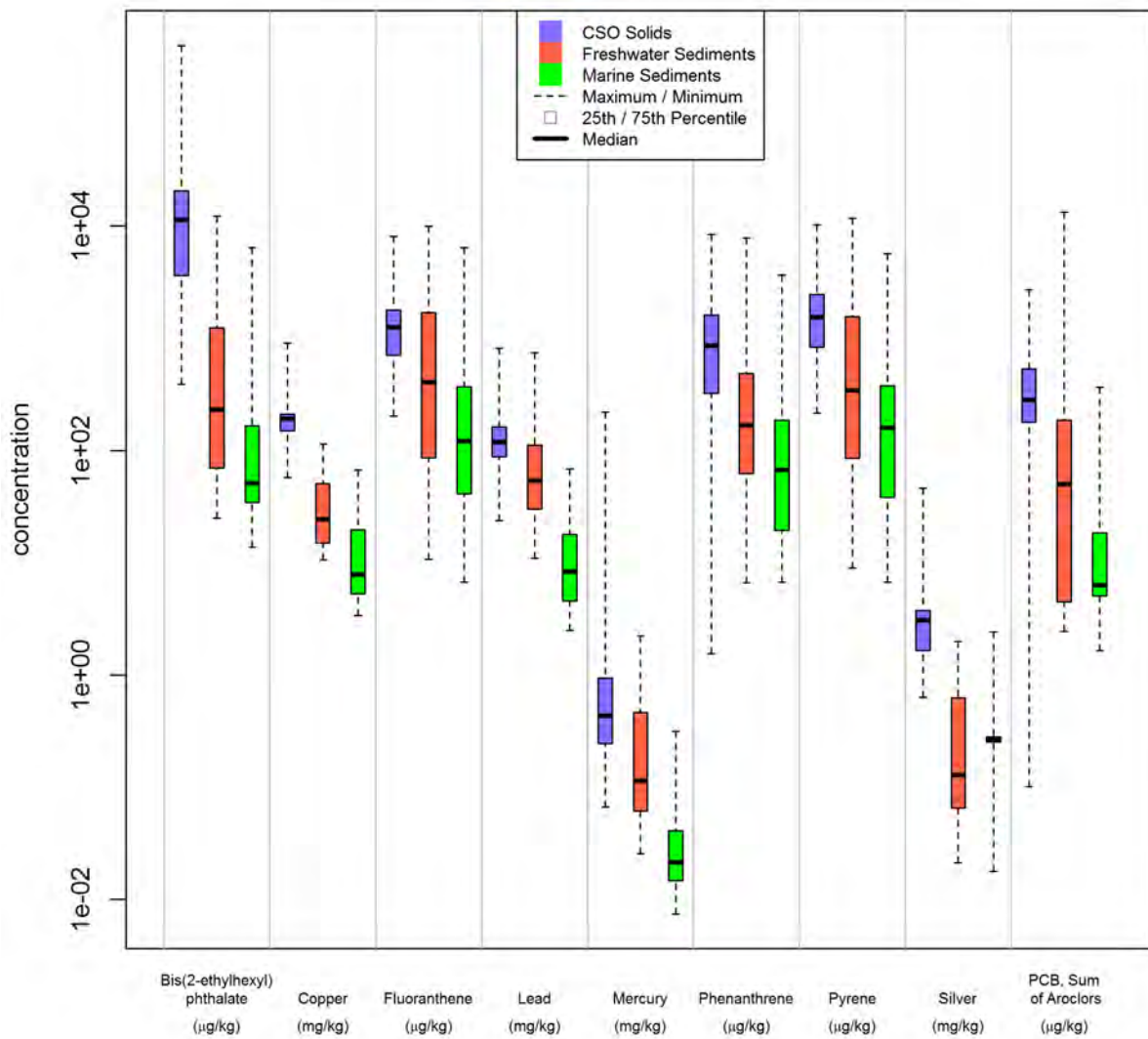


**Figure 16. Range of concentrations observed in CSO solids and ambient sediments.**

## 7.2 Verification Evaluation

This analysis is predicated on the concept that solids in CSO discharges will settle and accumulate in the ambient sediments surrounding the CSO. Locations that receive the greatest deposition from CSO discharges should have elevated concentrations of compounds that are found in CSO solids at elevated concentrations. The pattern of elevated concentration should be consistent across multiple chemicals, in that areas with the higher deposition rates should have higher sediment concentrations than areas with lower sediment deposition rates. The sediment

concentration of each chemical will vary depending on the source concentration, ambient deposition, water–sediment partitioning, biological uptake, or degradation. However, most processes are proportional to the concentration, so locations with higher concentrations should remain high relative to other locations. The concentration ratio between high and low deposition sites is expected to vary by chemical because of the differences in chemical properties. As a result, each chemical is expected to have higher sediment concentrations in areas of higher deposition than in other areas.

There may also be location-dependent conditions that affect the amount of sediment retained at each location. This may include spatial variation in the rate of pore water exchange and sediment scour from currents or vessel traffic. In these cases, it would be expected that all chemical compounds would be lower (or higher) than predicted.

To evaluate the pattern of solids deposition predicted by the EFDC model, the spatial pattern of multiple chemicals is compared to the model deposition rate. Assuming the current and historic CSO discharges have been elevated in these compounds, ambient sediment samples should be elevated in all of these compounds in areas that receive higher depositional rates of CSO solids. If a pattern is not apparent, either

- the CSO depositional rate is too low to overcome analytical and natural variability
- nearby source(s) are elevating concentrations of some chemicals at different locations
- sediment resuspension from either natural (tides) or human (boats) processes is causing sediment to be redistributed
- other processes not included in the modeling are modifying the sediment concentrations

Three figures explore the model deposition rates and sediment chemistry data at each CSO location. The first graphic overlays the sediment chemistry data over the spatial distribution of the modeled depositional rates. Sediment chemistry at each sampling location is shown as a pie graph where each “slice” corresponds to one chemical and the length of the slice represents the concentration. To help patterns be more apparent, the length corresponds to the logarithm of the concentration, normalized to the average concentration of all the stations shown at each site. The red circle represents the average concentration. Non-detected compounds are shown as open pie segments, with the length representing the MDL. In calculating the average concentration, one-half of the MDL was used for non-detected compounds. For example, a station with a chemical above the average concentration at that CSO station group would have a pie segment extend beyond the circle while a chemical below the average would have the segment not reach the circle. Concentrations of these chemicals above the average would occur wherever CSO solids deposited at higher rates compared to background sedimentation and would be below the average in areas not getting much CSO solids deposition. Conversely, little variation from the average across all stations occur at sites with low deposition and likely represent the natural variability in background concentration.

The second graphic plots the concentration of the nine chemicals identified as markers for CSO solids against the concentration of the other eight chemicals. An area with accumulation of CSO solids should show a high degree of correlation between the chemical concentrations; particularly those that have similar chemical properties.

The third graphic plots the concentration of the same nine chemicals against the predicted CSO deposition rate at each sampling location. The modeled deposition rate will be correlated to the observed sediment chemistry if the model predicts a similar spatial pattern and the signal is above the natural and analytical variability. Non-detected compounds are plotted with a “+” symbol at one-half the MDL. Detected compounds are plotted with an “o” symbol. Both the detected and non-detected values are included in determining the linear least-squares regression line. MDL levels expressed as dry-weight concentrations vary between samples because of the total solids in the sample. Separating detects and non-detects aids in interpretation. For instance, a correlation between sediment concentration and deposition rate is not expected if all samples were below the MDL. However, a correlation would be expected if some samples were below detection, but others had detectable levels.

### 7.2.1 North Beach Pump Station

In general, the sediment concentrations near the North Beach CSO were slightly higher directly offshore of the discharge at CSO\_NB-3 (Figure 17). The results for bis(2-ethylhexyl)phthalate in the samples collected in 2011 were all laboratory qualified because of high concentrations in laboratory blanks.

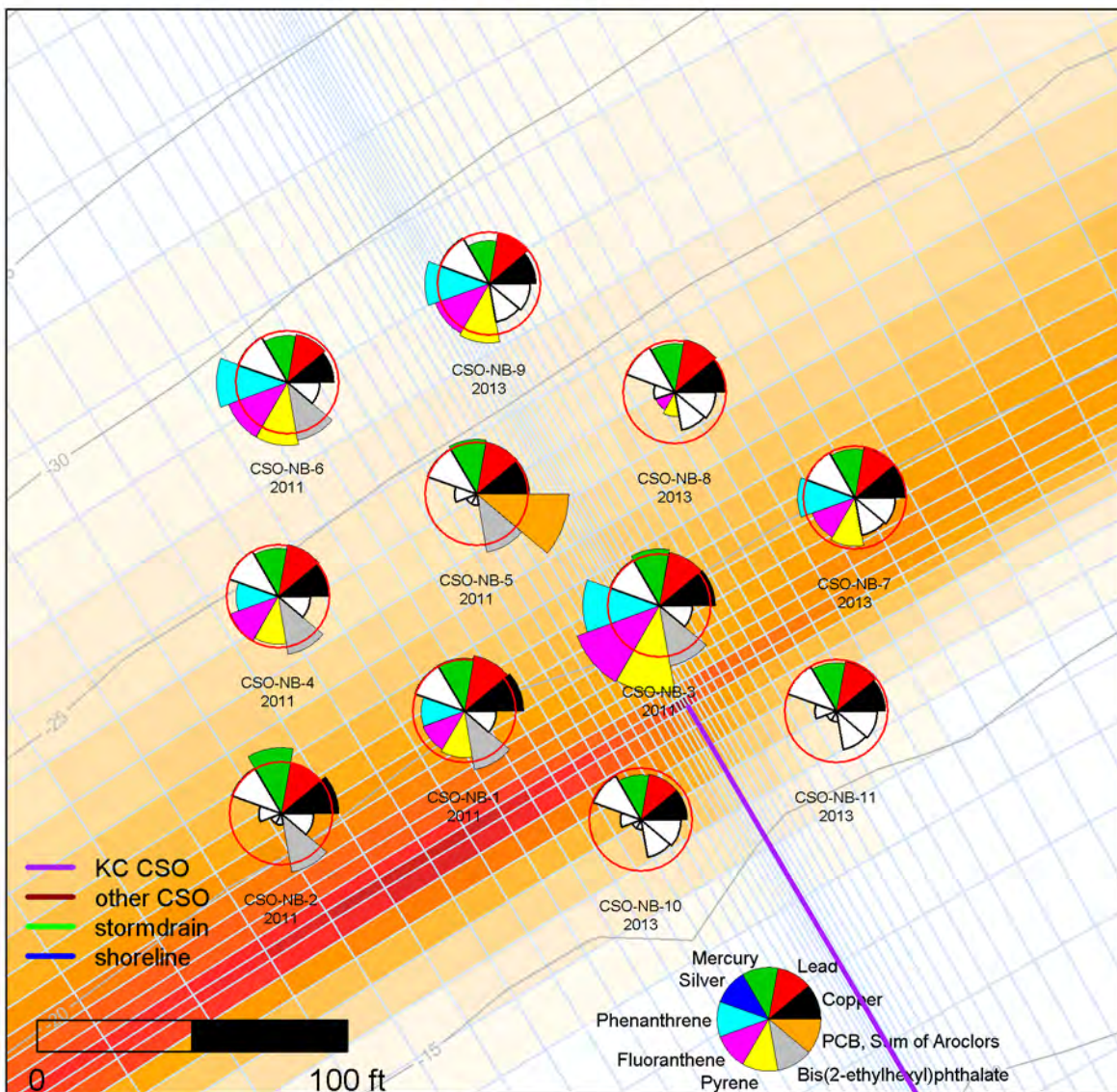
The pair-wise plots (Figure 18) show good correlation between phenanthrene, fluoranthene, and pyrene, but little to no correlation with other chemicals. A high degree of correlation between phenanthrene, fluoranthene, and pyrene is expected because all three are polycyclic aromatic hydrocarbons, whose primary source in urban environments is thought to be formation during combustion processes. There also appears to be some correlation between copper, lead, and mercury, but little to no correlation with other chemicals. The range of detected concentrations for copper and lead is relatively small, implying a lower confidence in the correlation. The two sets of correlated parameters may indicate a different source for the metal and organic parameters, or natural variability in the sediment composition.

Comparing the correlation of sediment chemical concentrations to the predicted CSO solids deposition rate (Figure 19), there is no correlation for most compounds. This suggests two possible interpretations. The first interpretation is that there was insufficient deposition from the North Beach CSO at any of the sampling sites to elevate the chemical concentrations. The model predicted deposition rates below 0.1 mm/yr beyond 20 ft from the discharge. With a characteristic Puget Sound sedimentation rate of 1 cm/yr, this suggests that an insufficient chemical mass was deposited at any of the sampling locations to have a significant influence on chemical concentrations, and the variability observed is a result of other processes.

The alternative interpretation is that the model has poor performance in predicting the deposition pattern, resulting in little correlation with the observed data. However, the sediment concentrations have generally low correlation between chemicals, suggesting that there is not a consistent deposition pattern of elevated concentrations. The higher PAH concentrations at the station closest to the discharge (CSO\_NB-3) are suggestive of the CSO discharge as the source. Although this cannot be entirely ruled out, the lack of elevated concentrations in other compounds at this site is indicative that there is not a high rate of CSO solids accumulation at this site.

The lack of an apparent spatial pattern in the sediment chemistry suggests no conclusion can be made about the accuracy of the EFDC model prediction. With the low deposition rates predicted at North Beach, the chemical signature of the CSO discharge may be less than the natural variability of background concentrations (or laboratory accuracy), and thus a spatial pattern is not apparent in the data. However, the higher PAH concentrations at CSO-NB-3, the station closest to the discharge, are suggestive that the CSO discharge is the source of these compounds. This would indicate that the model may underestimate deposition offshore of the discharge. However, it is unclear why the furthest offshore sites (CSO-NB-6, CSO-NB-9) also have elevated PAH concentrations. The range of concentrations observed may reflect variability of background concentrations more than the deposition pattern from the CSO discharge.

## North Beach CSO



Segment length proportional to logarithm of detected value, unfilled segments indicate MDL

**Figure 17. North Beach sediment concentrations for selected compounds.**

# North Beach CSO

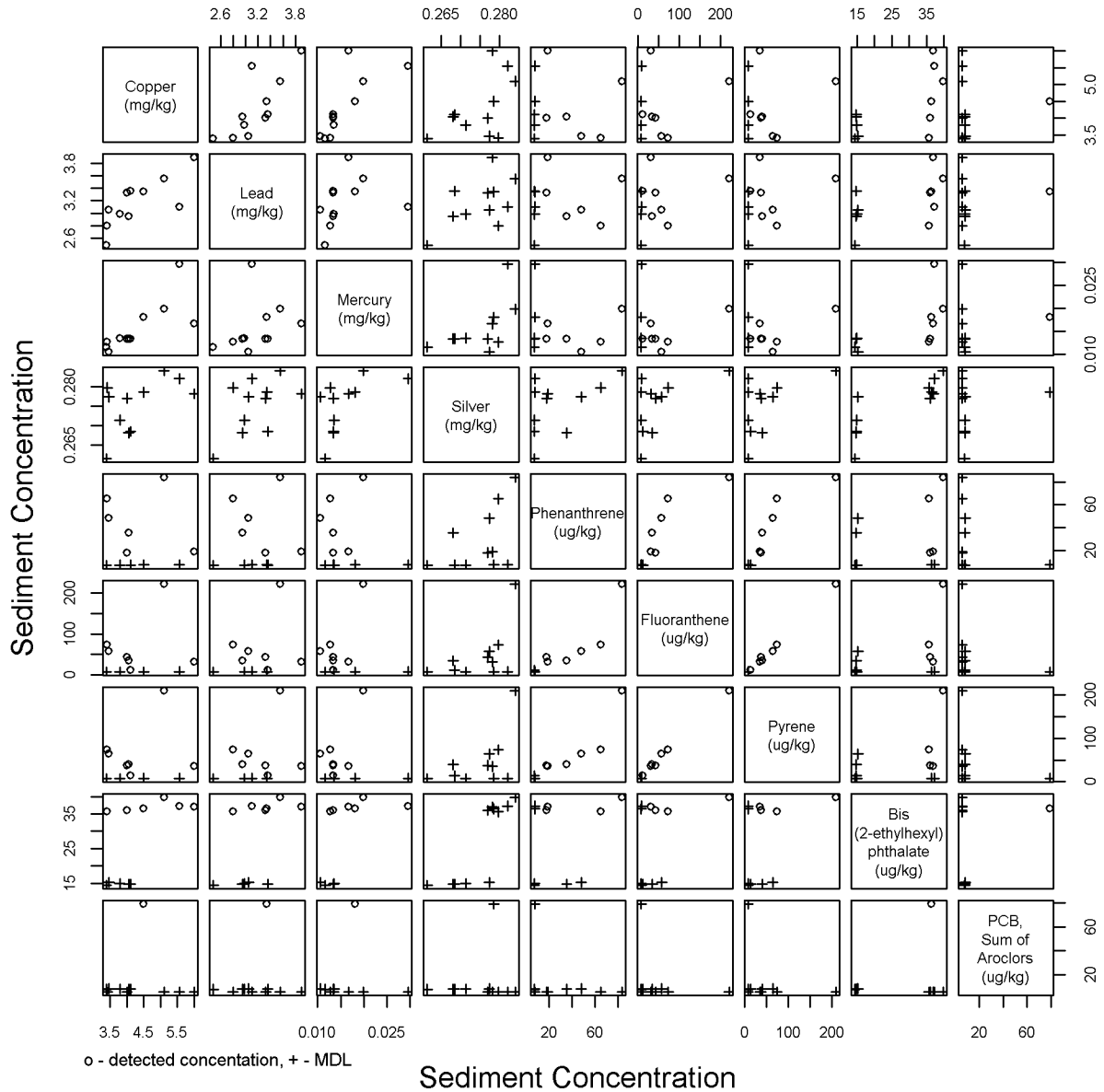


**Figure 18. Parameter-parameter plot of sediment concentrations at North Beach CSO.**

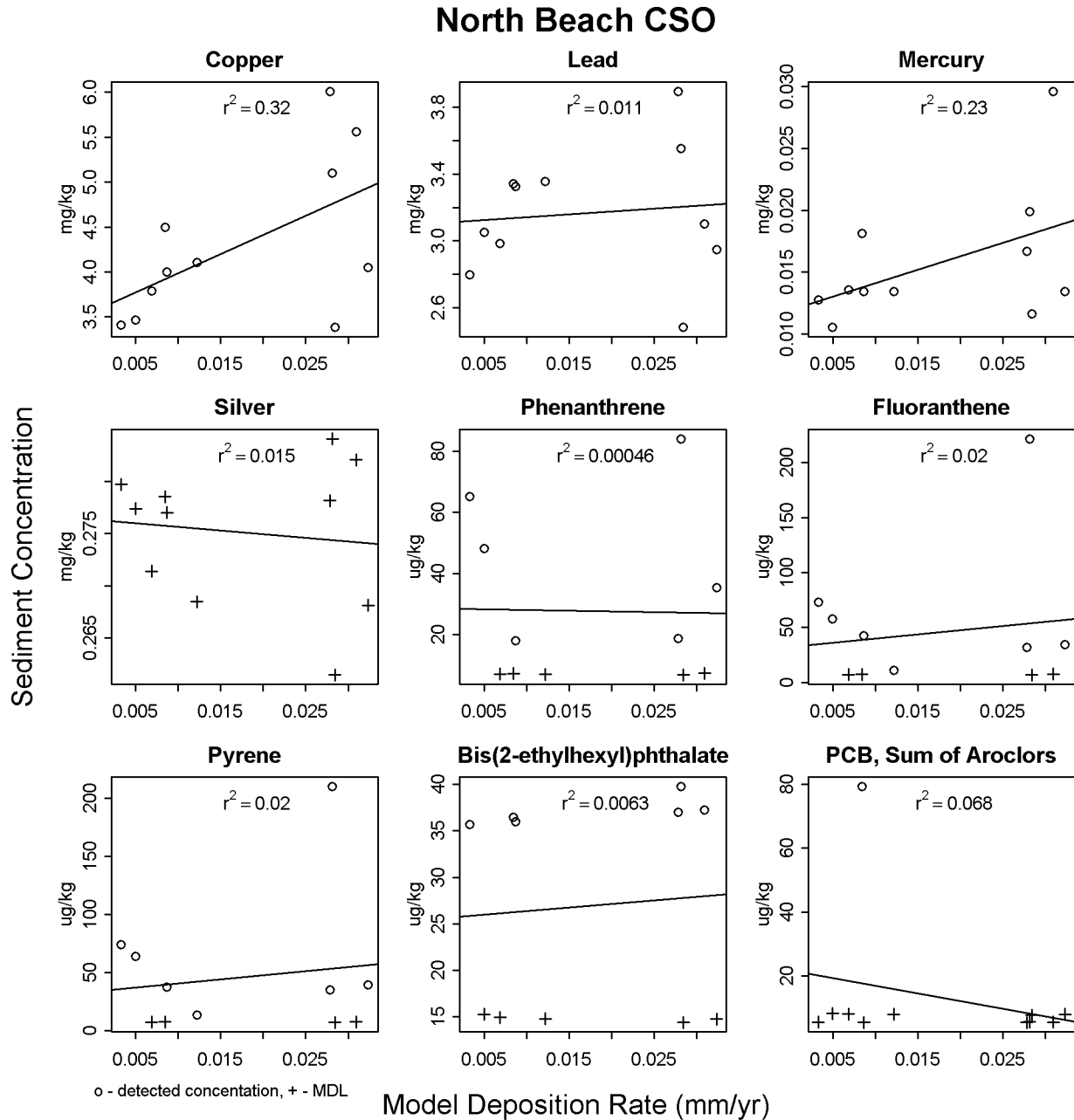


**Figure 19. Sediment concentrations versus predicted sediment depositional rates at North Beach CSO**

### 7.2.2 South Magnolia CSO

In general, sediment concentrations near the Magnolia CSO were slightly higher for inshore samples compared to offshore samples (Figure 20). Bis(2-ethylhexyl)phthalate, copper, and lead appeared slightly elevated at CSO-MG-2. Station CSO-MG-7 was added to sample in the depositional pattern suggested by the EFDC model. The copper concentrations were higher at this station.

The pair-wise plots (Figure 21) show good correlation between fluoranthene and pyrene, but little to no correlation with other chemicals. Some correlation is apparent between lead and bis(2-ethylhexyl)phthalate.

In contrast to the pair-wise plots and other compounds, there is an apparent correlation between sediment copper concentrations and the predicted CSO solids deposition rate (Figure 22). Compared to the North Beach CSO, the range of copper concentrations is larger (more than a factor of 2) and the predicted deposition rate is an order of magnitude larger, suggesting that this may be more than natural variability. With the exception of the lower concentrations at CSO-MG-7, a relationship also appears to exist between predicted depositional rates and both lead and bis(2-ethylhexyl)phthalate. The correlation is not apparent for the PAH compounds; however, the concentration range of these compounds is similar to the North Beach observations, suggesting other variability may dominate the distribution of these chemicals. Similarly, the concentration range of mercury, silver (not detected), and PCBs is low and, therefore, not good parameters at this location for comparison with model predictions.

A potential confounding factor is the location of the Magnolia CSO overflow directly west of the Elliott Bay marina (Figure 23). With extensive use of copper as a marine anti-fouling agent, it is possible that the marina contributes to the elevated sediment copper concentrations. Likewise, fuel and combustion sources at the marina could contribute to the PAH sediment concentrations, although there does not appear to be a spatial pattern in the distribution of these compounds.

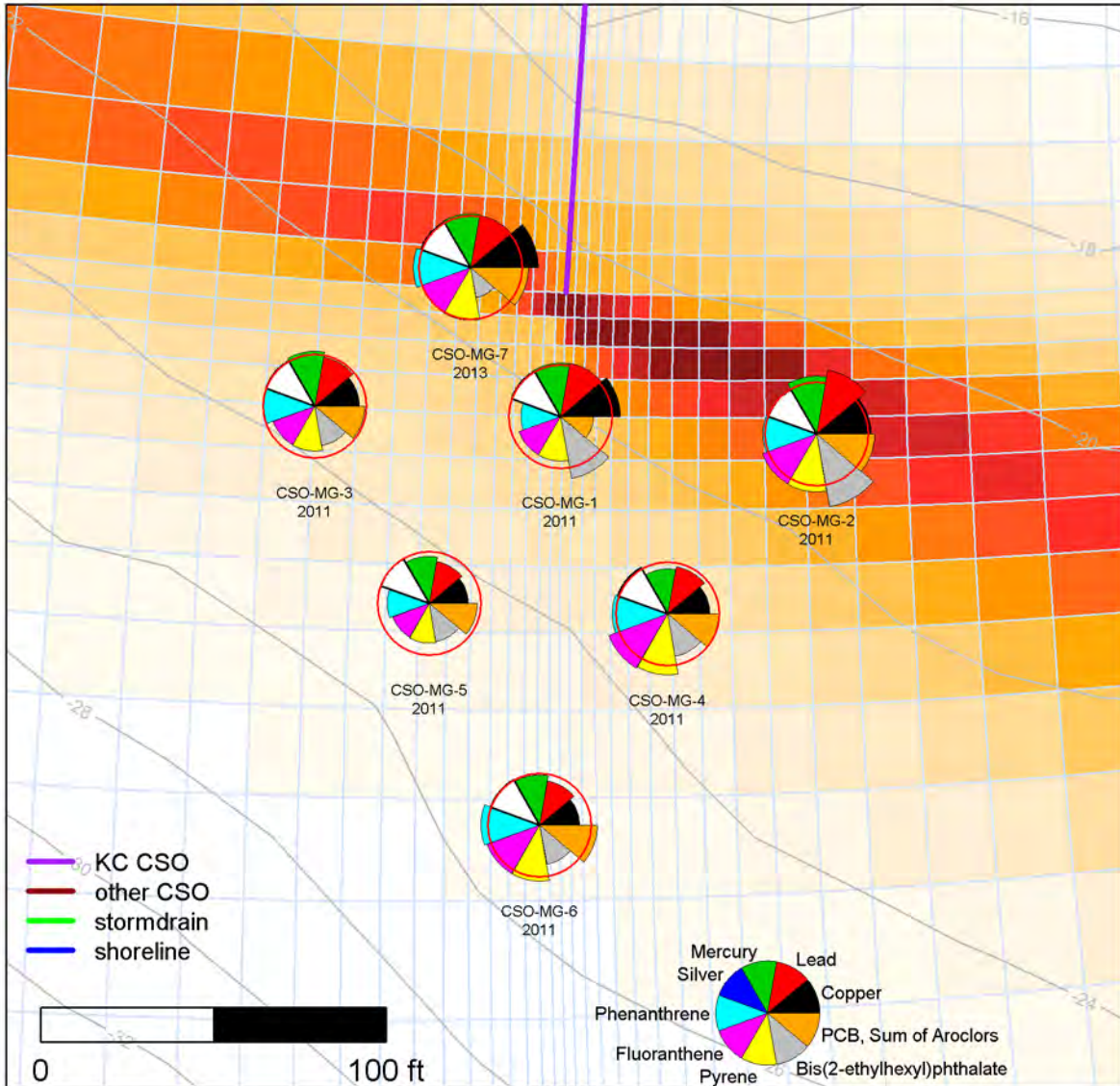
The outfall was relocated to its current alignment in 1999. With typical sedimentation rates of 0.3 to 1.4 cm/yr measured in Elliott Bay, the expected sediment accumulation is 4 to 17 cm while the sediment sampling targeted the top 10 cm. Although this is not expected to change the depositional pattern, vertical mixing could reduce the apparent increase.

The sediment concentrations seem to generally align with the model's predictions of higher deposition rates at the inshore sampling stations (CSO-MG-1, CSO-MG-2, CSO-MG-7). Beyond this general agreement, the lack of a consistent spatial pattern in the concentrations for multiple parameters suggests no conclusion can be made about the accuracy of the EFDC model prediction. While the predicted deposition rates are up to 0.4 mm/yr, the chemical signature of the CSO discharge may be less than the natural variability of background concentrations (or laboratory accuracy), and thus a spatial pattern is not apparent in the data. The chemical signature to background variability may vary by chemical, so the depositional pattern may be reflected in the copper, lead, and mercury concentrations while other chemical concentrations are dominated by the natural variability.

The original South Magnolia overflow was replaced in 1999 with the current outfall. Previously, the outfall had two branches: one extended approximately 300 ft further offshore and east of the current discharge and the other terminated approximately 400 ft further inshore and west of the current discharge. These discharges are sufficiently distant from the current outfall location that they are not anticipated to contribute to sediment concentrations around the current outfall. Depending on the local ambient sedimentation rate, the 10-cm-deep sediment samples may

include sediment deposited before the outfall construction, resulting in a dilution of the contribution of CSO solids in the sediment sample relative to a steady-state condition.

### Magnolia Overflow



Segment length proportional to logarithm of detected value, unfilled segments indicate MDL

**Figure 20. Magnolia sediment concentrations for selected compounds**

# Magnolia Overflow

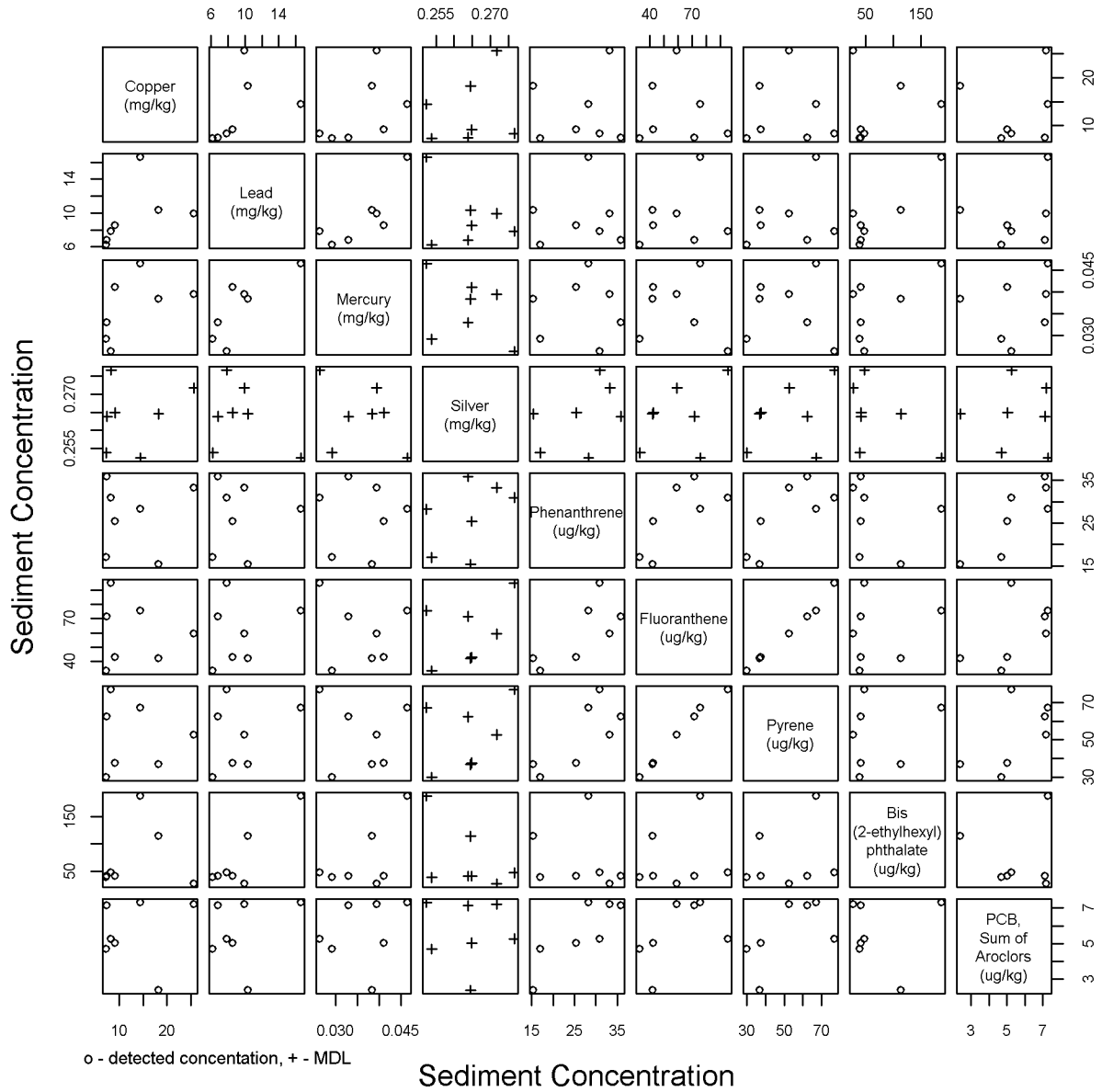


**Figure 21. Parameter-parameter plot of sediment concentrations at Magnolia CSO.**

## Magnolia Overflow

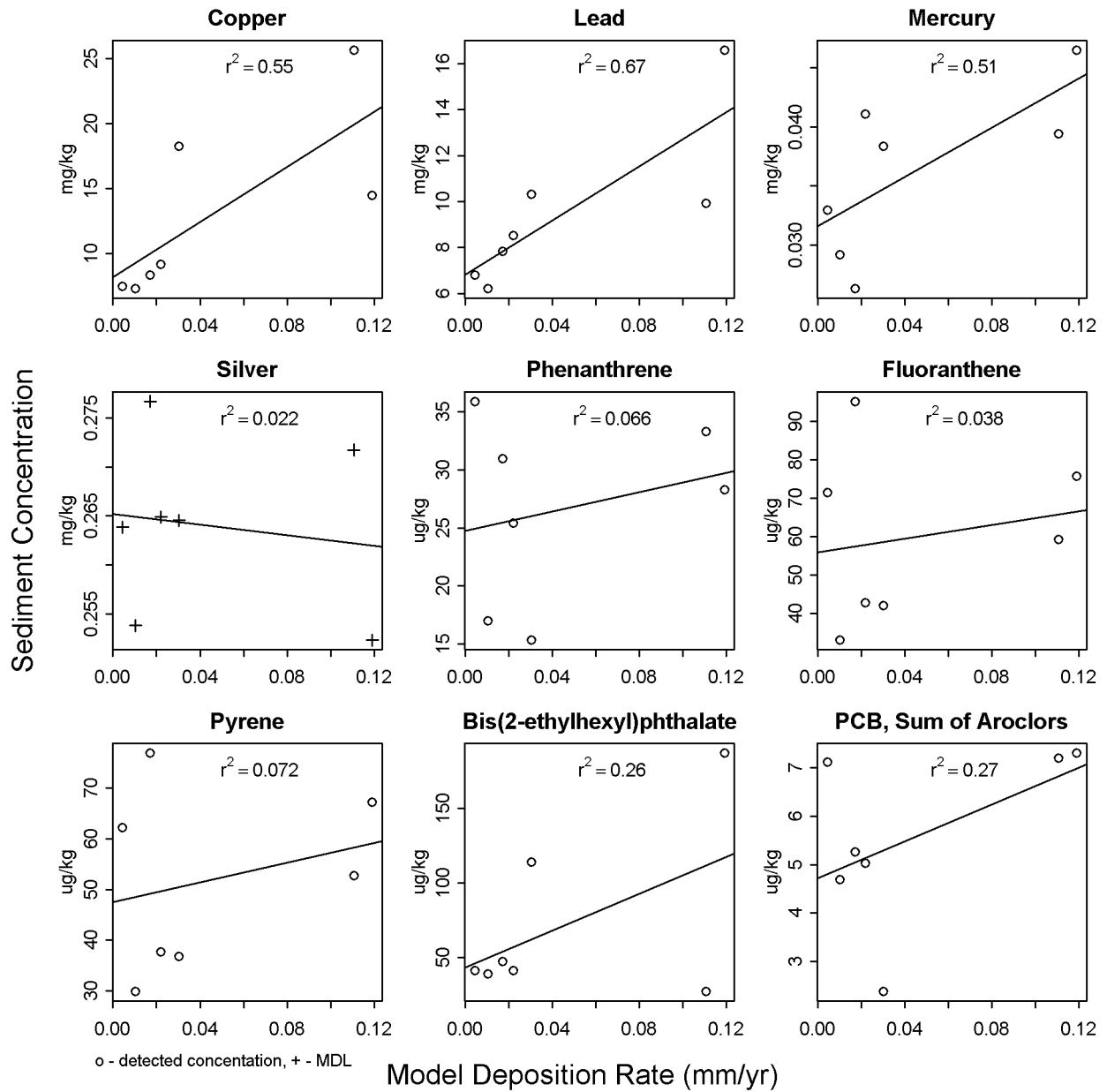


**Figure 22. Sediment concentrations versus predicted sediment depositional rates at Magnolia CSO.**



**Figure 23. South Magnolia Outfall in relation to Elliott Bay Marina.**

### 7.2.3 53rd Avenue Pump Station

Sediment concentrations near the 53rd Ave. Pump Station CSO were higher at the station closest to the CSO and at the station furthest offshore (Figure 24). Copper was significantly higher near the CSO at station CSO-53-1. Parameters such as lead and mercury appeared to increase with depth.

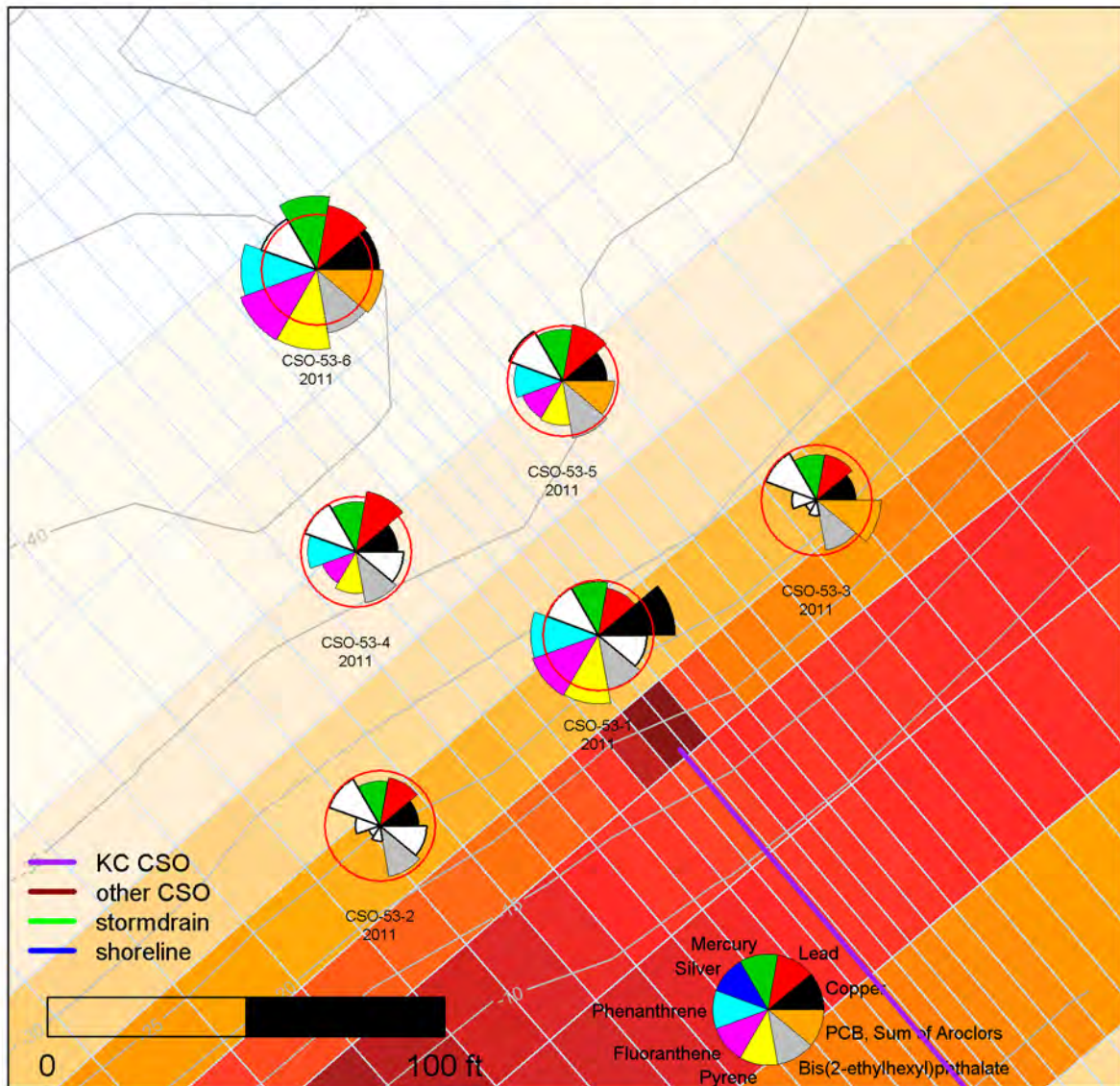
The pair-wise plots (Figure 25) show good correlation between the three PAH compounds (phenanthrene, fluoranthene, and pyrene). Although a lesser correlation may be apparent between the PAHs and bis(2-ethylhexyl)phthalate or mercury, a similar correlation also appears to exist with silver. Silver was not detected in any of these samples, and the values reflect the variation in total solids between samples. The MDLs shown for silver are identical for each sample on a wet-weight basis, and the conversion to a dry-weight basis results in the variation shown. This suggests that much of the variation seen is due to natural variation in the sediments.

A negative correlation exists between the predicted CSO solids depositional rate and most sediment chemical concentrations (Figure 26). Because of the infrequency of overflows at the 53rd Ave. CSO, the modeled depositional rate is the lowest of all CSOs simulated—less than 0.001 mm/yr at the sampling stations. As a result, the contribution of CSO discharges to sediment concentrations is likely very small and no pattern may be detectable.

Spatially, it seems plausible that the EFDC model might underpredict the deposition immediately offshore of the CSO, thereby underpredicting the depositional amount at sample location CSO-53-1. However, the higher concentrations at the offshore location CSO-53-6 appear not to be connected to the CSO discharge given the lower concentrations observed at the intermediate stations CSO-53-4 and CSO-53-5. Thus, it seems more likely that the elevated concentrations at CSO-51-1 and CSO-53-6 are related to factors other than the CSO discharge rather than the model exhibiting poor performance in predicting this deposition pattern.

The sediment concentrations at the 53rd Ave. SW CSO appear to be reflective of ambient concentrations, similar to other Puget Sound sites, supporting the low predicted deposition rates at this site. Variation in the sediment chemistry could be partially attributable to the original use of the 53rd St. outfall as a raw sewage discharge prior to operation of the Alki treatment plant in 1958, or natural variability. The lack of an apparent spatial pattern in the sediment chemistry suggests no conclusion can be made about the accuracy of the EFDC model prediction beyond deposition rates are sufficiently small at a maximum of 0.003 mm/yr that only the natural variability of background concentrations (or laboratory accuracy) is expected.

## 53rd Avenue SW



Segment length proportional to logarithm of detected value, unfilled segments indicate MDL

**Figure 24. 53rd Ave. sediment concentrations for selected compounds.**

## 53rd Avenue SW

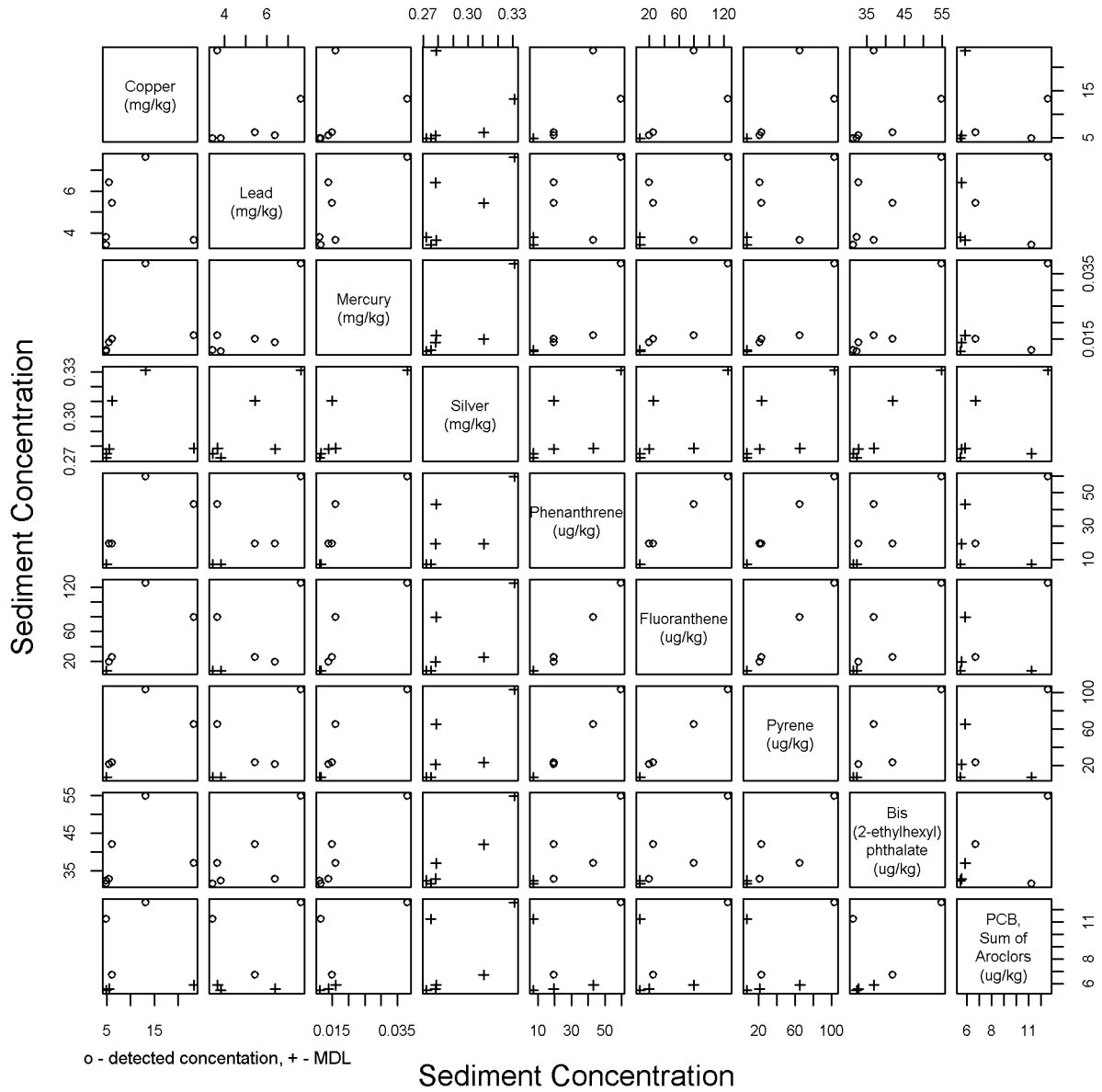


**Figure 25. Parameter-parameter plot of sediment concentrations at 53rd Ave. CSO.**

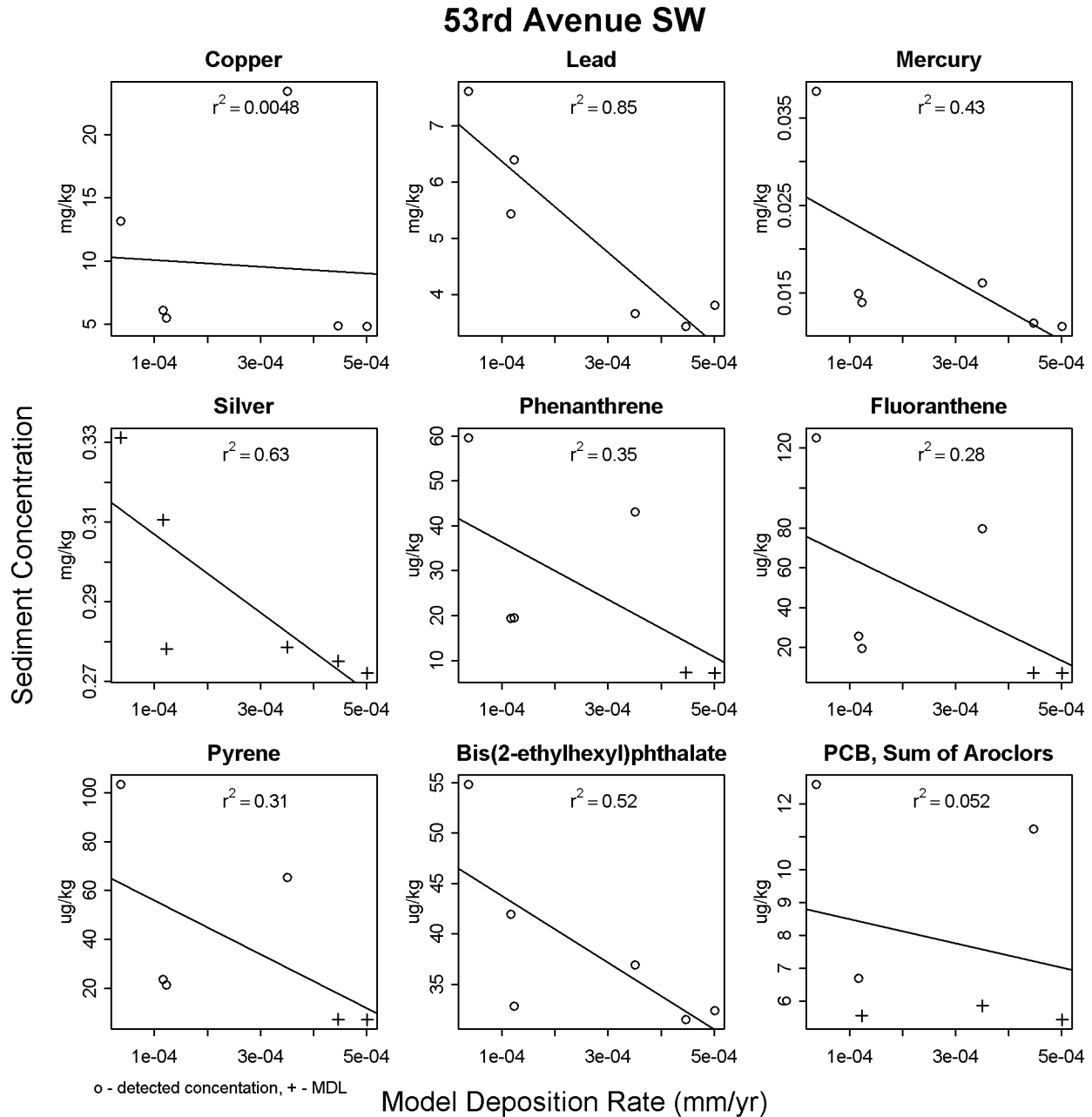


**Figure 26. Sediment concentrations versus predicted sediment depositional rates at 53rd Ave. CSO.**

### 7.2.4 Murray Avenue Pump Station

The sediment sampling locations around the Murray Ave. Pump Station CSO were originally set based on a significant offshore momentum of the discharge. It was later realized that flowrates were overestimated by omitting a hydraulic constraint and that the horizontal spreading of the buoyant plume would reduce the effect of the offshore momentum. Samples were subsequently collected closer to the CSO and to the north at stations CSO-MY-8 through CSO-MY-13, based

on the EFDC deposition pattern (Figure 27). The PAH concentrations are dominated by high values at CSO-MY-9. Because other chemicals do not have extremely high values at this station, it seems appropriate to consider if another source could be the cause. The EFDC model predicted higher depositional rates to the north of the CSO, and copper and lead have slightly higher values to the north.

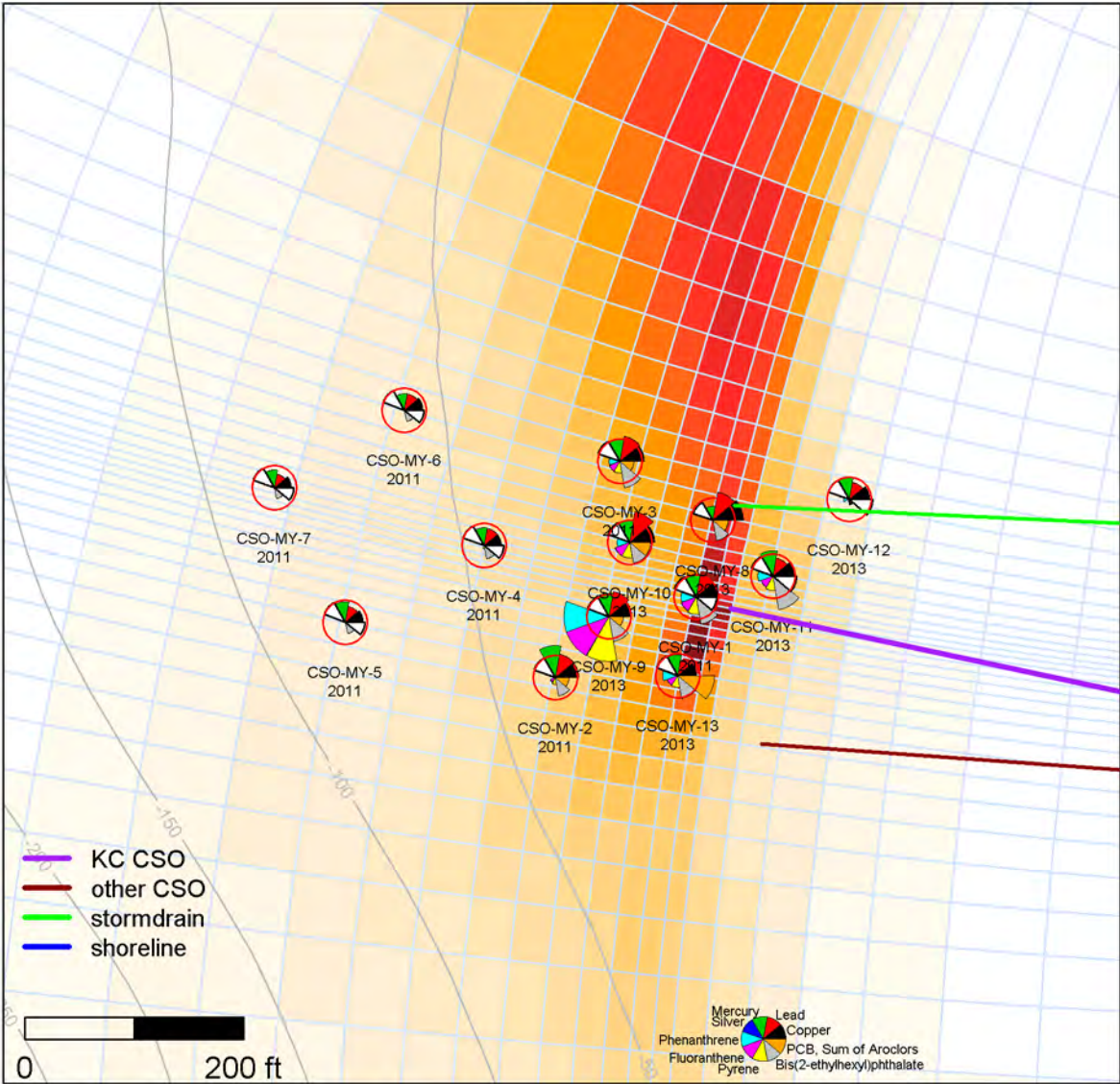
The pair-wise plots (Figure 28) show some correlation between copper and lead; otherwise, highly correlated parameters are not discernable.

Comparing sediment concentrations and the predicted CSO solids deposition rate (Figure 29), a loose correlation exists for several chemicals: copper, lead, and bis(2-ethylhexyl)phthalate. Although the correlation with the model predictions is not high, the spatial distribution of chemicals (Figure 27) does suggest a cluster of stations with higher copper and lead concentrations at CSO-MY- 1,3,8,9,13, generally to the north of the CSO discharge. This cluster of stations appears to be consistent with the deposition pattern from the CSO discharge, but the stormwater outfall to the north of the CSO may also be an influence on the concentrations. The local collection system CSO outfall to the south may also contribute to the spatial concentration variability.

Compared to the North Beach CSO, the predicted deposition rates at the sampling locations is similar (0 to 0.02 mm/yr at Murray, 0 to 0.027 mm/yr at North Beach), whereas the range of copper concentrations in the sediment samples was about a factor of two larger (4 to 15 mg/kg at Murray, 3.5 to 6 mg/kg at North Beach), and even greater for lead (4 to 22 mg/kg at Murray, 2.6 to 3.8 mg/kg at North Beach). With similar deposition rates, similar chemical concentrations would be expected, supporting the concept that the increased chemical concentrations result from the nearby stormwater and CSO discharge. Similar to North Beach, the low deposition rates predicted by the model suggest a de minus increase in sediment concentrations from the CSO. While Murray and North Beach are similar in being submerged discharges at similar depths in Puget Sound (Table 1), Murray has approximately double the annual CSO discharge of North Beach (Table 5), a larger outfall pipe, and much higher flowrates. The alternate possibility is that the model should predict higher deposition rates at Murray, explaining the higher sediment concentrations and poor spatial correlation with the observations.

The concentration of the PAH compounds (phenanthrene, fluoranthene, and pyrene) at CSO-MY-9 was about 20 times larger than any other sediment sample near the Murray CSO. The concentration of these three PAHs exceeded the 75th percentile concentration in solids collected from within the CSO pipes (Appendix B). Because the correlations with these compounds are dominated by this high value, the plots discussed above are repeated with these high values omitted (Figure 30 to Figure 32). A general correlation between the PAHs and bis(2-ethylhexyl)phthalate and a general correlation between concentration and the predicted depositional rate can be seen.

# Murray Avenue



Segment length proportional to logarithm of detected value, unfilled segments indicate MDL

**Figure 27. Murray Ave. CSO sediment concentrations for selected compounds.**

# Murray Avenue

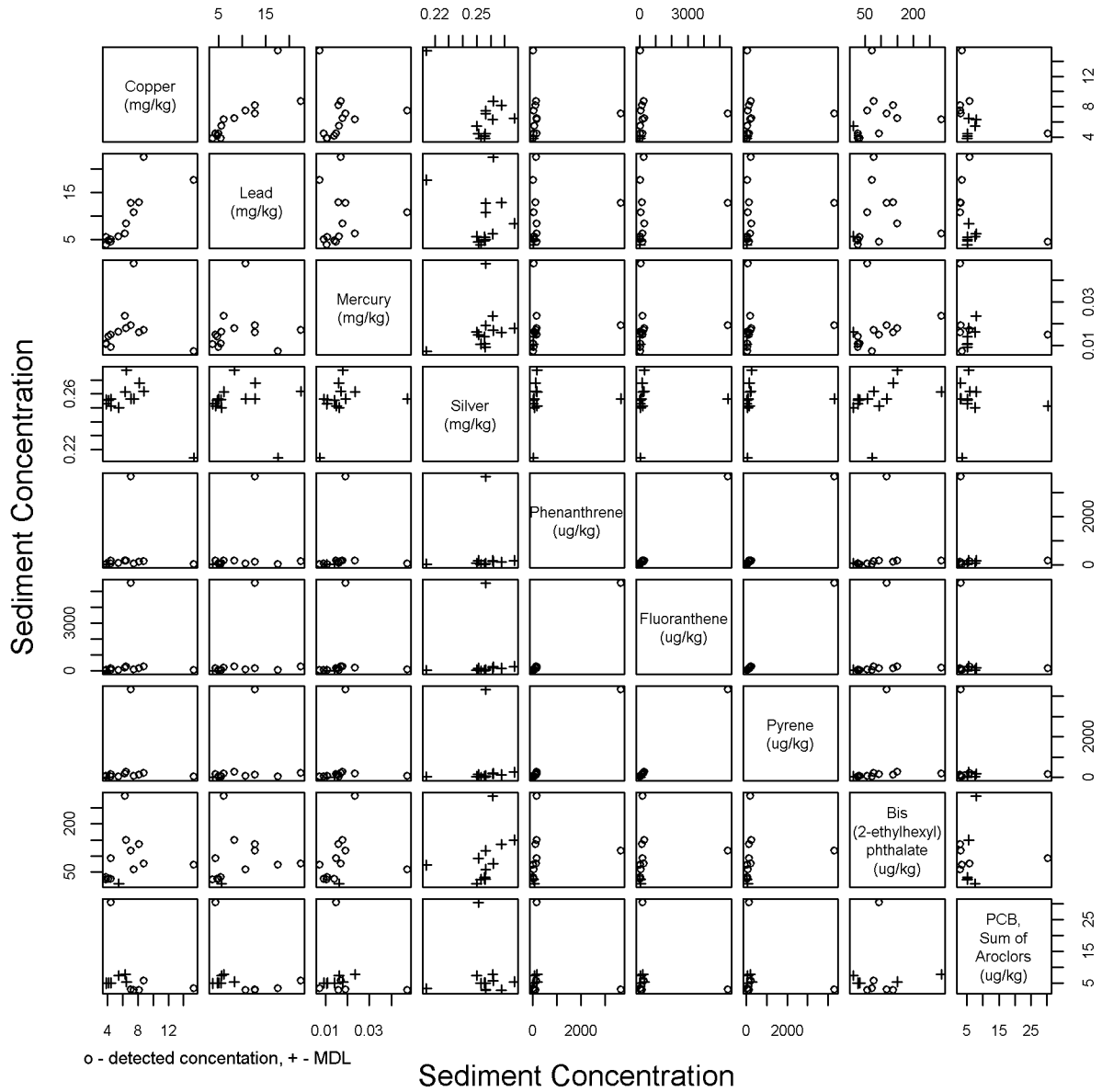


**Figure 28. Parameter-parameter plot of sediment concentrations at Murray CSO.**

## Murray Avenue

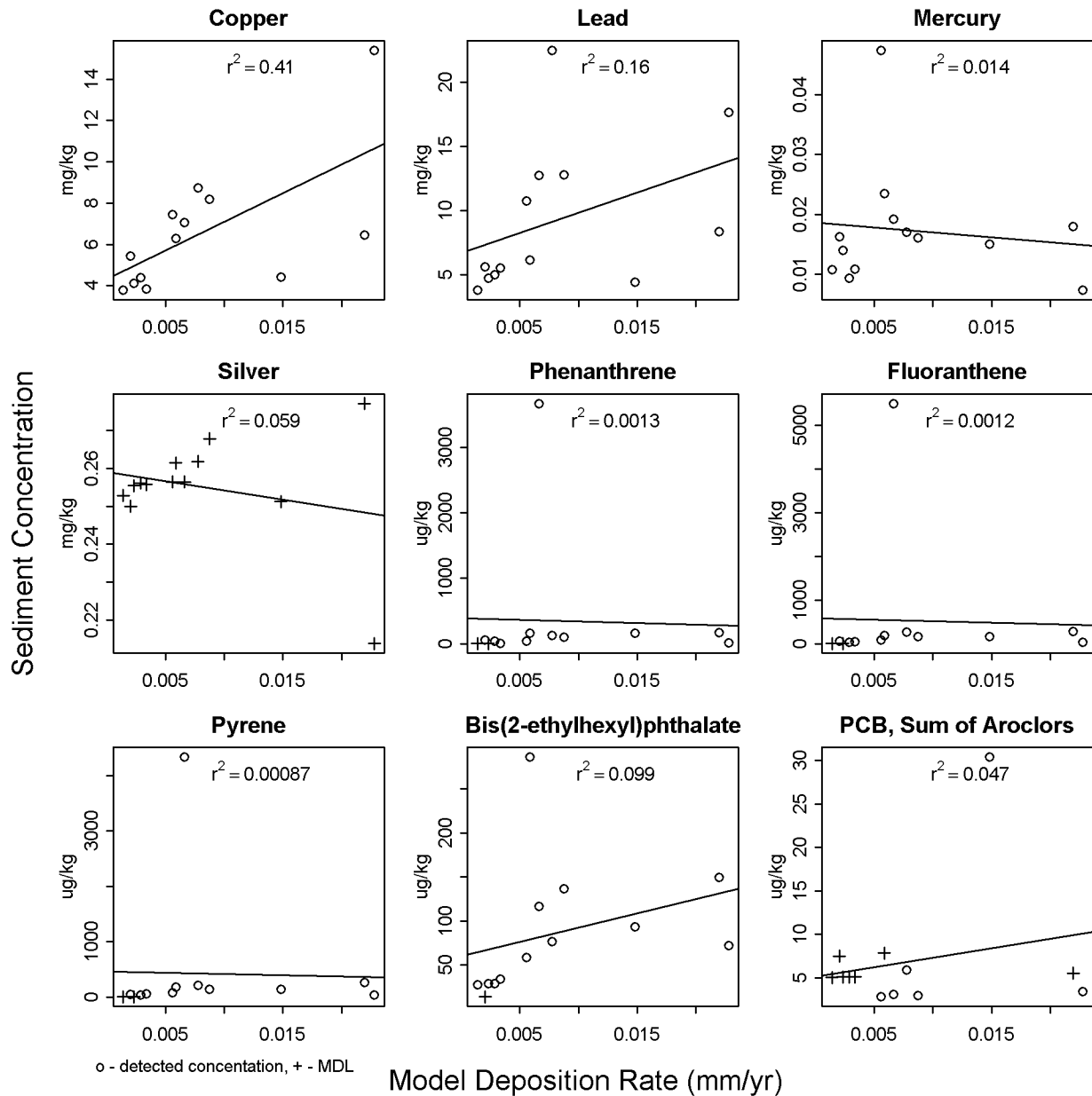
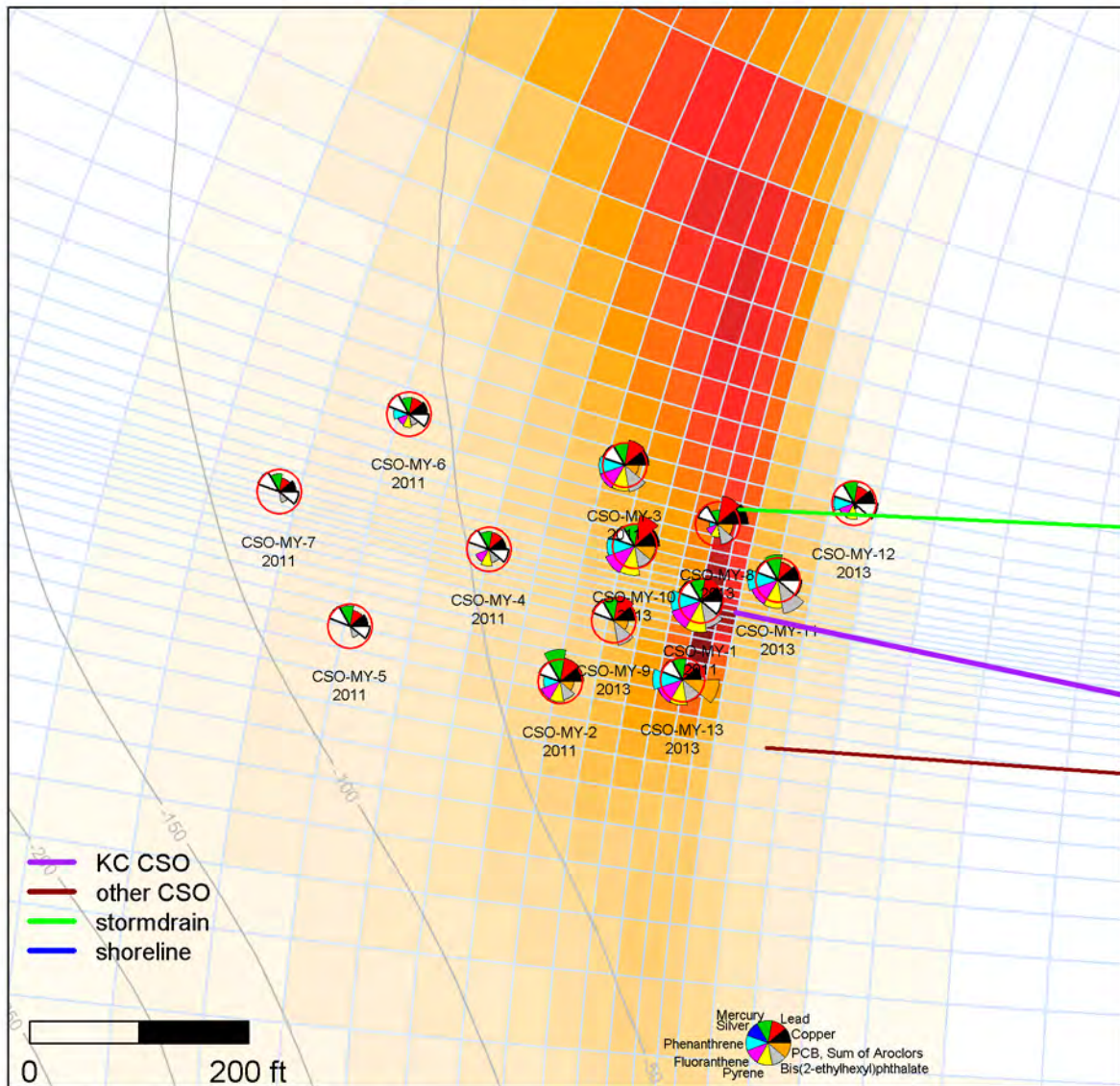


**Figure 29. Sediment concentrations versus predicted sediment depositional rates at Murray Ave. CSO.**

## Murray Avenue outlier removed



Segment length proportional to logarithm of detected value, unfilled segments indicate MDL

**Figure 30. Murray Ave. CSO sediment concentrations without PAH values at CSO-MY-9.**

# Murray Avenue outlier removed

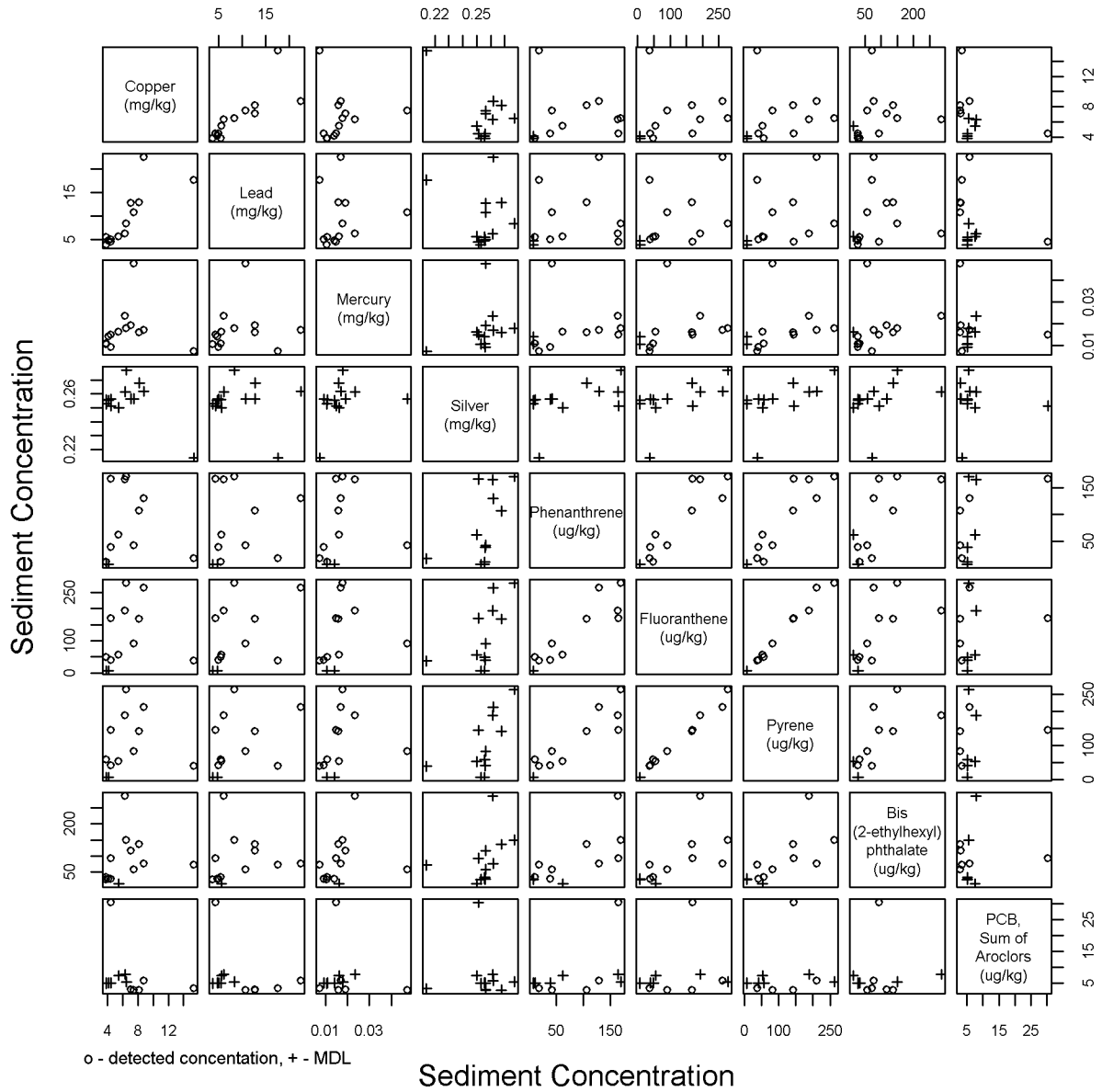
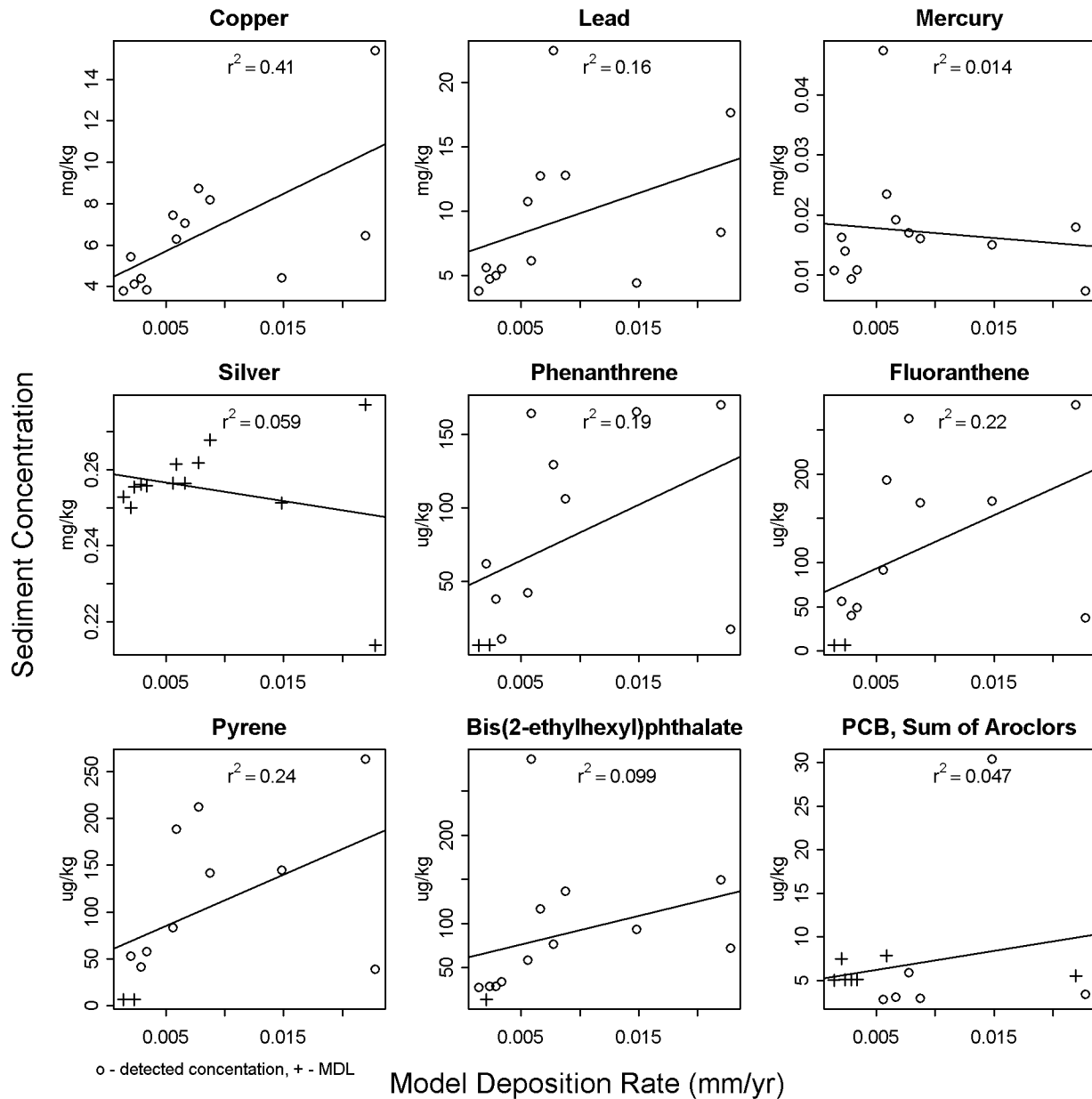


Figure 31. Parameter-parameter plot at Murray CSO without PAH values at CSO-MY-9.

## Murray Avenue outlier removed



**Figure 32. Sediment concentrations versus predicted sediment depositional rates at Murray Ave. CSO without PAH values at CSO-MY-9.**

### 7.2.5 Barton Street Pump Station

The initial sediment sampling results around the Barton St. Pump Station CSO were atypically high in most PAHs and difficult to interpret. All sampling sites plus additional sites to the north and shoreward were sampled again in 2016 (Figure 33, Figure 33). Because all stations were resampled in 2016, all data presented here are from the 2016 sampling event. Similar to Murray, a stormwater outfall exists to the north of the CSO discharge and a local collection system CSO

discharge exists to the south. Sediment concentrations may also be affected by the ferry terminal 250 ft to the south.

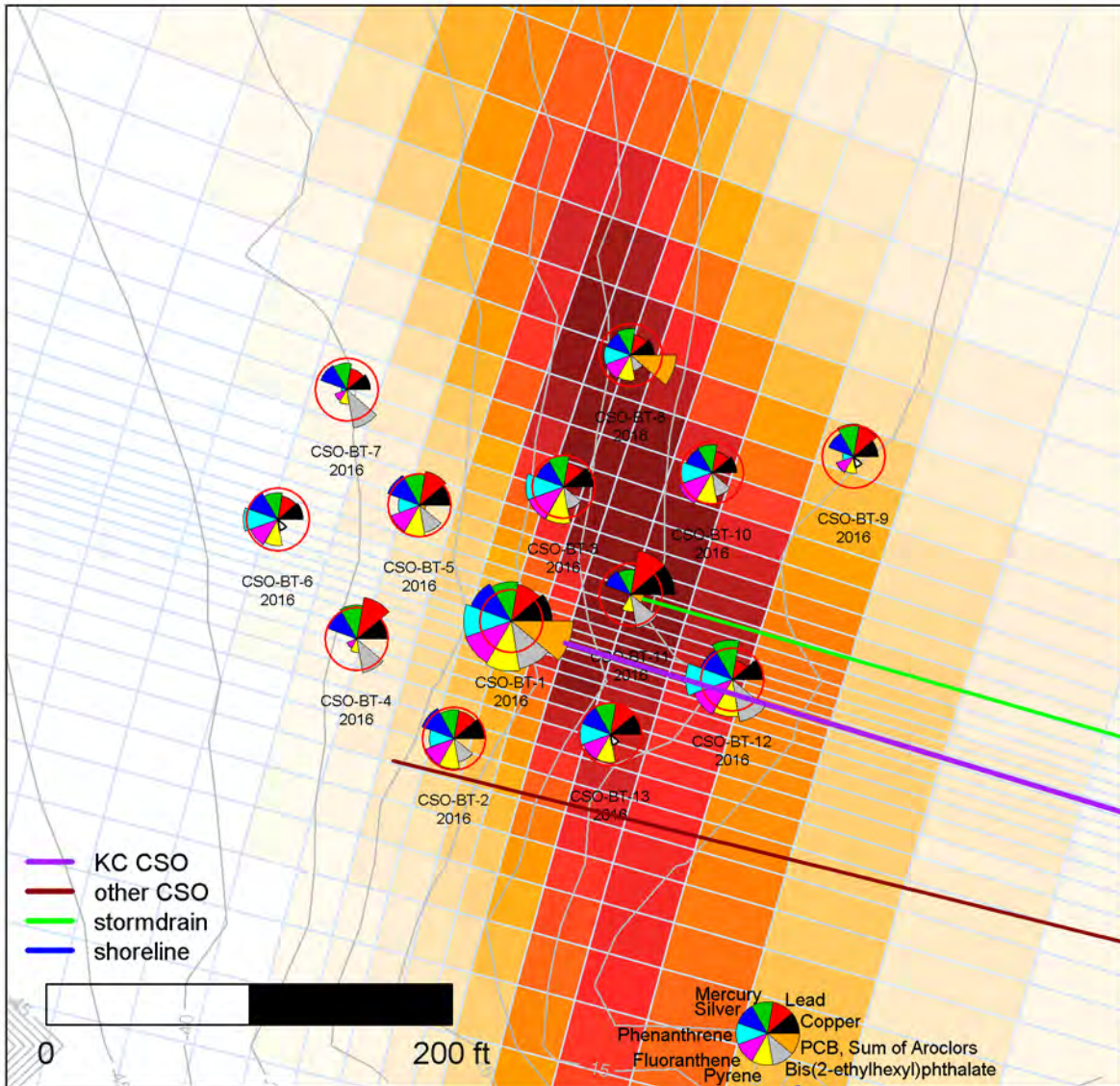
The pair-wise plots (Figure 34) show good correlation between the three PAH compounds (phenanthrene, fluoranthene, and pyrene) and lesser correlations between the metals and bis(2-ethylhexyl)phthalate.

Comparing sediment concentrations and the predicted CSO solids deposition rate (Figure 35), no particular correlation is apparent. The sediment chemistry at locations with higher predicted deposition rates (CSO-BT-3,8,10,11,13) did not have a consistent pattern of high concentrations. However, the generally higher concentrations at CSO-BT-1 suggest that the EFDC model might underpredict the deposition immediately offshore of the CSO.

Barton is generally similar to the previous CSO discharges, serving a primarily residential area with a submerged discharge into Puget Sound. Sediment concentrations at Barton tend to be higher than the previous CSOs. Predicted deposition rates at sampling locations tend to be higher than previous CSOs mostly due to locating sampling sites within the predicted region of deposition. Similar to Murray, higher concentrations of copper and lead at CSO-BT-11 suggest the stormwater outfall may be contributing to those concentrations.

The sediment concentrations at Barton St CSO appear to be complicated by the presence of a stormwater outfall to the north and a SPU CSO outfall to the south, contributing to this site not being informative of the model's ability to predict deposition rates. Additionally, the predicted deposition rates are relatively low and the chemical signature of the CSO discharge may be less than the natural variability of background concentrations. This and potential nearby sources suggests no conclusion can be made about the accuracy of the EFDC model prediction at this site.

## Barton Street



Segment length proportional to logarithm of detected value, unfilled segments indicate MDL

**Figure 33. Barton St. CSO sediment concentrations for selected compounds.**

# Barton Street

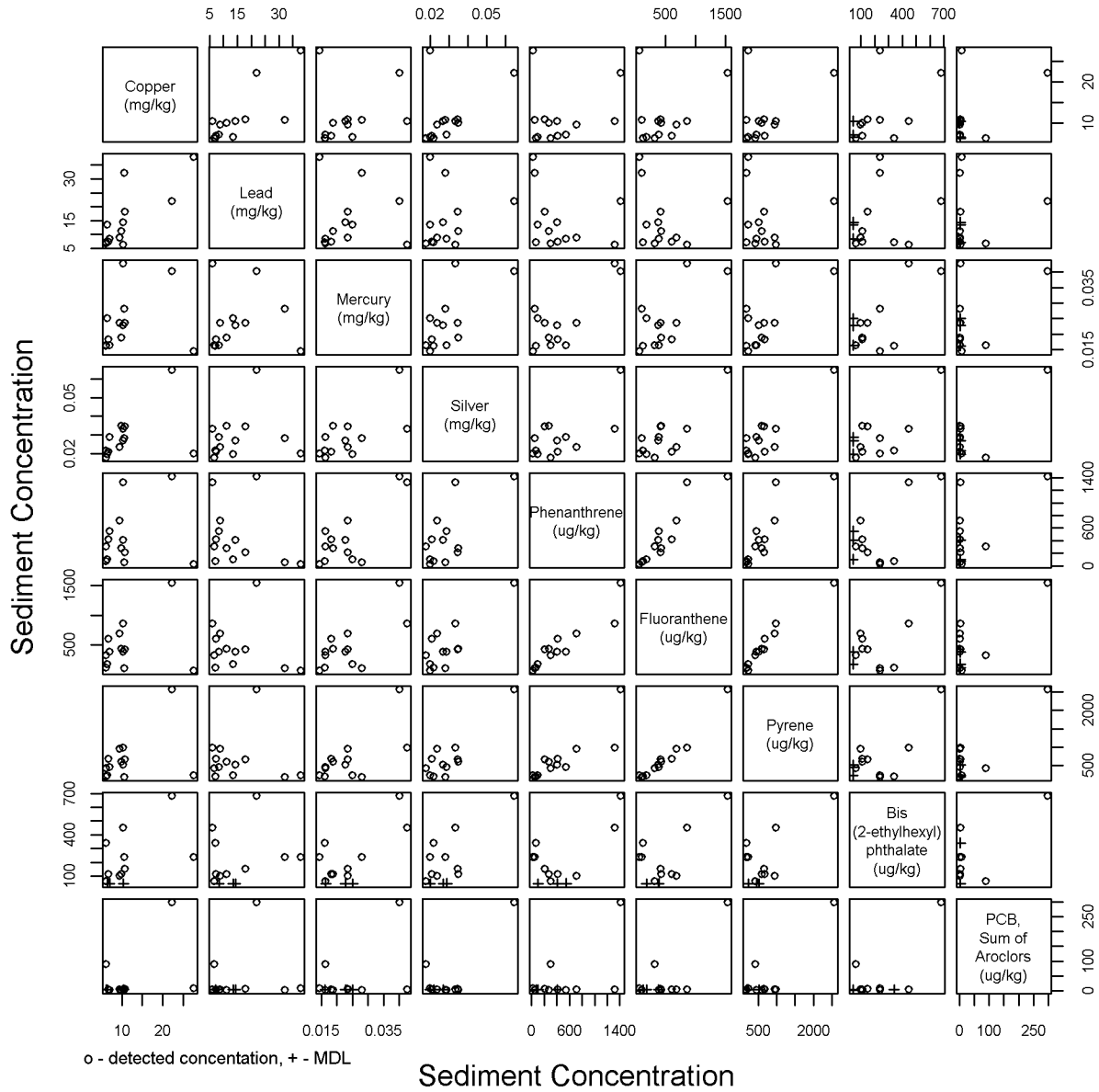
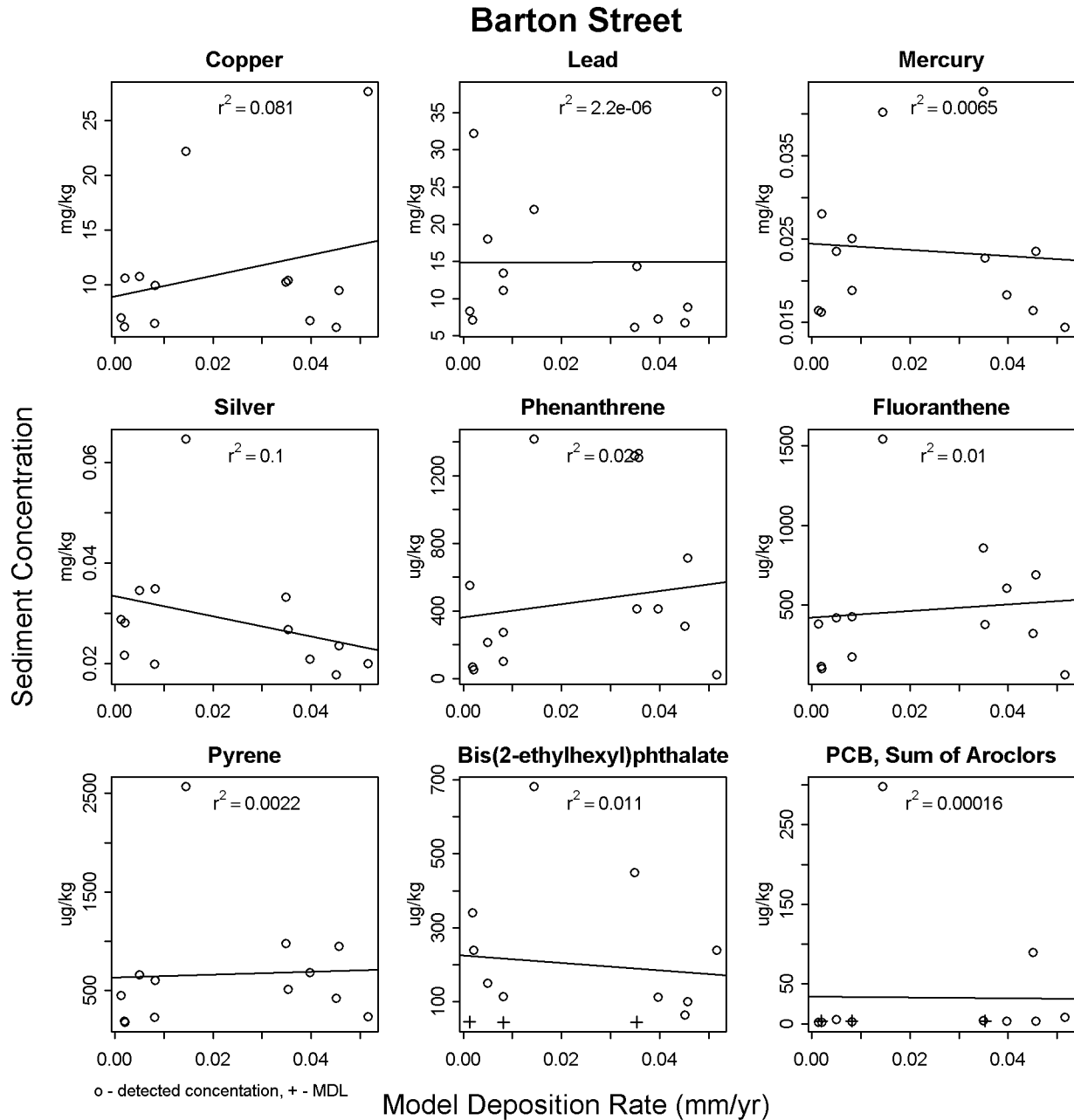


Figure 34. Parameter-parameter plot of sediment concentrations at Barton St. CSO.



**Figure 35. Sediment concentrations versus predicted sediment depositional rates at Barton St. CSO.**

### 7.2.6 Brandon Street CSO

Sediment concentrations near Brandon St. CSO were highest at the station closest to the CSO (CSO-BR-1) and at the station to the north (CSO-BR-3) (Figure 36). Mercury and PCBs were highest near the CSO outfall, while PAHs were significantly higher at CSO-BR-5 than all other stations. In general, a systematic pattern does not appear to exist with the sediment concentrations. Although Mercury and PCBs were elevated near the discharge (CSO-BR-1), the

other seven chemicals had relatively low concentrations. Concentrations of the three PAH compounds (phenanthrene, fluoranthene, and pyrene) at CSO-BR-3 are about 7 times larger than the other samples near the Brandon CSO. The concentration of these three PAHs exceeded the 75th percentile concentration in solids collected from within the CSO pipes (Appendix B). Because the correlations with these compounds are dominated by this high value, the plots discussed above are repeated with these high values omitted (Figure 39 to Figure 41).

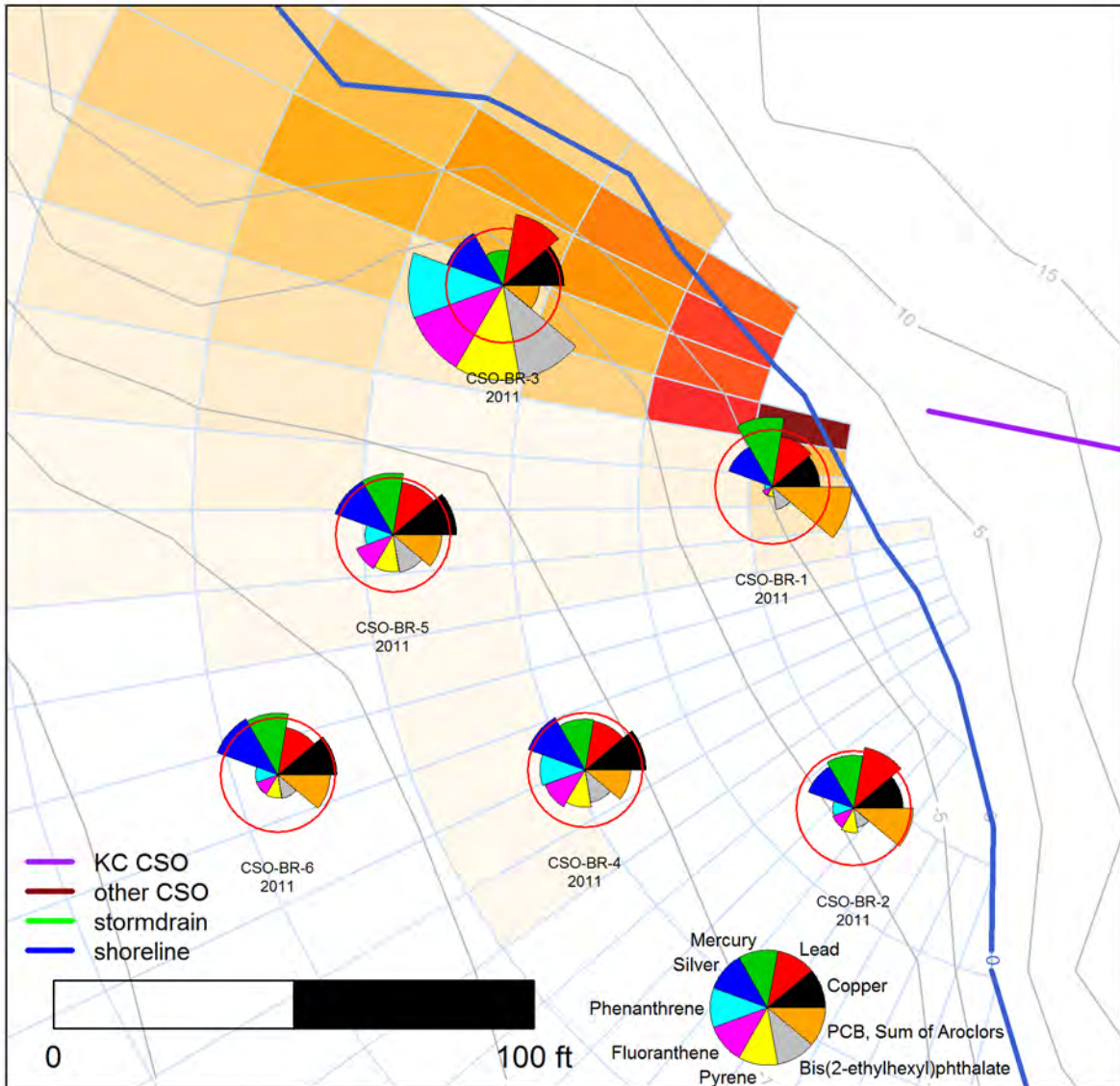
The pair-wise plots (Figure 37 or Figure 40) show the correlations between compounds. The PAH chemicals (phenanthrene, fluoranthene, and pyrene) and bis(2-ethylhexyl)phthalate appear correlated with each other. PCBs and mercury appear to have some correlation, whereas mercury and lead may have a negative correlation.

The correlations between predicted CSO solids depositional rate and sediment chemical concentrations (Figure 38 or Figure 41) have minimal correlation, with the exception of PCBs due to high deposition and concentration at CSO-BR-1.

Compared to the Puget Sound CSO sites above, sediment concentrations at Brandon are generally higher, reflective of the higher ambient concentrations in the LDW relative to Puget Sound.

The two sediment sampling stations around the Brandon St. CSO that correspond to the highest predicted depositional rates (CSO-BR-1 and CSO-BR-3) had the highest chemical concentrations. This would indicate good agreement with the model predictions, except that the chemicals are not consistently high at both locations.

## Brandon Street



Segment length proportional to logarithm of detected value, unfilled segments indicate MDL

**Figure 36. Brandon St. CSO sediment concentrations for selected compounds.**

# Brandon Street

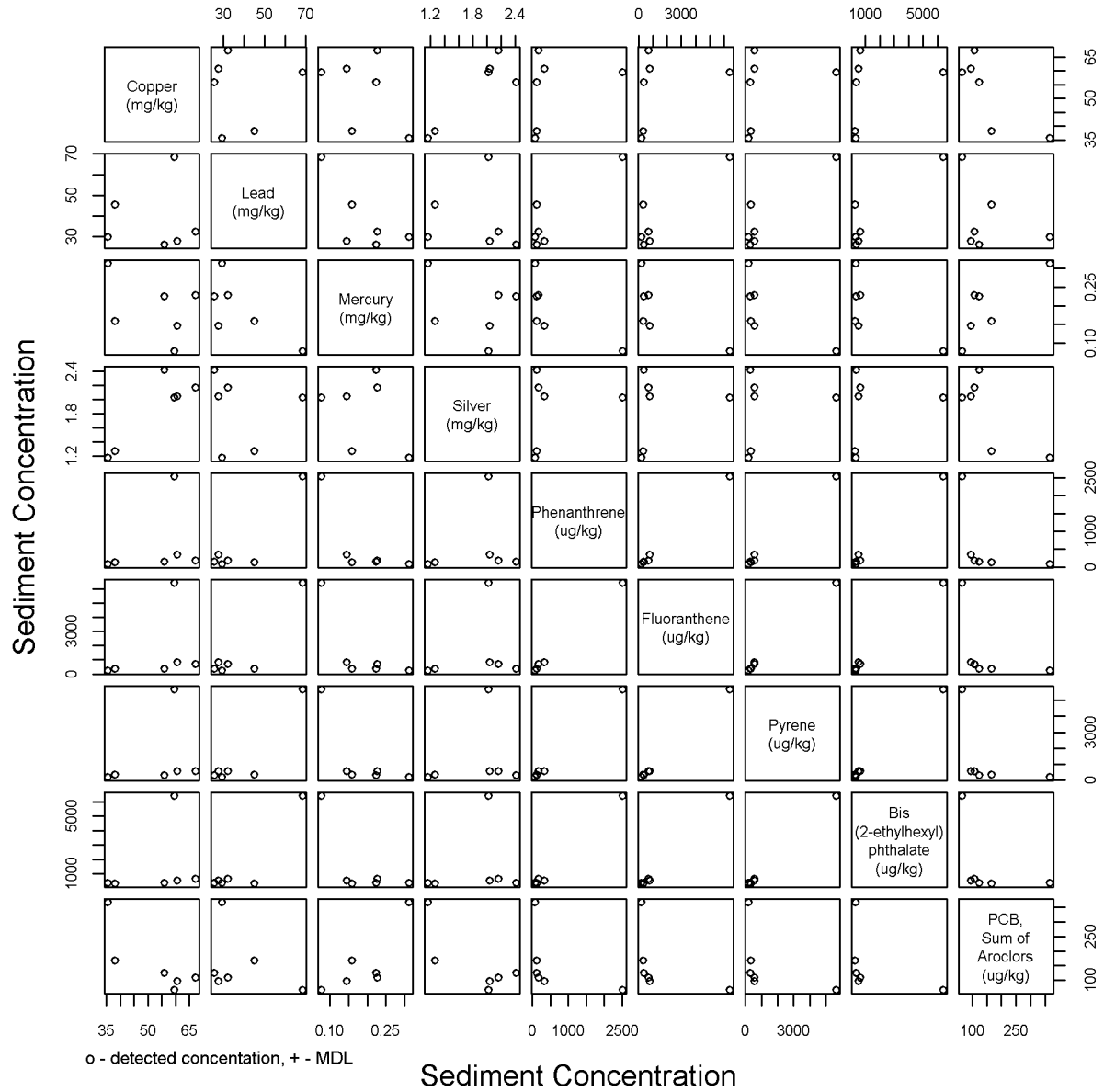


**Figure 37. Parameter-parameter plot of sediment concentrations at Brandon St. CSO.**

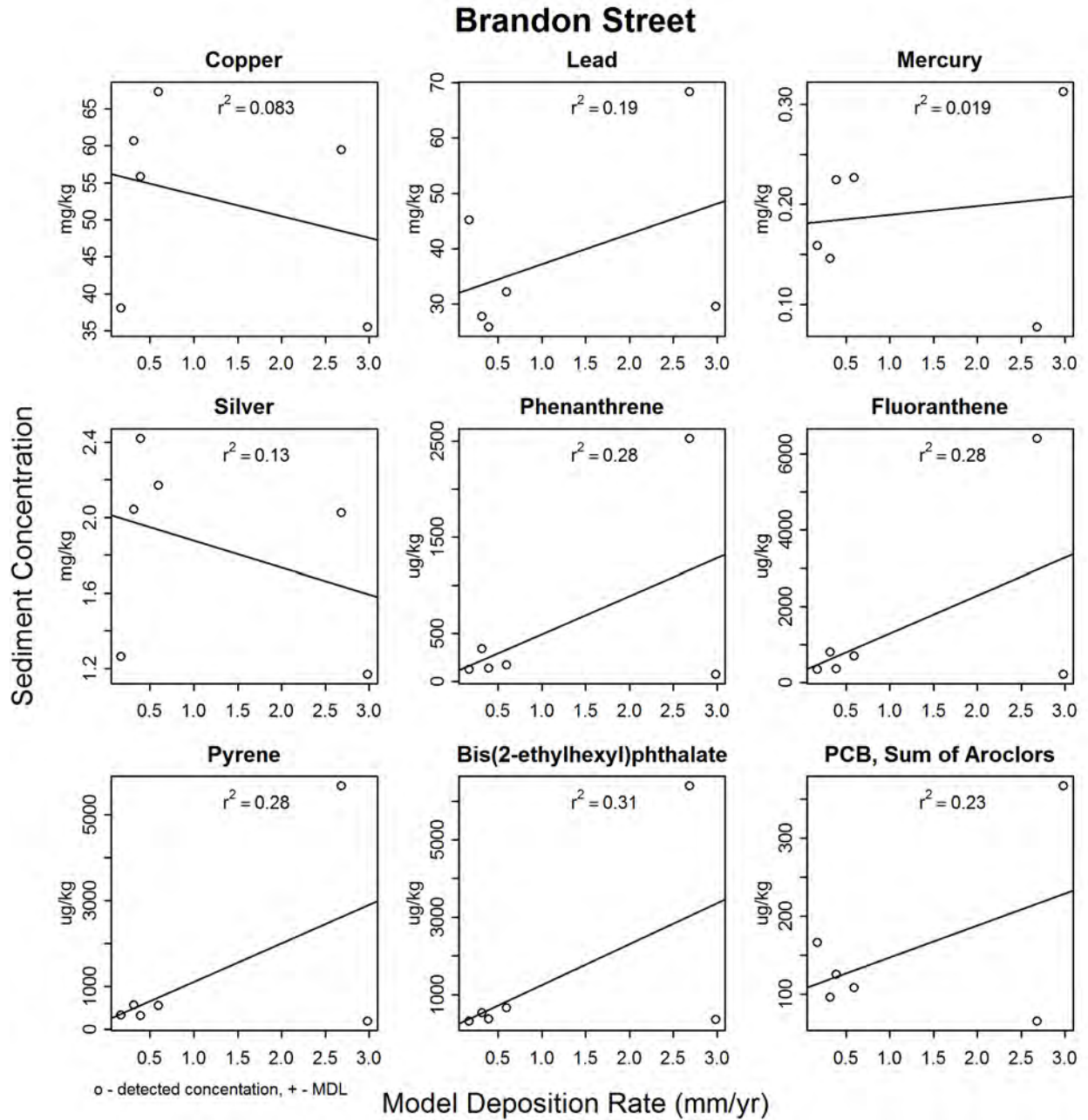
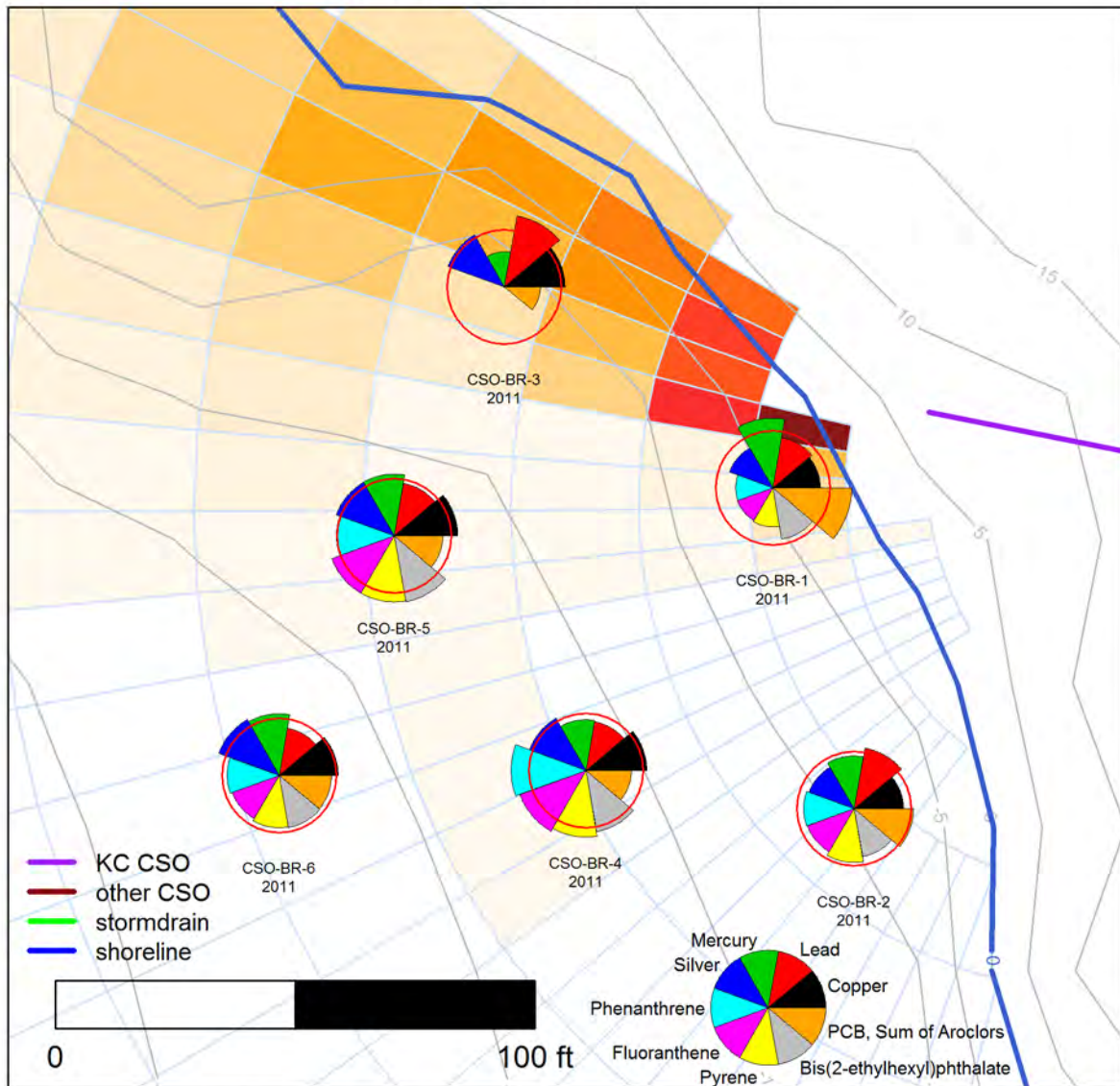


**Figure 38. Sediment concentrations versus predicted sediment depositional rates at Brandon St. CSO.**

## Brandon Street outlier removed



Segment length proportional to logarithm of detected value, unfilled segments indicate MDL  
**Figure 39. Brandon St. CSO sediment concentrations without PAH values at CSO-BR-3.**

## Brandon Street outlier removed

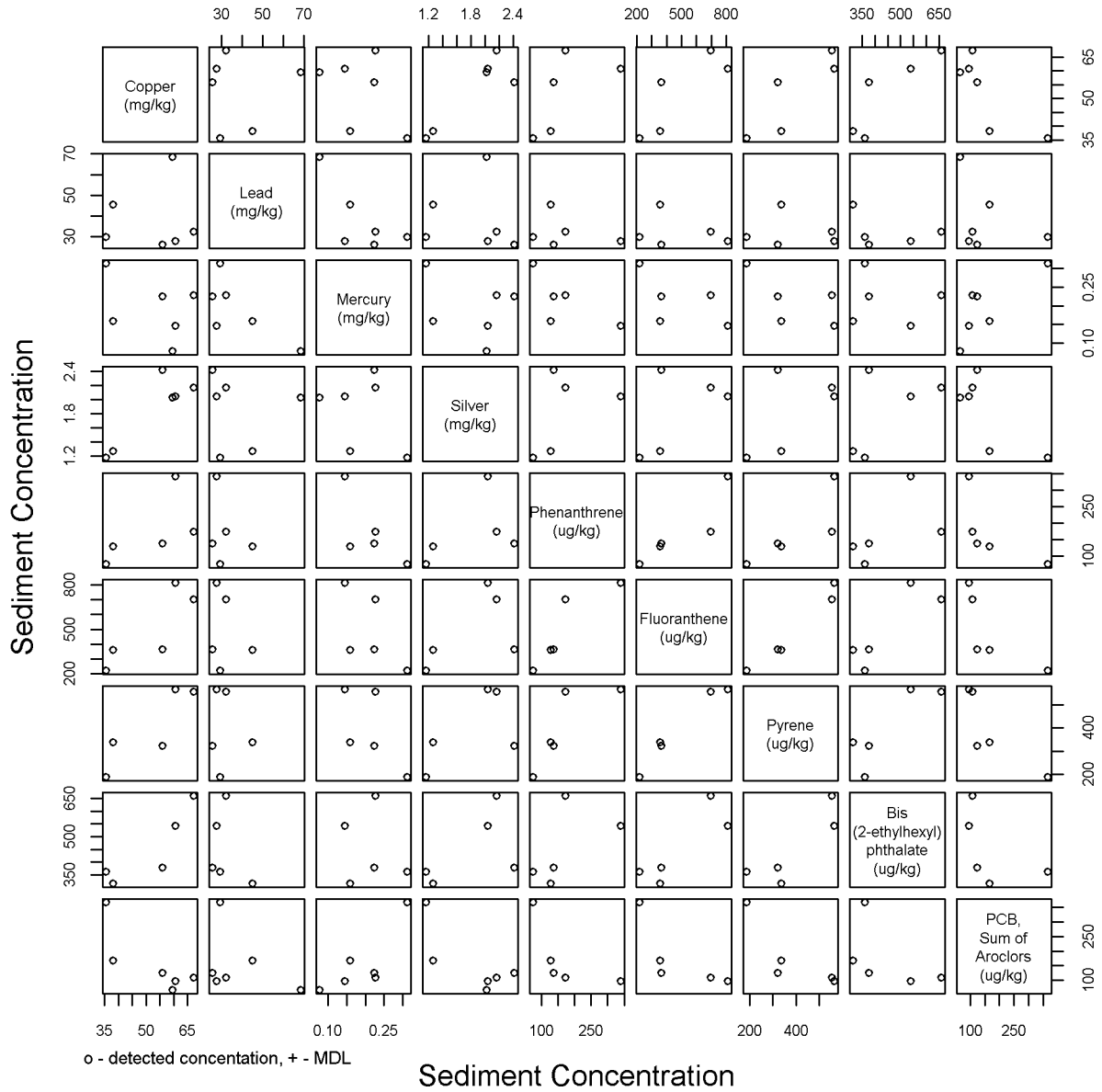


**Figure 40. Parameter-parameter plot at Brandon St. CSO without PAH values at CSO-BR-3.**

## Brandon Street outlier removed

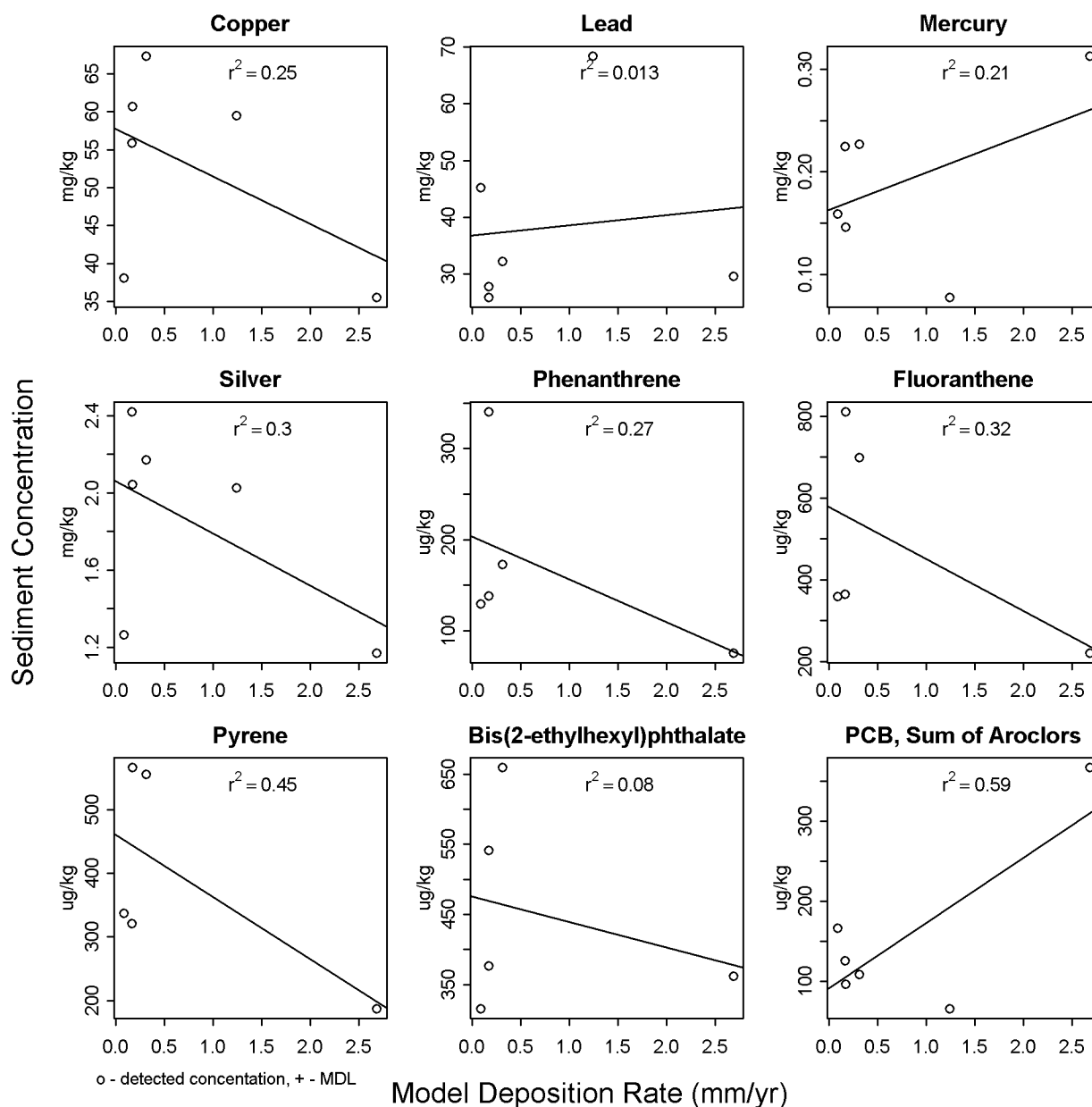


**Figure 41. Sediment concentrations versus predicted sediment depositional rates at Brandon St. CSO without PAH values at CSO-BR-3.**

### 7.2.7 Chelan Avenue CSO

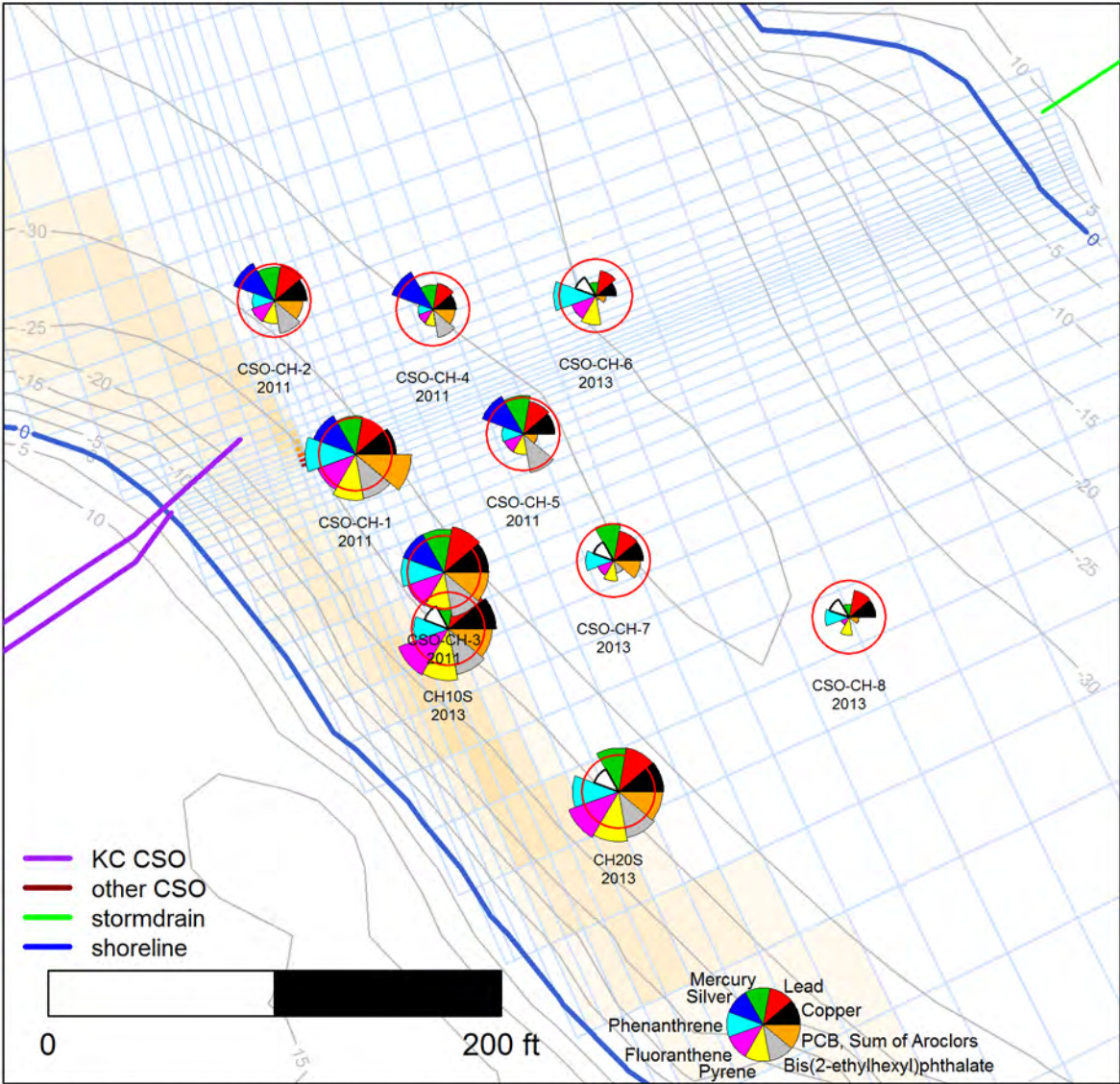
Sediment concentrations near the Chelan Ave. CSO were higher at the inshore stations, more so at the station closest to the CSO and to the southeast of the CSO. The outfall location on Figure 41 has been updated to reflect a refinement of the outfall coordinates that occurred after the sampling and modeling simulation. Spatially, the deposition pattern is primarily inshore of the sample locations.

The pair-wise plots show good correlation between the two HPAH compounds (fluoranthene and pyrene), and lesser correlations between copper, mercury, phenanthrene, and bis(2-ethylhexyl)phthalate.

While the model predicts very low deposition rates (less than 0.005 mm/yr) at the sampling locations, a reasonable correlation ( $r^2 = 0.2$  to  $0.8$ ) exists between the predicted CSO solids depositional rate and most sediment chemical concentrations (Figure 26). The relatively good model correlation with the data suggests that the EFDC model might underpredict the offshore motion of the CSO discharge.

The sediment concentrations at the Chelan CSO appear to be slightly lower than around the upstream Brandon St. CSO, but generally higher than the Puget Sound CSO sites above.

# Chelan Avenue



Segment length proportional to logarithm of detected value, unfilled segments indicate MDL

**Figure 42. Chelan Ave. CSO sediment concentrations for selected compounds.**

# Chelan Avenue

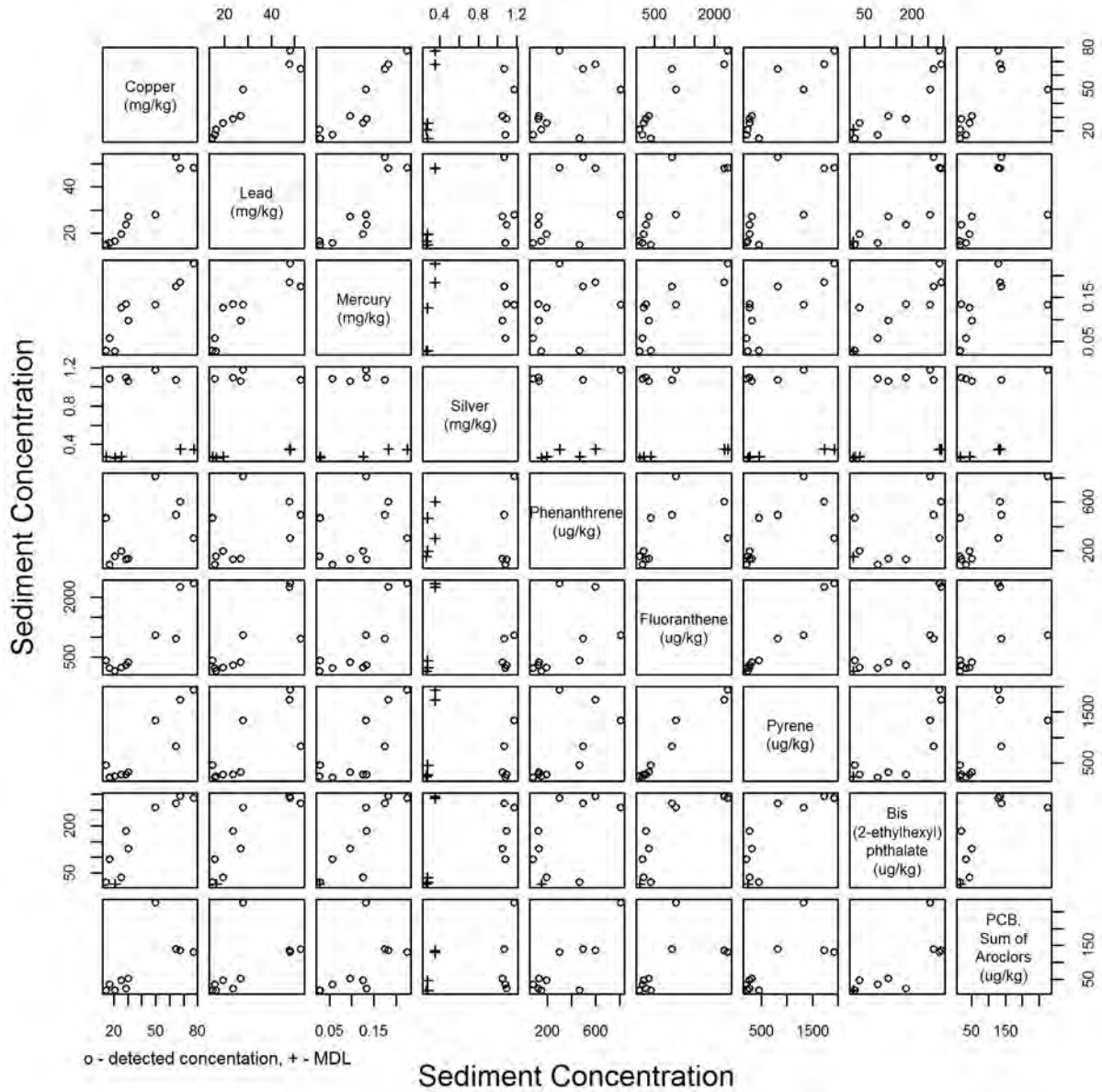


**Figure 43. Parameter-parameter plot of sediment concentrations at Chelan Ave. CSO.**

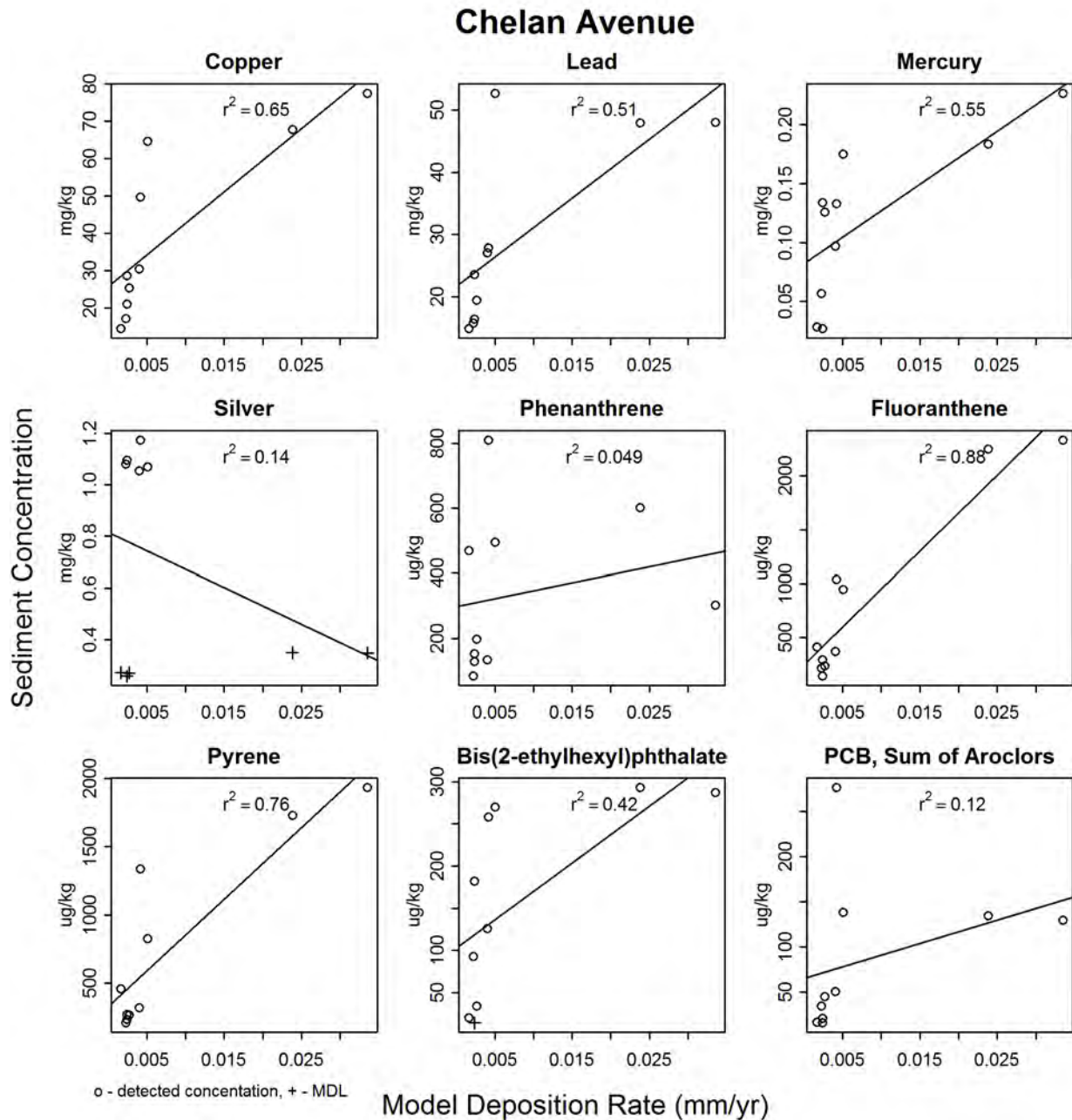


**Figure 44. Sediment concentrations versus predicted sediment depositional rates at Chelan Ave. CSO.**

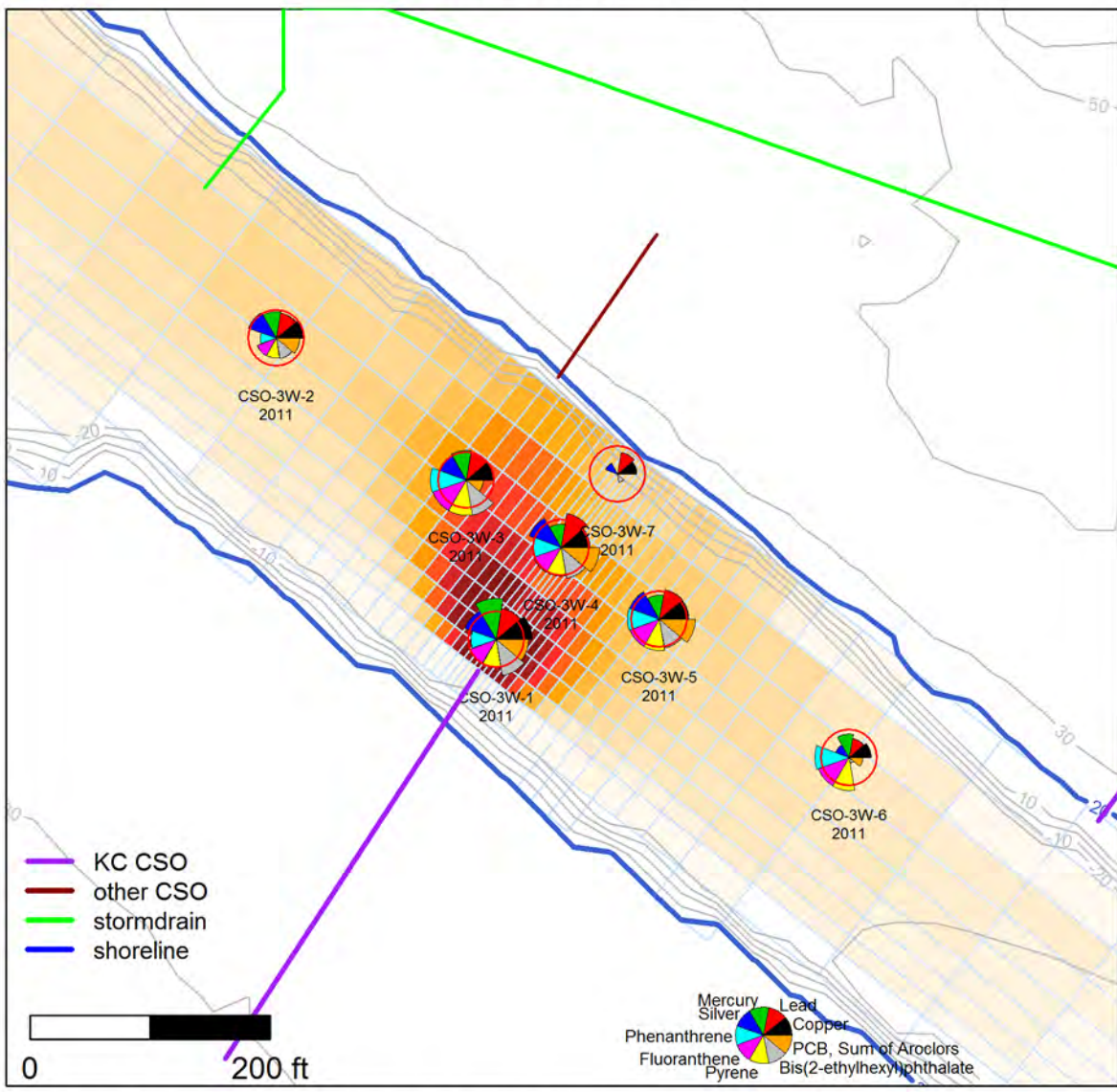
### 7.2.8 3rd Avenue West CSO

Sediment concentrations near the 3rd Ave. West CSO did not have an obvious spatial pattern (Figure 45). Copper and mercury were highest near the CSO at station CSO-3W-1. Lead, silver, and PCBs were highest offshore of the discharge in the center of the canal. Station CSO-3W-7 on the opposite side of the canal had consistently low concentrations.

The pair-wise plots (Figure 46) show good correlation between the three PAH compounds (phenanthrene, fluoranthene, and pyrene), and lesser correlations between copper, lead, mercury, silver, bis(2-ethylhexyl)phthalate, and PCBs. Spatially, the PAHs did not appear related to the CSO, suggesting that there may be one or more other sources of these compounds.

The model correlation with sediment data was reasonably good for copper and mercury, but dominated by a single data point. In general, the four samples closest to the discharge tended to have the highest sediment concentrations and the highest predicted depositional rates, without any clear pattern. With multiple other sources in the area (SPU CSO, SPU storm drain, local industrial sources, and vessel berths), the sediment signature of the CSO discharge may be hard to discern. The influence of other sources can be seen in the different correlation patterns shown in the parameter-parameter plot than seen at other County CSOs.

### 3rd Ave West



Segment length proportional to logarithm of detected value, unfilled segments indicate MDL

**Figure 45. 3rd Ave. W CSO sediment concentrations for selected compounds.**

### 3rd Ave West

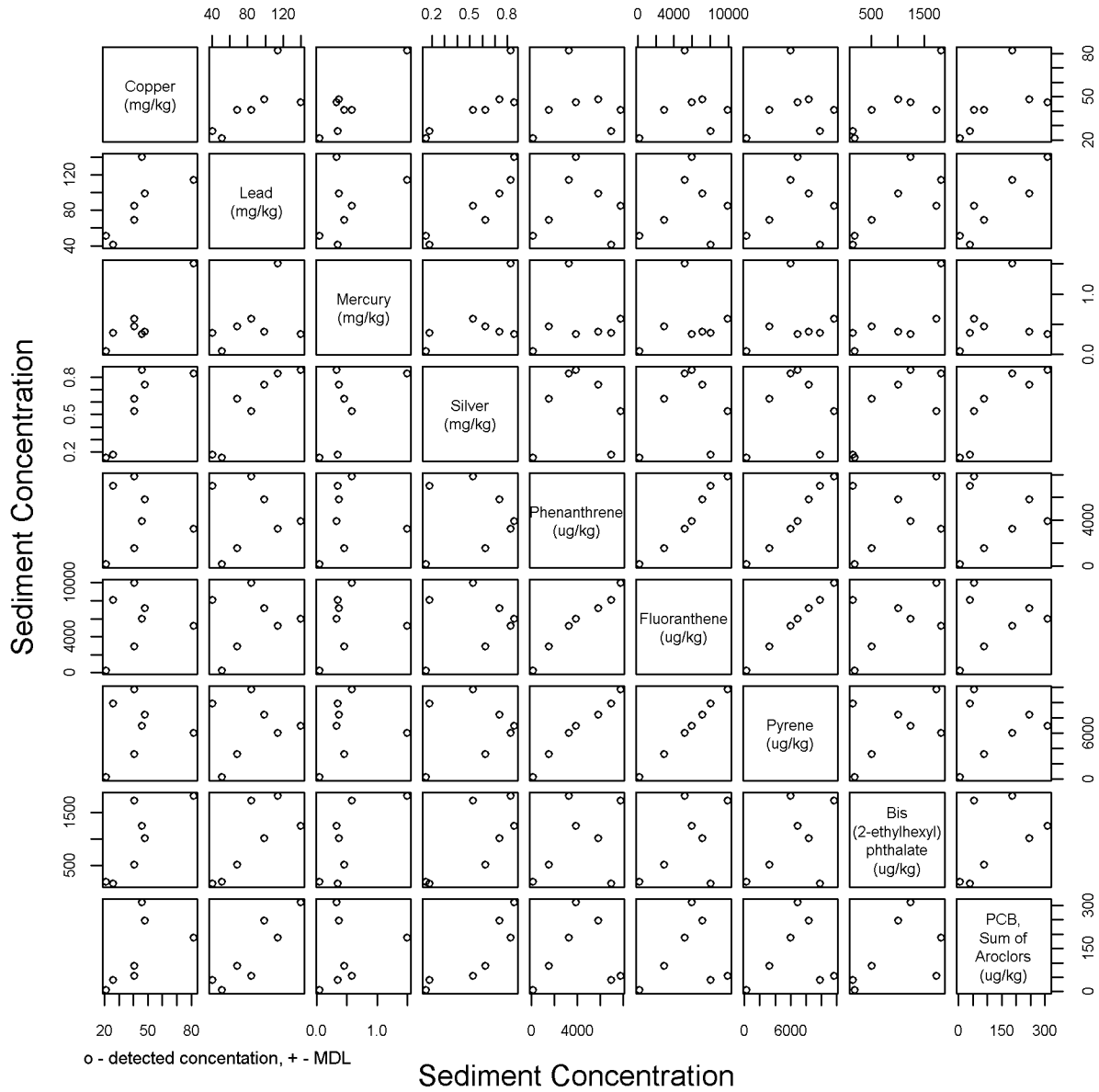


**Figure 46. Parameter-Parameter plot of sediment concentrations at 3rd Ave. W CSO.**

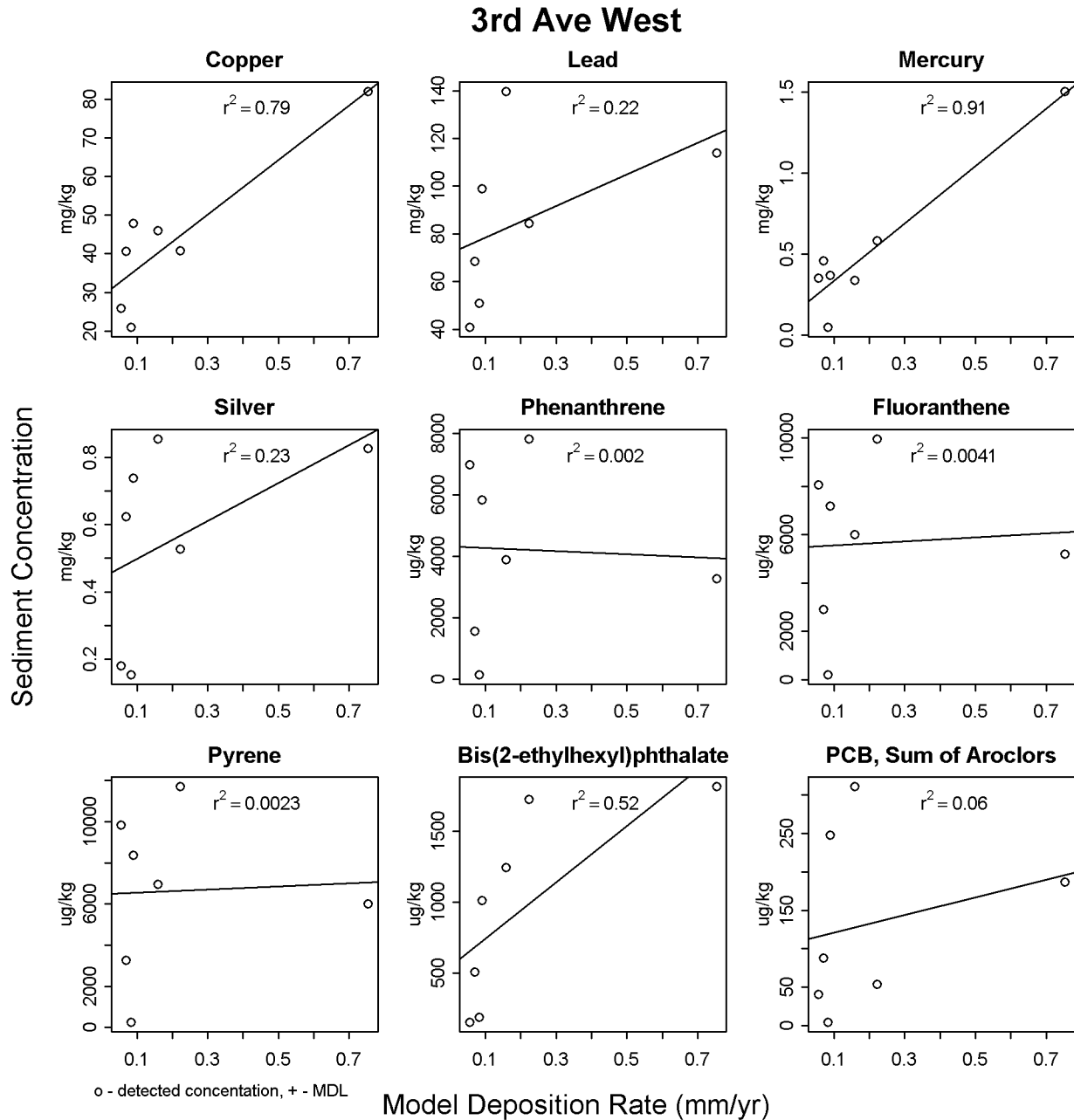


**Figure 47. Sediment concentrations versus predicted sediment depositional rates at 3rd Ave. West CSO.**

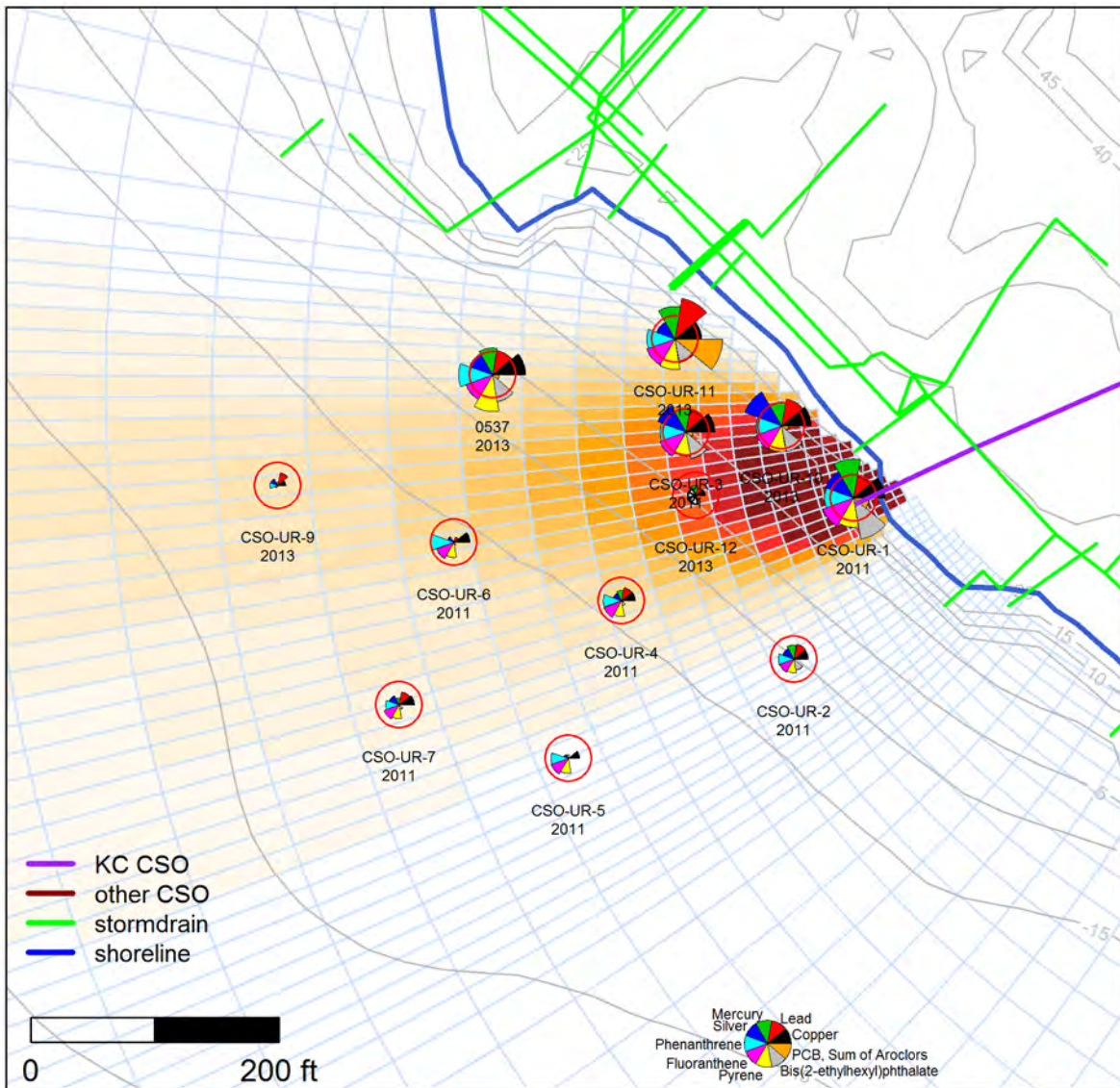
### 7.2.9 University Regulator

Sediment concentrations near the University Regulator CSO have an obvious spatial pattern of elevated concentrations off the CSO and along the shoreline to the northwest. The pattern appears similar to the EFDC prediction for CSO solids, except the sediment data are higher further to the north. The EFDC model predicts significant deposition at CSO-UR-12, but low sediment concentrations were observed. This may be due to a very hard substrate at this location. Multiple attempts were required to collect this sample, suggesting that any sediment deposited at this location may be subsequently scoured.

Sediments at CSO-UR-11 have the highest concentrations of PCBs and lead, suggesting that there may be another source of these chemicals. Other possible sources include storm drains from the University of Washington and activities at the University of Washington Oceanography Dock, where research ships are moored. The pair-wise plots show good correlation between copper and the three PAH compounds (phenanthrene, fluoranthene, and pyrene). The model correlation with sediment data was reasonably good for most parameters, and indicates that the high value for lead and PCBs is not consistent with the model's prediction.

Removing the sample at CSO-UR-11 from the analysis, the relationship between sediment concentrations and the model are illustrated in Figure 51, Figure 52, and Figure 53. These figures show higher sediment concentrations in areas with higher predicted deposition rates. The pair-wise plot shows reasonable correlation between chemical concentrations, or locations tend to have relatively high or low concentrations for all nine chemicals. The regression between the observed concentrations and the predicted deposition rates suggest the model is able to explain 50% to 70% of the observed variability.

# University Regulator



Segment length proportional to logarithm of detected value, unfilled segments indicate MDL

**Figure 48. University Regulator CSO sediment concentrations for selected compounds.**

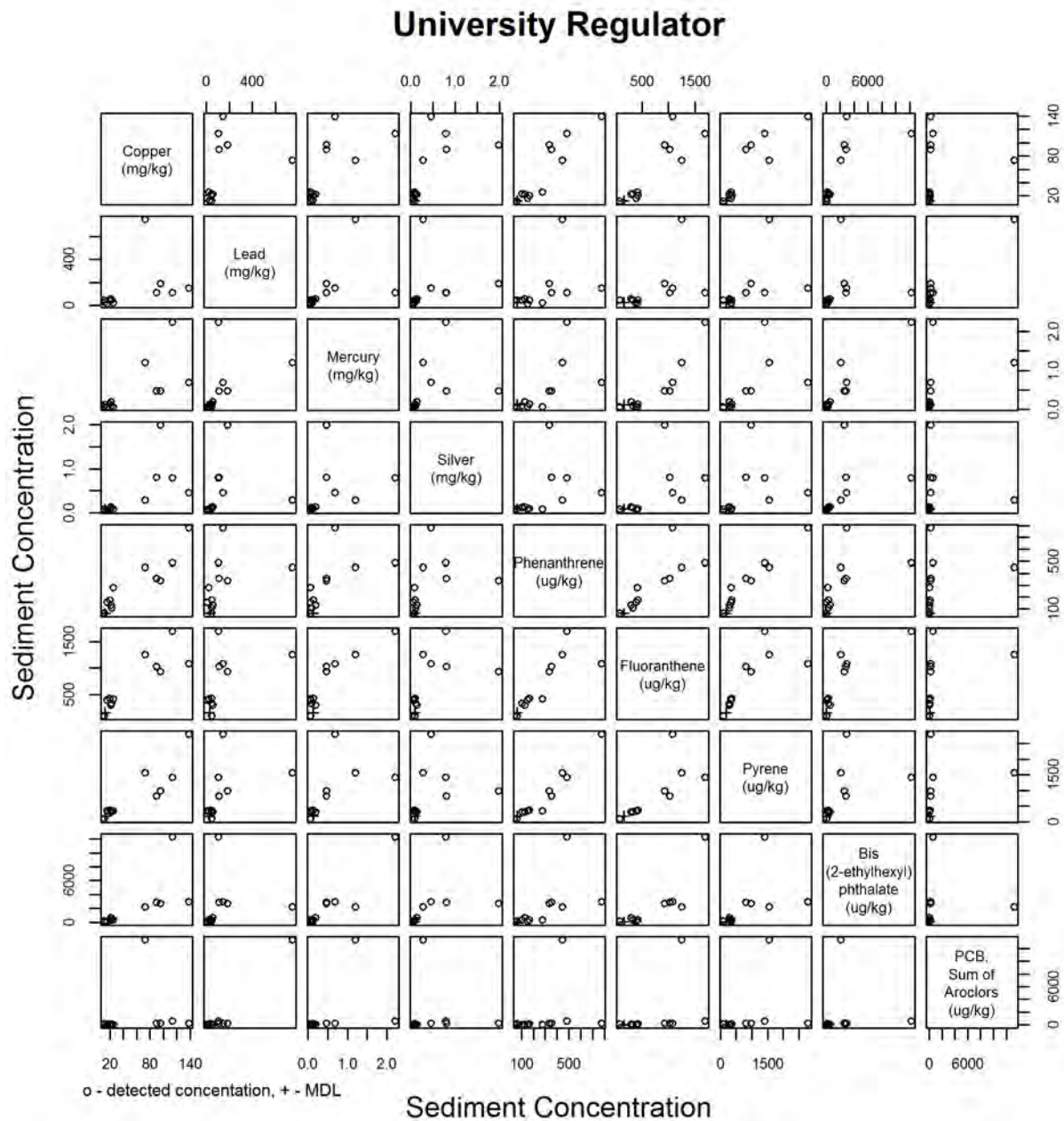


**Figure 49. Parameter-parameter plot of sediment concentrations at University CSO.**

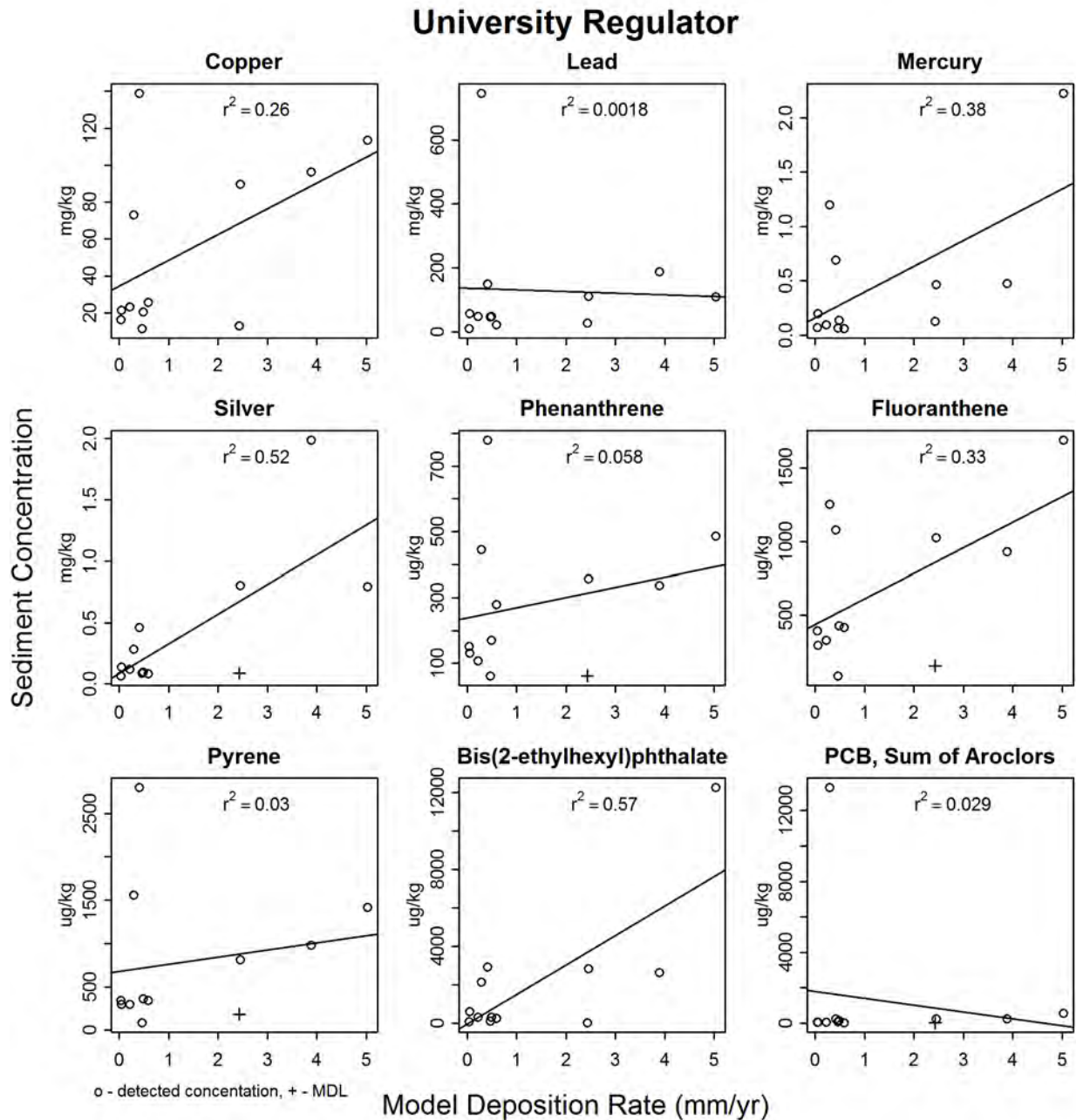


**Figure 50. Sediment concentrations versus predicted sediment depositional rates at University Regulator CSO.**

## University Regulator outlier removed

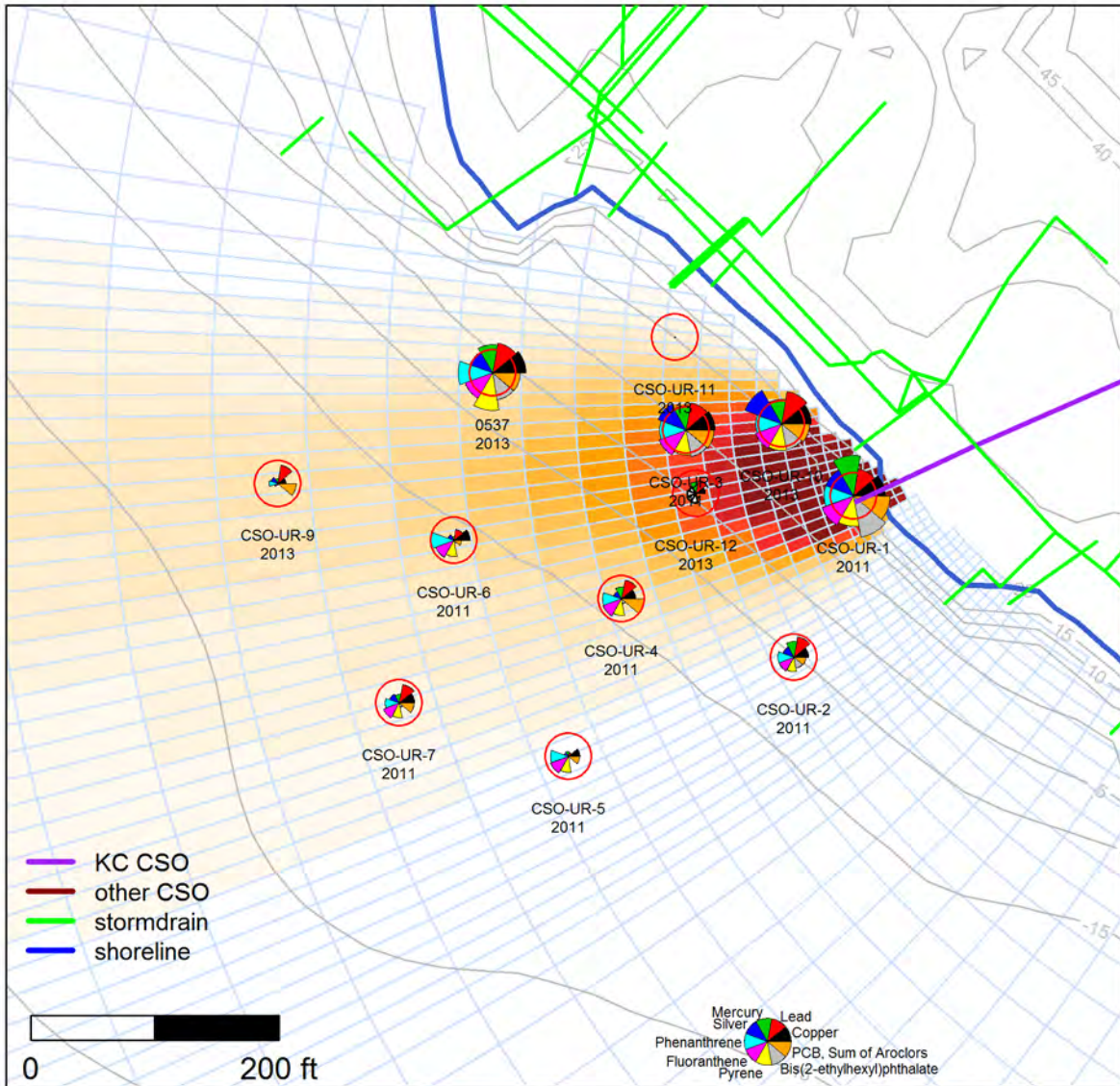


**Figure 51. University Regulator CSO sediment concentrations without values at CSO-UR-11.**

## University Regulator outlier removed

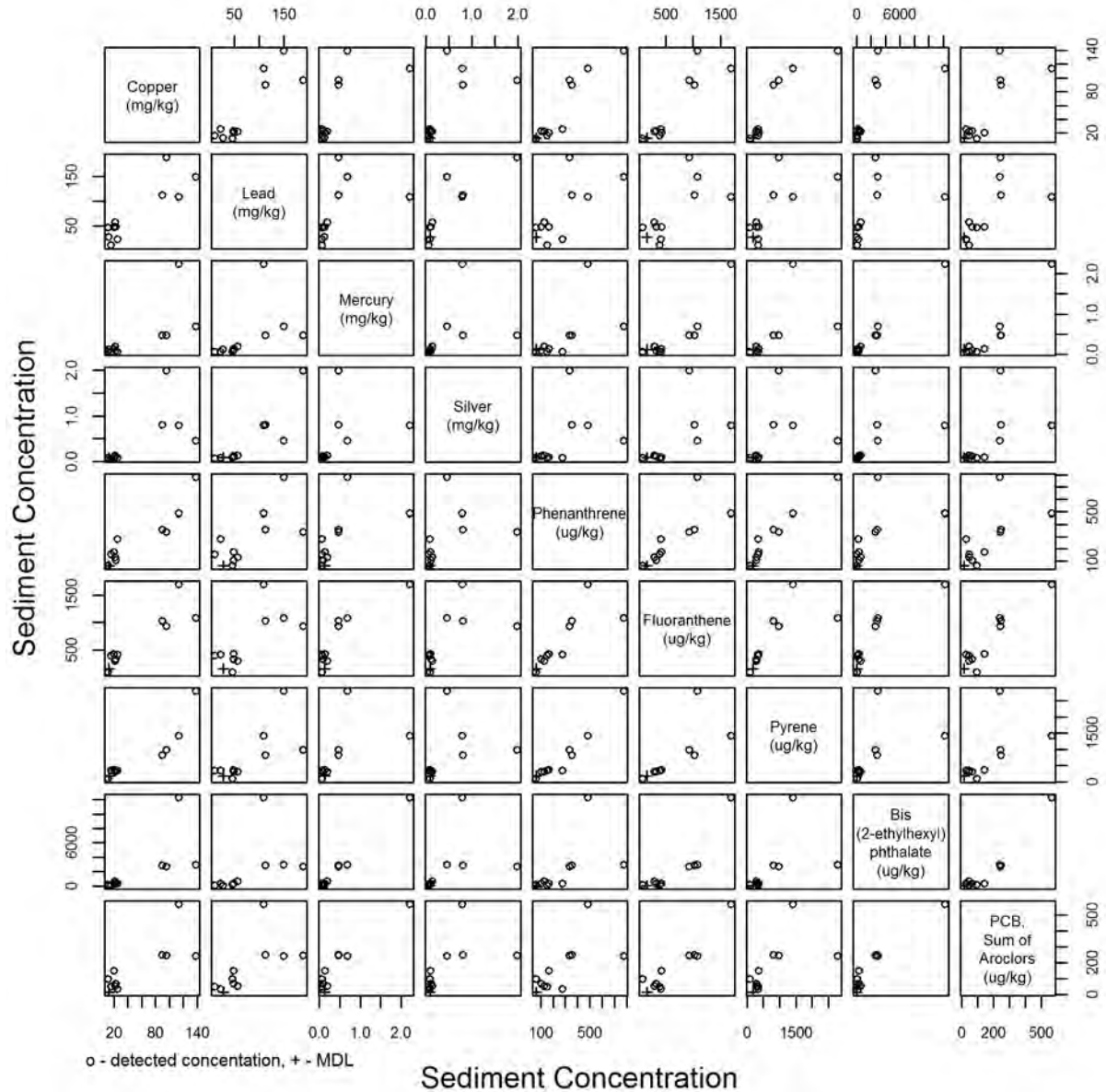


**Figure 52. Parameter-parameter plot at University Regulator CSO without values at CSO-UR-11.**

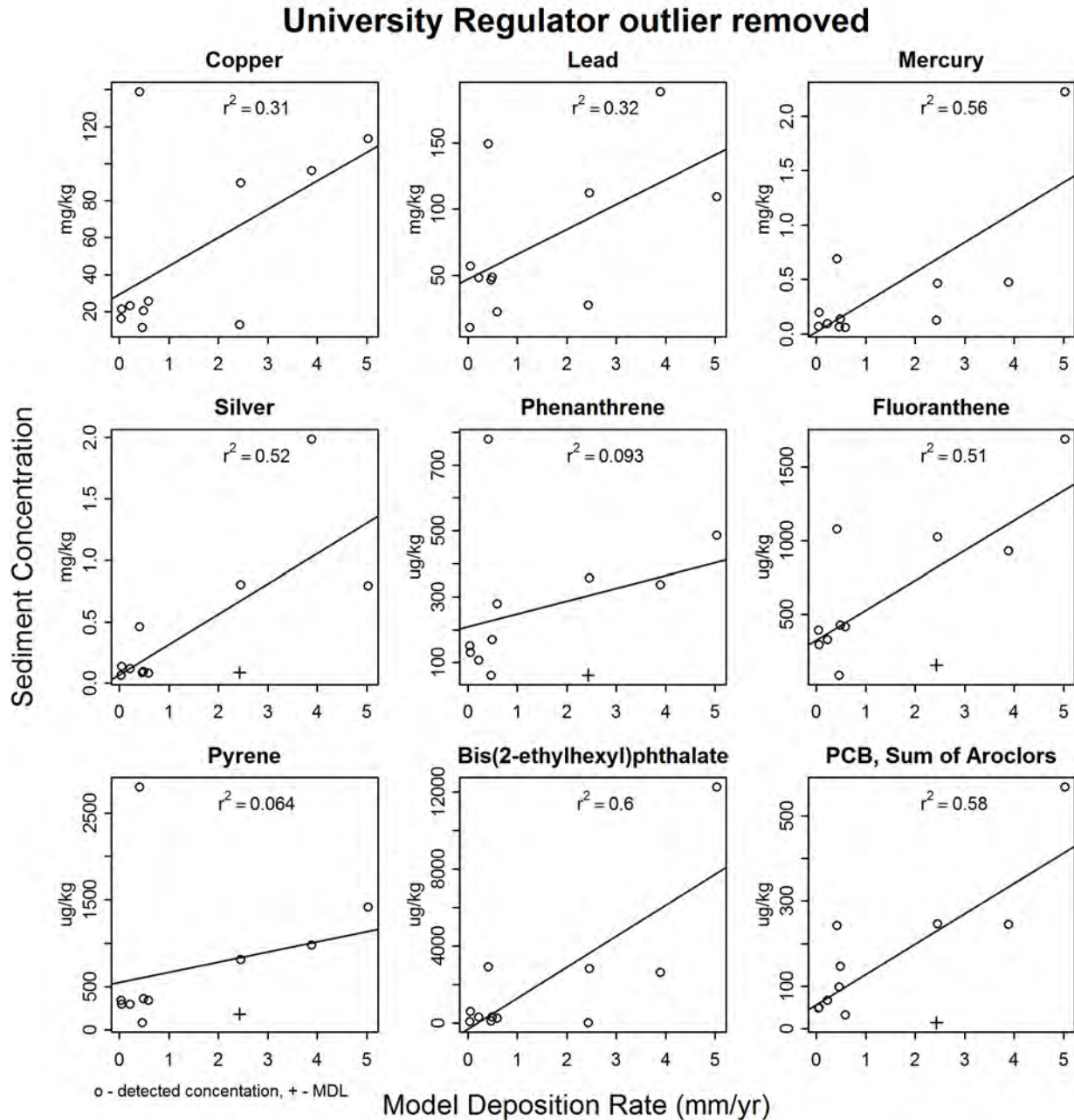


**Figure 53. Sediment concentrations versus predicted sediment depositional rates at University Regulator CSO without values at CSO-UR-11.**

### 7.2.10 Montlake CSO

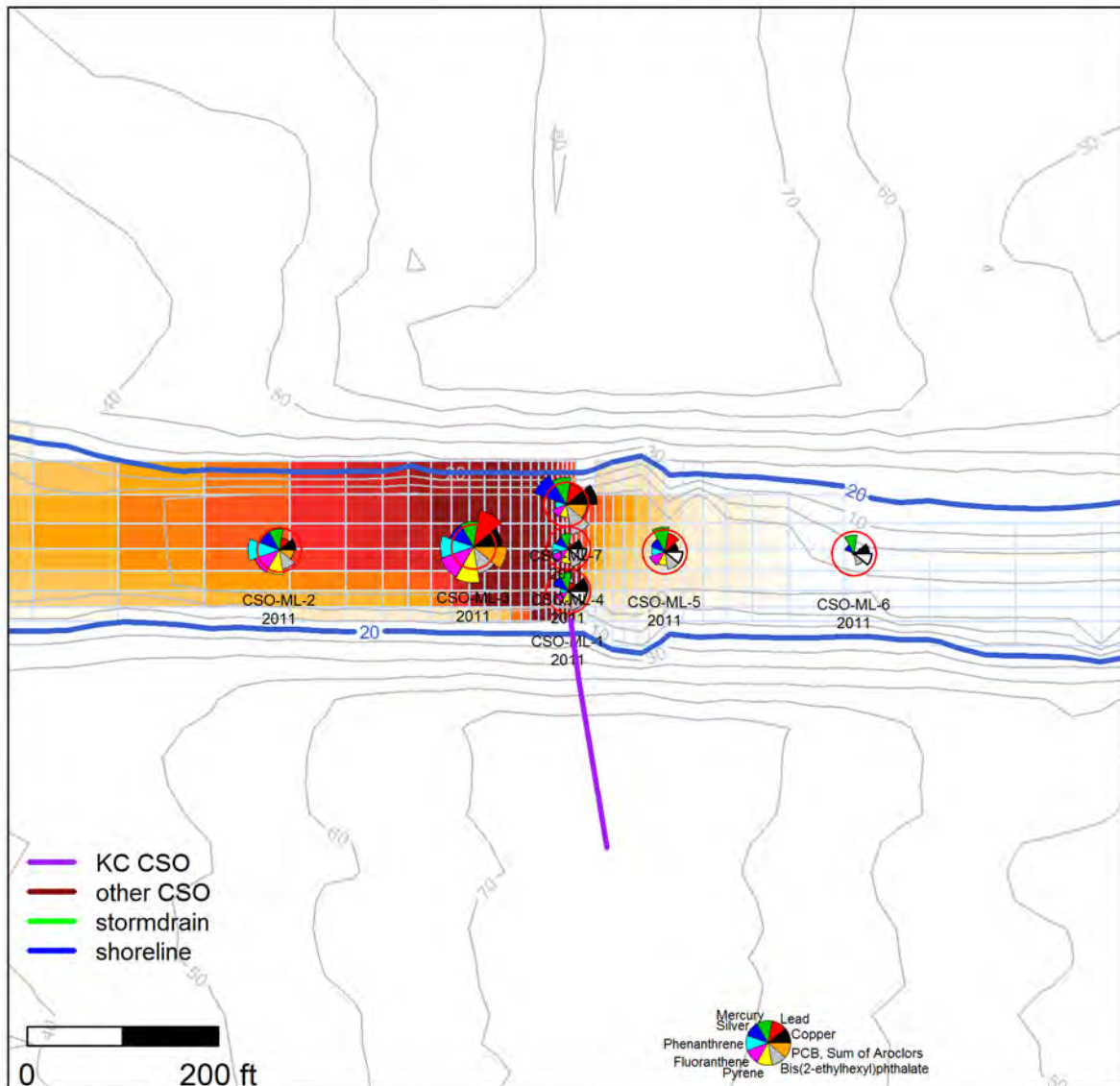
In general, the model did not do a good job of predicting sediment concentrations around the Montlake CSO. Sediment concentrations immediately off the CSO discharge location (Figure 54) at CSO-ML-1 and CSO-ML-4 were not as high as at the station further offshore (CSO-ML-7) or at the station further west (CSO-ML-3). Subsequent review identified an inaccuracy in the

model configuration. The model has the discharge entering the water at right angles to the southern shoreline, whereas the drawings show the discharge pipe is angled approximately 14 deg to the west. Modifying this discharge angle would reduce the sediment deposition rates at CSO-ML-1, CSO-ML-4, and CSO-ML-7.

The pair-wise plots (Figure 55) showed limited correlations. The lead concentration of 565 mg/kg at CSO-ML-3 is above the concentration associated with CSO solids (160 mg/kg) and above the surrounding samples, suggesting this could be an outlier or a nugget. Excluding this value, copper, lead, mercury, silver, and bis(2-ethylhexyl)phthalate concentrations had some correlation. The PAH compounds (phenanthrene, fluoranthene, and pyrene) had less correlation with each other than at most other sites, and little correlation with other compounds

Omitting the high lead value from CSO-ML-3, lead showed good correlation with mercury and reasonable correlation with silver and bis(2-ethylhexyl)phthalate. With the value removed, lead showed no correlation with the predicted model deposition rates.

# Montlake CSO



Segment length proportional to logarithm of detected value, unfilled segments indicate MDL

**Figure 54. Montlake CSO sediment concentrations for selected compounds.**

# Montlake CSO

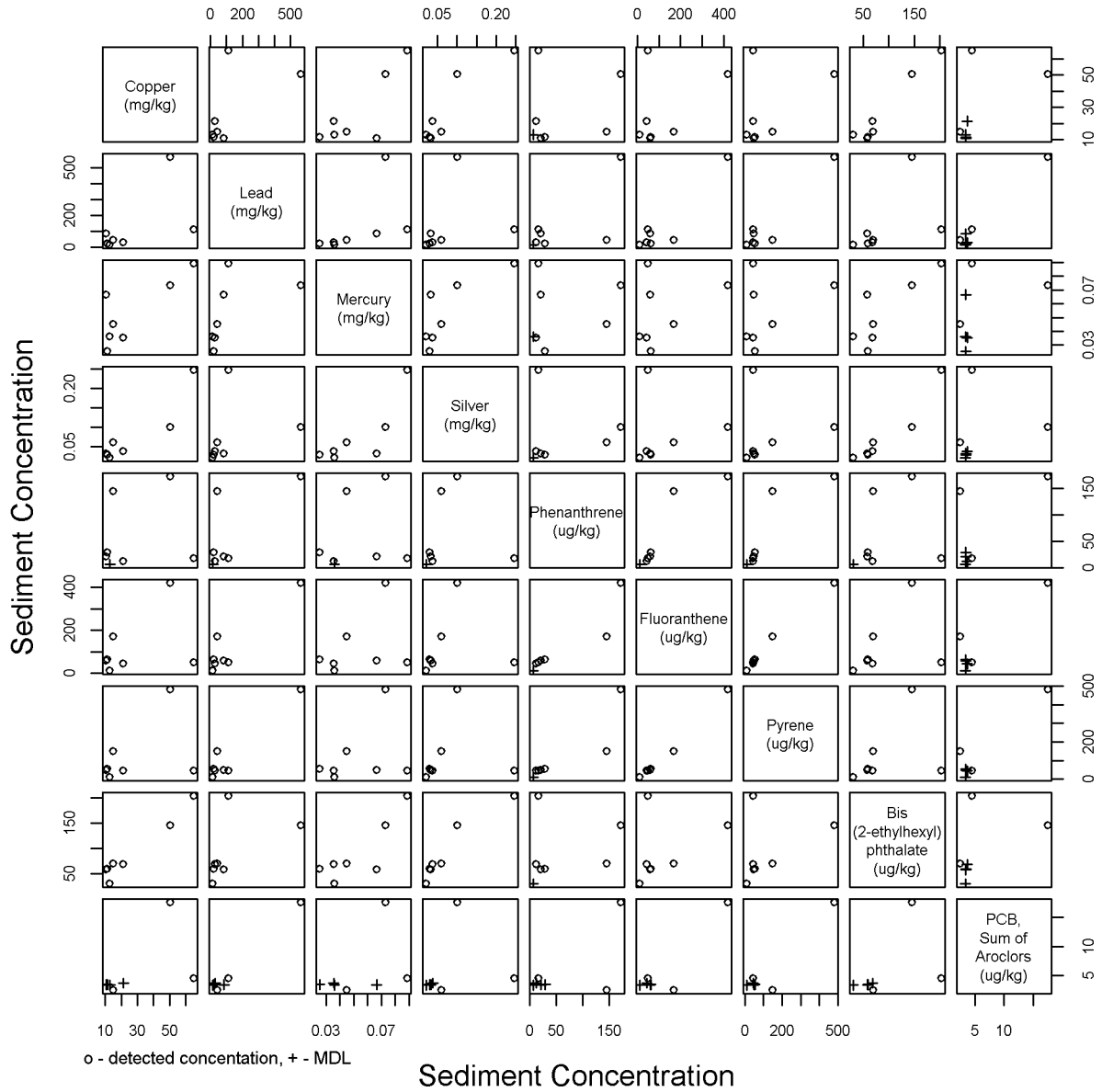


**Figure 55. Parameter-parameter plot of sediment concentrations at Montlake CSO.**

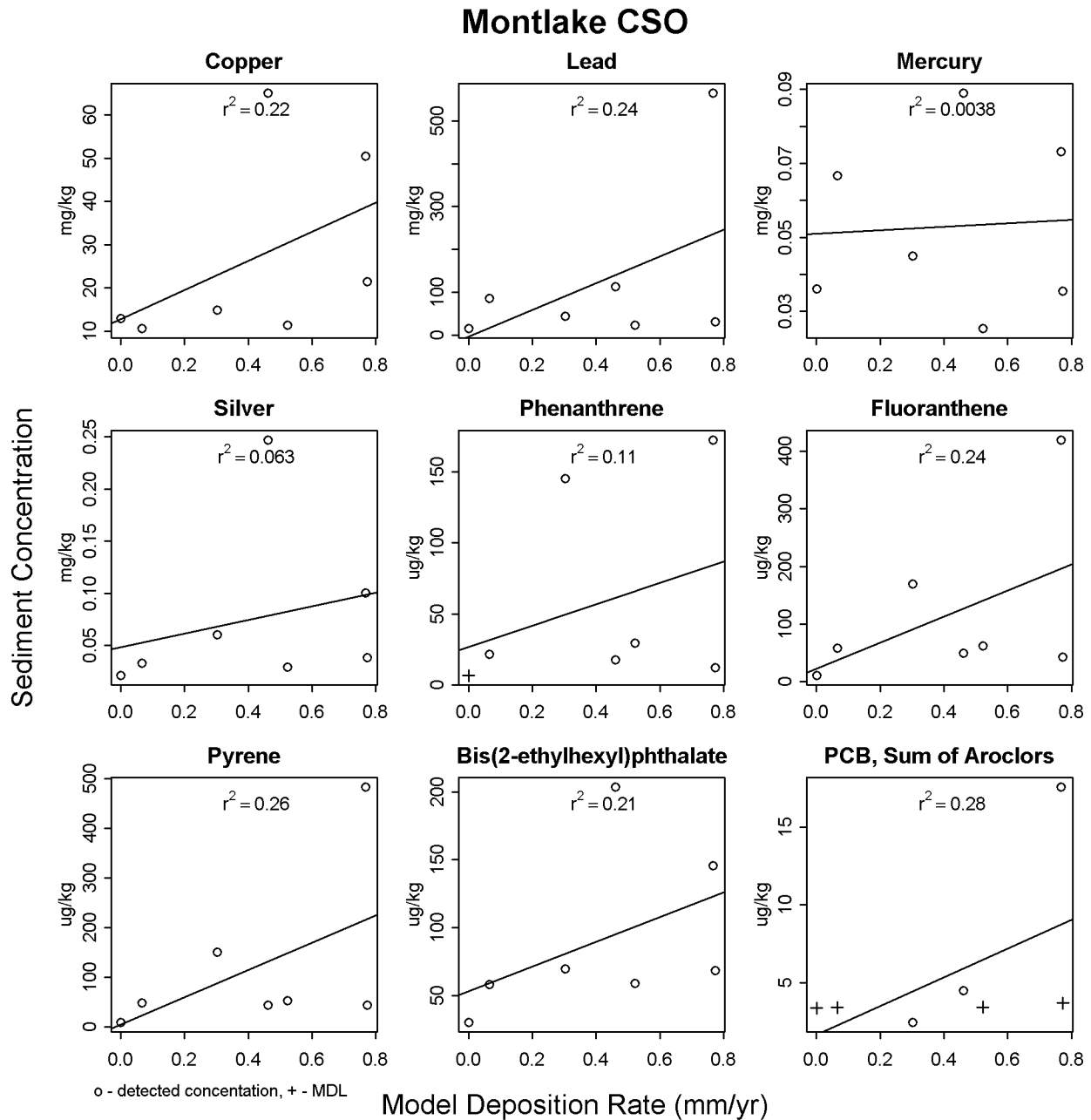


**Figure 56. Sediment concentrations versus predicted sediment depositional rates at Montlake CSO.**

### 7.3 Verification Summary

Verifying the accuracy of the model predictions is difficult without measurements of the same parameter predicted by the model; depositional rates for this model. Lacking data for direct comparison, the model predictions were compared to sediment concentrations collected around each CSO discharge. Presumably, higher sediment deposition rates should correspond to higher

sediment concentrations for those chemicals with elevated concentrations in the discharge relative to the ambient environment and the variability in ambient sedimentation rates. Because of the large amount of uncertainty in the volume of previous CSO discharges, the chemical concentrations associated with those discharges, and the historic ambient conditions, a quantitative comparison was not undertaken. The qualitative comparison focused on comparing the spatial depositional pattern predicted by the model with the spatial variation in chemical concentrations.

Nine compounds expected to be good indicators for deposited CSO solids were identified by comparing the concentrations measured in solids collected from the CSO system to the concentrations measured in the collected ambient sediment samples. Assuming the concentrations of these nine compounds is high in the deposited CSO solids relative to the ambient background, locations with high CSO solids deposition rates should have elevated concentrations for all nine compounds.

With the exception of the sample at CSO-UR-11, samples collected around the University Regulator are a good example of this. The pair-wise plots of sediment concentrations (Figure 52) show a reasonable correlation between chemical concentrations of all nine chemicals. This suggests that the CSO solids have a significant contribution to the sediment, which is supported by the magnitude of the predicted depositional rates. Predicted depositional rates of CSO solids varied from 0 to 5 mm/year, compared to a 3-mm/year estimate for Lake Washington sedimentation. With a strong signal of the CSO depositional pattern in the sediment chemistry, the model has a reasonable correlation coefficient ( $r^2$ ) of 0.5 to 0.7 between the predicted depositional rates and the sediment concentrations.

The other two freshwater CSO discharges, 3rd Ave. W and Montlake, have less coherence between different chemical concentrations and between the model predictions and the sediment concentrations. At Montlake, the sediment deposition is predicted to occur primarily to the west of the discharge, in agreement with the higher sediment concentrations. However, the lower concentrations observed at stations in front of the outfall suggest that the sediment should settle further to the west than the model predictions. One possible cause would be an underestimate of the ambient current during discharge events. The model was configured based on the mean wet season flow through the locks, but the discharge could be higher during storm events when the CSO is discharging. A second cause could be that the discharge was modeled as entering directed north, while the overflow pipe is angled about 14 deg to the west. The predicted depositional rate of CSO solids at sampling stations varied from 0 to 0.8 mm/year, and the lower relative contribution of CSO solids may contribute to the lower correlation between chemical concentrations.

At 3rd Ave W, there appeared to be some correlation between the model predictions and observed sediment concentrations, with the highest sediment concentrations tending to be found in the four samples closest to the discharge. With a predicted depositional rate at the sampling stations of 0 to 0.7 mm/year and contributions from numerous other sources in the area (SPU CSO, SPU stormwater outfall, local industrial sources, and vessel berths), the sediment signature of the CSO discharge may be harder to discern. The influence of other sources can be seen in the different correlation patterns shown in the parameter-parameter plot (Figure 46).

Both Montlake and 3rd Ave West discharge directly into the navigation channel. That depth varies from \_\_\_ to \_\_\_ with frequent vessel traffic including some large ships. Resuspension throughout the channel would make deposition patterns difficult to distinguish. University, being farther from the navigation channel, would be less subject to such effects.

Of the marine discharges, the Brandon CSO has the largest predicted depositional rate at 0 to 2.5 mm/yr. Although previous work (King County, 2011) indicated the EFDC model did an acceptable job of predicting the sediment deposition at Brandon, comparison with the sediment chemistry (Figure 41) does not show a correlation. In general, low concentrations observed at CSO-BR-1 and high concentrations at CSO-BR-3 (Figure 33) make this location very difficult to interpret; therefore, it is unlikely the model will produce good correlations. One possibility is the shallow location of CSO-BR-1 may accumulate sediment mobilized from ship wake.

The Magnolia overflow did not show correlations with many parameters, and the parameter-parameter plot did not indicate a high degree of correlation between chemicals. It may be that the 0- to 0.4-mm/yr depositional rate is too low here to detect a pattern (concentration not elevated above the variability in the ambient concentration), or that there is some active sediment movement that obscures the pattern.

The remaining discharge locations had low predicted depositional rates at the sediment sampling locations, up to 0.06 mm/yr. With the limited ability to observe a chemical signature with discharge rates an order of magnitude larger, the lack of an apparent pattern at any of these sites is to be expected. The lack of an apparent pattern in sediment chemistry supports the model predictions of very low sedimentation rates at these locations.

Several of these marine discharges, notably North Beach, 53rd Ave. SW, Barton St., and Chelan, tended to have higher sediment concentrations in the sample located just offshore of the discharge point. In all cases, the model predicted the discharge would rise quickly in the water column and not deposit solids offshore of the discharge. Simple plume analysis supports the notion that these discharges are primarily buoyant plumes that would rise quickly. However, future investigations could examine the potential mechanisms that would result in solids being deposited further offshore.

Discerning a spatial pattern is complicated by samples with high concentrations of one or more chemicals, seemingly unrelated to nearby concentrations. In this analysis, a reanalysis has been done with the high concentrations removed as an outlier. These outliers are suspected to reflect “nuggets”, or particles of or with very high concentrations that are not reflective of the local sediment concentration. Historically, resampling or reanalysis of the sample have resulted in significantly lower concentrations. Currently, the amount of small scale variability in sediment concentrations, and the impact of CSO discharges on the variability is unknown. Samples having these effects complicates discerning patterns although they are likely an indication of CSO solids deposition. While an indicator of depositional pattern, it is a confounding factor in determining if sediment quality concerns exist near a CSO.

## 8 Model Output Quality (Usability) Assessment

---

Without comparable measurements of solids deposition rates, the model accuracy cannot be quantified. However, for freshwater discharges with high deposition rates, the modeled deposition pattern appears similar and consistent with the sediment chemistry at University CSO, with the exception of one sample (CSO-UR-11). Conversely, at marine CSOs where very low deposition rates are predicted, no discernable pattern is evident in the sediment chemistry data. As a result, the model appears to be predictive of the general deposition pattern in most conditions, and is appropriate for use as a screening level tool to determine if a CSO is likely to create sediment exceedances over a broad enough area to be a concern.

The modeling and sediment sampling results suggest that creating sampling patterns based on discharge momentum length scales as discussed in King County's Post Construction Monitoring Plan (King County, 2012) is not appropriate for submerged buoyant discharges. The sampling pattern appears appropriate for surface and freshwater discharges. Future sampling and characterization events in marine waters should revise the sampling pattern to reflect the discharge buoyancy and predominate alongshore deposition pattern predicted from the model.

## 9 References

---

King County, 2011. Discharge modeling for the contaminated sediment cleanup decisions: A summary and supplemental analyses. Department of Natural Resources and Parks, Wastewater Treatment Division.

King County, 2012. Post Construction Monitoring Plan for King County CSO Controls, Appendix H to 2012 King County Long-term CSO Control Plan Amendment. Department of Natural Resources and Parks, Wastewater Treatment Division.

## Appendix A. Data Tables

Station	Model Deposition Rate (mm/yr)	Copper (mg/kg)	Lead (mg/kg)	Mercury (mg/kg)	Silver (mg/kg)	Phenanthrene (µg/kg)	Fluoranthene (µg/kg)	Pyrene (µg/kg)	Bis(2-ethylhexyl) phthalate (µg/kg)	PCB, Sum of Aroclors (µg/kg)
CSO-3W-1	0.753	82.0	113.9	1.50 J	0.83	3264	5207	6003	1815	186.8 C
CSO-3W-2	0.070	40.7	68.5 J	0.46	0.62	1560	2916	3274	506	88.4 C
CSO-3W-3	0.222	40.7	84.4	0.58	0.53	7823 J	9953 J	11711 J	1726 J	54.2 C
CSO-3W-4	0.159	46.0	139.7	0.34	0.85	3898	5997	6957	1243	310.5 C
CSO-3W-5	0.090	47.9	99.0	0.37	0.74	5837	7176	8370	1012	247.5 C
CSO-3W-6	0.055	25.9	40.9	0.35	0.18	6991	8070	9852	152 B2	40.6 C
CSO-3W-7	0.083	21.0	51.0	0.05 J	0.15	143	209	246	189 B2	4.5 C
0537	0.411	139.0	149.3	0.69 J	0.46 J	779	1080	2798	2930	242.3 C
CSO-UR-1	5.027	113.5	109.2	2.23	0.79	487	1692	1419	12265	567.4 C
CSO-UR-10	3.884	96.2	188.6 J	0.47	1.99 J	338	932	981	2644 J	245.5 C
CSO-UR-11	0.290	73.1	746.1	1.20 J	0.28	446	1254	1560 J	2139	13300.3 C
CSO-UR-12	2.429	13.0 J	27.6	0.13 J	0.09 U	62 UJ	156 UJ	184 UJ	25 J	14.5 UC
CSO-UR-2	0.049	21.6	57.1	0.20	0.14	131	297	299	602	50.8 C
CSO-UR-3	2.452	89.6	112.2	0.46	0.80	357	1027	811	2842	247.3 C
CSO-UR-4	0.488	20.7	48.7	0.14	0.10	171	427	365	325 B2	147.0 C
CSO-UR-5	0.038	16.4	10.9	0.07 J	0.07 J	153	394	344	80 B	48.9 C
CSO-UR-6	0.587	25.6	22.6	0.06 J	0.08	278	416	341	260 B2	32.7 C
CSO-UR-7	0.220	23.2	48.2	0.10 J	0.12 J	108	329	299	311 B2	67.4 C
CSO-UR-9	0.466	11.6	46.5	0.07 J	0.09	62	86	85	115	98.1 C
CSO-53-1	0.000	23.5	3.7 J	0.02 J	0.28 U	43	79	65	37 B	5.9 UC
CSO-53-2	0.001	4.8	3.8 J	0.01 J	0.27 U	7 U	7 U	7 U	32 B	5.4 UC
CSO-53-3	0.000	4.9	3.4 J	0.01 J	0.28 U	7 U	7 U	7 U	31 B	11.2 C
CSO-53-4	0.000	5.5	6.4 J	0.01 J	0.28 U	19	20	21	33 B	5.6 UC

Station	Model Deposition Rate (mm/yr)	Copper (mg/kg)		Lead (mg/kg)		Mercury (mg/kg)		Silver (mg/kg)		Phenanthrene (µg/kg)		Fluoranthene (µg/kg)		Pyrene (µg/kg)		Bis(2-ethylhexyl) phthalate (µg/kg)		PCB, Sum of Aroclors (µg/kg)		
CSO-53-5	0.000	6.1		5.4	J	0.01	J	0.31	U	19		26		24		42		B	6.7	C
CSO-53-6	0.000	13.2		7.6	J	0.04	J	0.33	U	60		125		103		55		B	12.6	C
CSO-BR-1	2.980	35.6		29.6		0.31		1.17	J	75		220		187		362			367.0	C
CSO-BR-2	0.168	38.1		45.2		0.16		1.27	J	129		359		337		315			166.1	C
CSO-BR-3	2.681	59.5		68.4		0.08		2.03		2528		6411		5670		6397			65.3	C
CSO-BR-4	0.315	60.7		27.8		0.15		2.04		340		811		566		541			96.1	C
CSO-BR-5	0.595	67.3		32.3		0.23		2.17		173		699		556		659			108.2	C
CSO-BR-6	0.390	55.9		25.9		0.22		2.42		138		364		321		377		B2	125.3	C
CSO-BT-1	0.014	22.2		22.0		0.04	J	0.06	JG	1418		1542		2570	JL	682		JL	297.9	C
CSO-BT-10	0.040	6.8		7.3		0.02	J	0.02	J	414		604		679		113			3.4	JC
CSO-BT-11	0.052	27.6		37.8		0.01	J	0.02	J	22	J	62		231		239			8.5	C
CSO-BT-12	0.035	10.3		6.2	J	0.04	J	0.03	J	1320		858		975		449			3.8	JC
CSO-BT-13	0.035	10.4		14.3		0.02	J	0.03	J	411		379		511		44		U	3.3	UC
CSO-BT-2	0.008	10.0		11.1		0.02	J	0.03	J	274		428		599		113			2.2	JC
CSO-BT-3	0.046	9.5		8.9		0.02	J	0.02	J	713		688		947		101			3.3	JC
CSO-BT-4	0.002	10.6		32.2		0.03	J	0.03	J	52		100		174		239			2.0	JC
CSO-BT-5	0.005	10.8		18.1		0.02	J	0.03	J	215		419		656		150			5.2	JC
CSO-BT-6	0.001	7.0		8.4		0.02	J	0.03	J	551		383		447		45		U	1.6	JC
CSO-BT-7	0.002	6.2		7.1		0.02	J	0.02	J	68		117		188		341			3.4	UC
CSO-BT-8	0.045	6.2		6.7		0.02	J	0.02	J	309		320		422		63		J	89.8	C
CSO-BT-9	0.008	6.5		13.5		0.03	J	0.02	J	102		176		225		44		U	3.3	UC
LSVV01	0.000	5.4		5.7	J	0.02	J	0.34	U	27		24		38		23		J,B	13.4	UC
CH10S	0.034	77.5		48.1		0.23		0.35	U	303		2334	J	1934	J	287			129.4	C
CH20S	0.024	67.7		48.0		0.18		0.35	U	602		2251		1731		293			134.2	C
CSO-CH-1	0.004	49.8		27.9		0.13		1.17	J	810		1042		1336		259		B2	276.5	C

Station	Model Deposition Rate (mm/yr)	Copper (mg/kg)	Lead (mg/kg)	Mercury (mg/kg)	Silver (mg/kg)	Phenanthrene (µg/kg)	Fluoranthene (µg/kg)	Pyrene (µg/kg)	Bis(2-ethylhexyl) phthalate (µg/kg)	PCB, Sum of Aroclors (µg/kg)							
CSO-CH-2	0.004	30.5	27.0	0.10	1.05	J	134	373	319	126	B	50.6	C				
CSO-CH-3	0.005	64.6	52.7	0.17	1.07	J	496	947	827	270	B2	137.9	C				
CSO-CH-4	0.002	17.2	15.8	0.06	J	1.08	J	84	215	208	93	B	34.3	C			
CSO-CH-5	0.002	28.7	23.6	0.13	1.10	J	129	294	270	182	B2	20.7	C				
CSO-CH-6	0.002	14.5	14.9	0.03	J	0.27	U	470	415	458	20	J	16.1	JC			
CSO-CH-7	0.003	25.4	19.5	0.13	0.27	U	199	236	266	34		45.0	C				
CSO-CH-8	0.002	21.1	16.4	0.03	J	0.26	U	154	142	233	14	U	15.6	JC			
CSO-MG-1	0.030	18.3	10.3	0.04	J	0.26	U	15	42	37	114	B	2.4	JC			
CSO-MG-2	0.119	14.5	16.6	0.05	J	0.25	U	28	76	67	187	B2	7.3	JC			
CSO-MG-3	0.022	9.2	8.5	0.04	J	0.26	U	25	43	38	41	B	5.0	JC			
CSO-MG-4	0.017	8.3	7.8	0.03	J	0.28	U	31	95	77	47	B	5.3	JC			
CSO-MG-5	0.010	7.3	6.2	J	0.03	J	0.25	U	17	33	30	39	B	4.7	JC		
CSO-MG-6	0.004	7.5	6.8	0.03	J	0.26	U	36	72	62	41	B	7.1	JC			
CSO-MG-7	0.111	25.7	9.9	0.04	J	0.27	U	33	59	53	27	J	7.2	JC			
CSO-ML-1	0.773	21.4	30.2	0.04	J	0.04	J	12	J	43	44	68	B	3.7	UC		
CSO-ML-2	0.303	14.9	43.7	0.04	J	0.06	J	145	170	150	70	B	2.4	JC			
CSO-ML-3	0.767	50.5	565.2	0.07	0.10		173	419	482	146	B2	17.6	C				
CSO-ML-4	0.523	11.4	22.4	0.03	J	0.03	J	30	62	53	59	B	3.4	UC			
CSO-ML-5	0.066	10.6	85.0	0.07	0.03	J	22	59	48	58	B	3.4	UC				
CSO-ML-6	0.000	13.0	15.2	0.04	J	0.02	J	7	U	11	J	9	J	30	B	3.4	UC
CSO-ML-7	0.461	65.1	J	112.2	0.09	0.25	J	18	50	44	204	B2	4.5	JC			
CSO-MY-1	0.022	6.5	8.4	0.02	J	0.28	U	170	278	263	150	B2	5.5	UC			
CSO-MY-10	0.008	8.7	22.5	0.02	J	0.26	U	130	J	263	J	212	J	77		5.9	JC
CSO-MY-11	0.006	6.3	6.1	J	0.02	J	0.26	U	165	193	188	286				7.8	UC
CSO-MY-12	0.002	5.5	5.6	J	0.02	J	0.25	U	62	56	53	14	U			7.5	UC

Station	Model Deposition Rate (mm/yr)	Copper (mg/kg)		Lead (mg/kg)		Mercury (mg/kg)		Silver (mg/kg)		Phenanthrene (µg/kg)		Fluoranthene (µg/kg)		Pyrene (µg/kg)		Bis(2-ethylhexyl) phthalate (µg/kg)		PCB, Sum of Aroclors (µg/kg)	
CSO-MY-13	0.015	4.4		4.4	J	0.02	J	0.25	U	166		170		144		93		30.4	C
CSO-MY-2	0.006	7.4		10.8		0.05	J	0.26	U	42		92		83		58	B	2.8	JC
CSO-MY-3	0.009	8.2		12.8		0.02	J	0.27	U	106		167		142		137	B2	2.9	JC
CSO-MY-4	0.003	3.8		5.5	J	0.01	J	0.26	U	11	J	49		58		34	B	5.1	UC
CSO-MY-5	0.002	4.1		4.7	J	0.01	J	0.26	U	7	U	7	U	7	U	29	B	5.1	UC
CSO-MY-6	0.003	4.4		5.0	J	0.01	J	0.26	U	38		40		41		29	B	5.1	UC
CSO-MY-7	0.001	3.8		3.8	J	0.01	J	0.25	U	7	U	7	U	7	U	27	B	5.1	UC
CSO-MY-8	0.023	15.4		17.6		0.01	J	0.21	U	18		37		39		72		3.4	JC
CSO-MY-9	0.007	7.1		12.7		0.02	J	0.26	U	3667		5500		4333		117		3.1	JC
CSO-NB-1	0.028	6.0		3.9	J	0.02	J	0.28	U	19		32		35		37	B	5.6	UC
CSO-NB-10	0.028	3.4		2.5	J	0.01	J	0.26	U	7	U	7	U	7	U	14	U	7.8	UC
CSO-NB-11	0.007	3.8		3.0	J	0.01	J	0.27	U	7	U	7	U	7	U	15	U	8.1	UC
CSO-NB-2	0.031	5.6		3.1	J	0.03	J	0.28	U	7	U	7	U	7	U	37	B	5.6	UC
CSO-NB-3	0.028	5.1		3.6	J	0.02	J	0.28	U	84		222		210		40	B	5.7	UC
CSO-NB-4	0.009	4.0		3.3	J	0.01	J	0.28	U	18		43		37		36	B	5.5	UC
CSO-NB-5	0.008	4.5		3.3	J	0.02	J	0.28	U	7	U	7	U	7	U	36	B	79.2	C
CSO-NB-6	0.003	3.4		2.8	J	0.01	J	0.28	U	65		73		74		36	B	5.6	UC
CSO-NB-7	0.032	4.0		2.9	J	0.01	J	0.27	U	35		35		40		15	U	8.0	UC
CSO-NB-8	0.012	4.1		3.4	J	0.01	J	0.27	U	7	U	11	J	13	J	15	U	8.1	UC
CSO-NB-9	0.005	3.5		3.1	J	0.01	J	0.28	U	48		58		64		15	U	8.3	UC

All concentrations reported on a dry weight basis

U – not detected. Value given is MDL

J – estimated value

JG – estimated value, probable low bias

Station	Model Deposition Rate (mm/yr)	Copper (mg/kg)	Lead (mg/kg)	Mercury (mg/kg)	Silver (mg/kg)	Phenanthrene (µg/kg)	Fluoranthene (µg/kg)	Pyrene (µg/kg)	Bis(2-ethylhexyl) phthalate (µg/kg)	PCB, Sum of Aroclors (µg/kg)
JL – estimated value, probable high bias										
B – the associated blank concentration is > MDL and the sample result is within 5 times the blank concentration										
B2 – the associated blank concentration is > MDL and the sample result is > 5 and < 10 times the blank concentration										
C – calculated value										